



UNIVERSITEIT VAN PRETORIA
UNIVERSITY OF PRETORIA
YUNIBESITHI YA PRETORIA

SINGLE-PHASE FORCED AND MIXED CONVECTION IN THE LAMINAR AND TRANSITIONAL FLOW REGIMES OF INCLINED SMOOTH TUBES WITH INLET DISTURBANCES

by

Abubakar Idris Bashir

Submitted in partial fulfilment of the requirements for the degree

**Doctor of Philosophy (PhD)
in Engineering**

**Department of Mechanical and Aeronautical Engineering
University of Pretoria**

December 2019

**Supervisor: Prof JP Meyer
Co-supervisor: Dr M Everts**

Abstract

Title: Single-phase forced and mixed convection in the laminar and transitional flow regimes of inclined smooth tubes with inlet disturbances

Supervisor: Prof JP Meyer

Co-supervisor: Dr M Everts

Department: Mechanical and Aeronautical Engineering

Degree: PhD (Mechanical Engineering)

Laminar and transitional flow regimes in tubes have been extensively investigated in the literature. However, there are several gaps in the forced and mixed convection literature, especially for inclined tubes with different inlet disturbances. The purpose of this study was to experimentally investigate the effect of tube inclination and inlet contraction ratio on the single-phase heat transfer and pressure drop characteristics in the laminar and transitional flow regimes for pure forced and mixed convection conditions.

An experimental set-up was designed, constructed and validated against literature with the test section in a horizontal and different vertical orientation. The test section was 4.6 m long and was made from a smooth hard drawn copper tube with measured inner and outer diameters of 5.1 mm and 6.3 mm, respectively. Experiments were conducted at various inclination angles from vertical upward flow (+90°) to vertical downward flow (-90°), with horizontal flow (0°) and several other angles in between. A total of 2 679 mass flow rate measurements, 174 135 temperature measurements and 2 679 pressure drop measurements were conducted using water (Prandtl numbers between 3.5 and 8.1) as working fluid. The Reynolds number range covered were from 400 to 6 000 at constant heat fluxes varying from 1 to 8 kW/m². Four different types of inlets namely; square-edged and re-entrant inlet with different inlet contraction ratios (5, 11, 14 and 33), as well as hydrodynamically fully developed and 90° bend inlets were used.

It was found that an increase in the inclination angle from horizontal flow (0°) to vertical ($\pm 90^\circ$) flow, decreased the buoyancy effects which led to decreased laminar heat transfer coefficients and friction factors for both upward and downward flows. The onset of buoyancy effects was significant near the vertical inclination angles and caused a rapid increase in the laminar heat transfer coefficients and friction factors when the inclination angles moved from vertical to

horizontal orientations. An inclined tube Grashof number which is a function of inclination angle was defined and used to express the laminar Nusselt numbers as a forced convection part plus an enhancement component owing to mixed convection. The laminar friction factors were expressed as a function of a forced convection/isothermal part multiplied by the mixed convection part. Furthermore, it was found that the critical Reynolds numbers at which transitional flow regime started increased as the inclination angles increased from horizontal to vertical, while the end of transitional flow regime were inclination angle independent. This caused the width of the transitional flow regime to decrease, as well as the transition gradients to increase, with increasing inclination angles at different heat fluxes. It was also found that the flow directions (upward and downward) had a negligible effect on the heat transfer coefficients and friction factors in the entire transition and quasi-turbulent regions.

The fully developed laminar forced convection Nusselt numbers were not constant at 4.36, but were a function of Reynolds number for Reynolds numbers higher than 1 000. Therefore, a revised laminar Nusselt number correlation for smooth circular tubes was developed. The fully developed laminar forced convection friction factors were, as expected, equal to $64/Re$. For both the forced convection heat transfer and pressure drop characteristics, transition occurred at the same mass flow rates for all the heat fluxes, including isothermal flow, but the critical Reynolds numbers increased with an increase in heat flux. For forced convection condition, the width of the transitional flow regime in the fully developed region remained constant for all heat fluxes.

For a square-edged inlet geometry, the transition from the laminar to the turbulent flow regimes occurred earlier as the inlet contraction ratio increased, while for the re-entrant inlet, transition was delayed. The transitional flow regime was significantly affected by smaller contraction ratios and this effect increased with increasing heat flux. However, it was found that the critical Reynolds numbers were independent of inlet geometry for contraction ratios larger than 33. For the 90° bend inlet, transition occurred earlier than all the other inlet geometries and contraction ratios.

Publications

The journal articles published and conference papers presented at international conferences during the progress, preparation and completion of this thesis are listed below:

Articles

1. J.P. Meyer, **A.I. Bashir**, M. Everts, Single-phase mixed convective heat transfer and pressure drop in the laminar and transitional flow regimes in smooth inclined tubes heated at a constant heat flux, *Experimental Thermal and Fluid Science*, vol. 109, (2019), 109890.
2. **A.I. Bashir**, M. Everts, J.P. Meyer, R. Bennacer, Single-phase forced convection heat transfer and pressure drop in circular tubes in the laminar and transitional flow regimes, *Experimental Thermal and Fluid Science*, vol. 109, (2019), 109891.
3. **A.I. Bashir**, M. Everts, J.P. Meyer, Influence of inlet contraction ratios on the heat transfer and pressure drop characteristics of single-phase flow in smooth circular tubes in the transitional flow regime, *Experimental Thermal and Fluid Science*, vol. 109, (2019), 109892.

Conference papers

1. **Bashir A.I.** and Meyer J.P.; Heat transfer in the laminar and transitional flow regimes of smooth vertical tube for upflow direction, *Proceedings of the 13th International Conference on Heat Transfer, Fluid Mechanics and Thermodynamics (HEFAT2017)*, pp. 29-34, Portorož, 17-19 July 2017.
2. **Bashir A.I.** and Meyer J.P.; Experimental investigation of convective heat transfer in the transitional flow regime of an inclined smooth tube, *Proceedings of the 16th International Heat Transfer Conference*, Beijing, IHTC16-23461, 10 – 15 August 2018
3. **Bashir A.I.**, Everts M., Bhattacharyya S. and Meyer J.P.; Effect of inclination buoyancy on the fully developed friction factors in the laminar and transitional flow regimes of smooth tube, *Proceedings of the 14th International Conference on Heat Transfer, Fluid Mechanics and Thermodynamics (HEFAT2019)*, pp. 470 – 475, Wicklow, 22 – 24th July.
4. **Bashir A.I.**, Everts M. and Meyer J.P.; Experimental investigation of transitional flow forced convection heat transfer through a smooth vertical tube with a square-edged inlet, *Proceedings of the 16th UK Heat Transfer Conference*, Nottingham, UKHTC2019-042, 8 - 10 September 2019.
5. Bhattacharyya S., Everts M., **Bashir A.I.** and Meyer J.P.; Experimental and numerical investigation of the heat transfer characteristics of laminar flow in a vertical circular tube at low Reynolds numbers, *Proceedings of the 16th UK Heat Transfer Conference*, Nottingham, UKHTC2019-060, 8 - 10 September 2019.

6. Everts M., **Bashir A.I.** and Meyer J.P.; Influence of free convection on fully developed transitional flow, Proceedings of the 22nd Congress in Thermal Science and Technology in Kocaeli, Turkey, 11 - 14 September 2019.

Declaration

All the work in the above papers were conducted by the author (AI Bashir) of this thesis under the supervision of the co-authors Prof JP Meyer and Dr M Everts. In article 2 Prof Bennecer (LMT, ENS-Cachan, CNRS, Université Paris Saclay, Cachan, France) assisted with the interpretation of the data while visiting the University of Pretoria on a short sabbatical that received funding from the European Union's Horizon 2020 research and innovation programme under the Marie Skłodowska-Curie grant agreement No. 778104.

In conference paper 5, the experimental data taken by the author of this thesis was made available for comparison purposes with simulations conducted by Dr S Bhattacharyya who was a postdoctoral fellow at the University of Pretoria in 2018/2019.

Prize

Best student paper (one of only five awards out of a total of 126 papers) for conference paper 4, at the 16th UK Heat Transfer Conference (UKHTC2019), 8 - 10 September, Nottingham, UK.

Dedication

This thesis is dedicated to my late parents; Alh. Idris Nayaya Bashir and Haj. Rukayya Idris Bashir. May their souls rest in Jannatul Firdaus, Amin Summa Amin.

Acknowledgements

Glory be to Allah, the self-sustainer and sustainer of all, by whose favour good deeds are accomplished. I thank Almighty Allah for His infinite mercies, His guidance, the knowledge, good health and the strength he bestowed on me to be able to reach this milestone.

I would like to express my sincere gratitude to my supervisors; Prof Josua P Meyer and Dr Marilize Everts for their valuable support, stimulating comments, guidance and encouragement. I owe my deepest gratitude to my deceased parents; may God shower his mercy upon their souls as they cherished me in childhood. I am very grateful to my lovely wife Saudah Ibrahim Kurfi and my daughter Ruqayya Abubakar Idris for their love, prayers, patience and encouragements throughout my programme. I would like to extend my appreciation to my brothers and sisters for their sincere love and supports.

The financial support of Tertiary Education Trust Fund (TETFund) through Bayero University, Kano and the University of Pretoria to this programme is tenaciously appreciated. I would also like to thank Bayero University Kano for approving my study fellowship.

I greatly appreciate the technical and support staff of Mechanical and Aeronautical Engineering department; Mr D Gouws, Mr C Moon, Mr P Kruger, Mr E Mohale, Mr W Murray, Mr KJ Mthombeni and Ms T Evans. Your help and advice are invaluable. Finally, to my family and friends, colleagues at University of Pretoria, I sincerely appreciate your encouragements.

Table of contents

Abstract.....	i
Publications.....	iii
Dedication.....	v
Acknowledgements.....	vi
Table of contents.....	vii
List of figures.....	xi
List of tables.....	xvi
Nomenclature.....	xvii
1. Introduction.....	1
1.1. Background.....	1
1.2. Problem statement.....	4
1.3. Aim.....	4
1.4. Objectives.....	5
1.5. Scope of work.....	5
1.6. Original outcomes.....	6
1.7. Layout of thesis.....	7
2. Literature review.....	8
2.1. Introduction.....	8
2.2. Dimensionless parameters.....	8
2.2.1. Reynolds number.....	8
2.2.2. Prandtl number.....	9
2.2.3. Graetz number.....	9
2.2.4. Nusselt number.....	9
2.2.5. Colburn j -factor.....	9
2.2.6. Grashof number.....	10
2.2.7. Rayleigh number.....	10

2.2.8.	Richardson number	10
2.2.9.	Fanning and Darcy friction factors	11
2.3.	Transitional flow nomenclature	11
2.3.1.	Start of the transitional flow regime, Re_{cr}	11
2.3.2.	Start of the quasi-turbulent flow regime, Re_{qt}	13
2.3.3.	Width of the transitional flow regime, ΔRe	13
2.3.4.	Transition gradient, TG	13
2.3.5.	Start of the turbulent flow regime, Re_t	14
2.4.	Developing and fully developed flows in tubes	14
2.5.	Forced convection heat transfer	17
2.5.1.	Laminar flow.....	17
2.5.2.	Transitional flow.....	20
2.5.3.	Quasi-turbulent and turbulent flow.....	20
2.6.	Mixed convection heat transfer	20
2.6.1.	Laminar flow: Horizontal tubes	21
2.6.2.	Laminar flow: Vertical tubes	22
2.6.3.	Laminar flow: Inclined tubes	23
2.6.4.	Transitional flow: Horizontal tubes	24
2.6.5.	Transitional flow: Vertical and inclined tubes.....	28
2.7.	Effects of inlet disturbances on transitional flow	29
2.7.1.	Inlet geometry	29
2.7.1.	Inlet contraction ratios	30
2.7.2.	Flow-calming section contents	32
2.7.3.	Multiple circular tubes	32
2.8.	Summary and conclusions.....	32
3.	Experimental set-up and data reduction.....	34
3.1.	Introduction	34
3.2.	Experimental set-up.....	34
3.2.1.	Flow-calming section and inlet section.....	35
3.2.2.	Test section	37

3.2.3.	Test bench	40
3.2.4.	Insulation.....	40
3.3.	Experimental procedure	40
3.4.	Data reduction	41
3.5.	Experimental test matrix	45
3.6.	Uncertainties.....	49
3.7.	Summary, conclusions and recommendations	50
4.	Validation.....	52
4.1.	Introduction	52
4.2.	Isothermal Pressure drops	52
4.3.	Laminar forced convection heat transfer.....	53
4.4.	Laminar mixed convection heat transfer	58
4.5.	Turbulent flow	59
4.6.	Conclusions and recommendations	60
5.	Mixed convection heat transfer and pressure drop	62
5.1.	Introduction	62
5.2.	Fully developed flow pressure drop	62
5.2.1.	Isothermal friction factors.....	62
5.2.2.	Diabatic friction factors	63
5.3.	Fully developed flow heat transfer	67
5.3.1.	Laminar flow.....	67
5.3.2.	Laminar Nusselt number and friction factor correlations	71
5.3.3.	Transitional flow	76
5.3.4.	Schematic summary	81
5.4.	Developing flow heat transfer for horizontal and vertical flow	83
5.5.	Conclusions and recommendations	85
6.	Forced convection heat transfer and pressure drop.....	87
6.1.	Introduction	87
6.2.	Laminar flow	87
6.2.1.	Heat transfer	87

6.2.2.	Pressure drop and heat transfer analogy	94
6.3.	Transitional flow	96
6.3.1.	Heat transfer.....	97
6.3.2.	Pressure drop in the transitional flow regime	101
6.4.	Conclusions and recommendations.....	102
7.	Effects of flow-calming section contents and inlet contraction ratios	104
7.1.	Introduction	104
7.2.	Calming section content.....	104
7.2.1.	Pressure drop characteristics.....	104
7.2.2.	Heat transfer characteristics	106
7.3.	Contraction ratio.....	108
7.3.1.	Pressure drop characteristics.....	108
7.3.2.	Heat transfer characteristics	110
7.3.3.	Schematic summary	114
7.4.	Conclusions and recommendations.....	116
8.	Summary, conclusions and recommendations	117
8.1.	Summary	117
8.2.	Conclusions	118
8.3.	Recommendations	119
References	121

List of figures

Fig. 2.1: Schematic representation of the different flow regimes in terms of the Nusselt number, Colburn j -factor, and friction factor as a function of Reynolds number. Adapted from Everts [65] and Everts and Meyer [21, 40].	12
Fig. 2.2: Schematic representation of the heat transfer coefficients, friction factors, velocity and temperature profiles for laminar flow in tubes [11].	15
Fig. 2.3: Schematic representation of buoyancy effects on the fluid flow and heat transfer in (a) horizontal, (b) inclined, and (c) vertical tubes for both upward and downward flows.	21
Fig. 2.4: Schematic representation of the different inlet geometries: (a) re-entrant, (b) square-edged, (c) bell-mouth, and (d) hydrodynamically fully developed. Adapted from Everts [65].	30
Fig. 3.1: Schematic layout of the experimental set-up.	35
Fig. 3.2: Schematic representation of the inlet mixer with (a) the original flow-calming section with a square-edged inlet, (b) the empty flow-calming section a re-entrant inlet, (c) the hydrodynamically fully developed inlet and (d) the 90° bend inlet. (All dimensions given in mm).	36
Fig. 3.3: Schematic representation of (a) the test section indicating the pressure taps (PT) and thermocouple stations (T), (b) the flow directions and (c) a cross section of the test section tube that shows the thermocouple positions per station.	38
Fig. 4.1: Validation of the fully developed isothermal friction factors for horizontal flow with literature.	52
Fig. 4.2: Validation of the local laminar Nusselt numbers as a function of the axial position for forced convection conditions at a heat flux of 280 W/m ² and bulk fully developed Reynolds number of 660.	53
Fig. 4.3: Comparison of local Nusselt numbers as a function of the axial position for vertical and horizontal flow orientations. The horizontal tube is at a bulk Reynolds number of 660 and a very low heat flux of 280 W/m ² . The flows for vertical upward and vertical downward orientations are at a bulk Reynolds number of approximately 1 050 and a high heat flux of 4 kW/m ² .	55
Fig. 4.4: Comparison of local Nusselt numbers as a function of the axial position at higher heat fluxes and a Reynolds number of approximately 2 100 for vertical upward and downward flows.	56
Fig. 4.5: Comparison of the average wall temperature differences between the top and bottom thermocouples for horizontal flow and vertical upward flow as a function of Reynolds number at different heat fluxes.	57

Fig. 4.6: Comparison of the laminar forced convection results on the flow regime map of Metzais and Eckert [129] for heat fluxes of 1 kW/m ² (pink), 2 kW/m ² (orange), 4 kW/m ² (blue), 6 kW/m ² (green) and 8 kW/m ² (red) for both vertical upward and downward flow at all the axial locations in the fully developed region ($416 < x/D_i < 857$).....	58
Fig. 4.7: Validation of the local Nusselt numbers as a function of the axial position for mixed convection conditions at a heat flux of 6 kW/m ² and bulk Reynolds number of 1 450.	59
Fig. 4.8: Comparison of the average fully developed turbulent Nusselt numbers as function of Reynolds number with literature. The Nusselt numbers were the average over the fully developed part and the Reynolds number was determined at the <i>b,FD</i> -point identified in Fig. 3.3.....	60
Fig. 5.1: Fully developed isothermal friction factors as a function of Reynolds number for different inclination angles in the upward and downward flow directions.	63
Fig. 5.2: Comparison of fully developed diabatic friction factors as a function of Reynolds number for different inclination angles at a heat flux of 6 kW/m ²	64
Fig. 5.3: Comparison of fully developed diabatic friction factors at a heat flux of 6 kW/m ² as a function of inclination angle at (a) different Reynolds numbers and (b) Reynolds number of 2 600.	65
Fig. 5.4: Reynolds numbers at which the transitional flow regime started (Re_{cr}) and ended (Re_{qt}) as a function of inclination angle for the diabatic friction factors in Fig. 5.2 at a heat flux of 6 kW/m ²	66
Fig. 5.5: Comparison of the local laminar Nusselt numbers as a function of the axial position for different inclination angles at a bulk Reynolds number of approximately 1 600 and a heat flux of 6 kW/m ² for (a) upward flow and (b) downward flow.	68
Fig. 5.6: Average Nusselt numbers as a function of inclination angle for fully developed laminar flow at different bulk Reynolds numbers and a heat flux of 6 kW/m ²	70
Fig. 5.7: Components of the buoyancy force for different tube orientations.....	71
Fig. 5.8: Average fully developed laminar Nusselt numbers as a function inclination angle for a bulk Reynolds number of 1 600 and a heat flux of 6 kW/m ²	72
Fig. 5.9: Comparison of the average laminar Nusselt number correlation Eq. 5.1 for fully developed flow with experimental results for the different inclination angles and heat fluxes using Eq. 6.5 and (a) Eq. 5.6 and (b) Eq. 5.7. The blue, green and red markers represent heat fluxes of 4 kW/m ² , 6 kW/m ² , and 8 kW/m ² , respectively.	74
Fig. 5.10: Comparison of average fully developed Nusselt number correlations, Eq. 5.1 (with Eq. 5.6 and Eq. 5.7) with the experimental data at a bulk Reynolds number of approximately 1 600 and a heat flux of 6 kW/m ² for different inclination angles.	75
Fig. 5.11: Comparison of the laminar fully developed diabatic friction factor correlations with the experimental results for the different inclination angles at different heat fluxes using (a) Eq. 5.8	

and (b) Eq. 5.9. The blue, green and red markers represent heat fluxes of 4 kW/m ² , 6 kW/m ² , and 8 kW/m ² , respectively.....	76
Fig. 5.12: Comparison of the average fully developed Colburn j -factors as a function of Reynolds number for upward flow at different inclination angles at constant heat flux of 6 kW/m ²	77
Fig. 5.13: Comparison of the Colburn j -factors at the start, j_{cr} , and end, j_{qt} , of the transitional flow regime as a function of inclination angle at a heat flux of 6 kW/m ²	78
Fig. 5.14: Comparison of transition gradients of the Colburn j -factors (TG_j) as a function of inclination angle at a heat flux of 6 kW/m ²	78
Fig. 5.15: Comparison of (a) the Reynolds numbers at which the transitional flow regime started and ended and (b) the width of the transitional flow regime as a function of inclination angle at a heat flux of 6 kW/m ²	80
Fig. 5.16: Schematic representation of (a) the Nusselt number and (b) the friction factor, as a function of Reynolds number for upward and downward flow at different inclination angles and a constant heat flux.	82
Fig. 5.17: Comparison of local developing and fully developed Colburn j -factors as function of (a) $x/D_i = 33$, (b) $x/D_i = 63$, (c) $x/D_i = 151$ and (d) $x/D_i = 592$, as a function of local Reynolds numbers for horizontal and vertical flow at a heat flux of 6 kW/m ²	83
Fig. 5.18: Comparison of the local critical Reynolds numbers as a function of axial location of the tube for developing and fully developed flows of horizontal and vertical inclinations in Fig. 5.17.	84
Fig. 6.1: Comparison of the average fully developed laminar Nusselt numbers as a function Reynolds number at various heat fluxes for vertical upward flow (forced convection heat transfer). Results for mixed convection horizontal flow (empty square markers) were included for comparison at the same heating conditions.	88
Fig. 6.2: Schematic representation of the variation of the mean fluid temperature, T_m , (red), viscosity, μ , (blue), Reynolds number, Re , (green), pressure drop, dP , (orange), heat transfer coefficient, h , (purple) and the Nusselt number, Nu , (grey) in the flow direction along the axial location of the test section tube for a constant heat flux boundary condition.	89
Fig. 6.3: Comparison for upward flow of (a) the heat transfer coefficients as a function mass flow rate and (b) the Nusselt numbers as a function of Reynolds number for different heat fluxes. ...	91
Fig. 6.4: (a) A linear curve fit through the average laminar forced convection Nusselt numbers as a function of Reynolds number and (b) Comparison of the revised fully developed laminar forced convection Nusselt number correlation (Eq. 6.5) with the vertical upward and downward flow experimental data at different heat fluxes.	94
Fig. 6.5: Comparison of the forced convection diabatic friction factors as a function of Reynolds numbers for vertical upward and downward flow at different heat fluxes.	95

Fig. 6.6: Comparison of (a) ratio of f/j as a function Reynolds numbers and (b) a linear curve fit through the experimental results for $(f/j)/Pr^{1/3}$ as a function of Reynolds number for both upward and downward flows at different heat fluxes. 96

Fig. 6.7: Average fully developed Nusselt numbers as a function of Reynolds number for vertical upward (●) and downward (○) flows at different heat fluxes. 97

Fig. 6.8: Comparison for vertical upward flow of (a) Reynolds numbers at which the transitional flow regime started, Re_{cr} , and ended, Re_{qt} and (b) width of the transitional flow regime, ΔRe , as a function axial location for different heat fluxes. 98

Fig. 6.9: Comparison of (a) $Re_{cr}/(Pr_b/Pr_w)$ as a function of axial location and (b) the critical Reynolds numbers calculated from Eq. 6.9 with experimental data for upward and downward flow at different heat fluxes. 100

Fig. 6.10: Comparison of (a) Re_{qt}/Pr^3 as a function of axial location and (b) the Reynolds numbers at which the transitional flow regime ended calculated from Eq. 6.10 with experimental data in the upward and downward flow directions at different heat fluxes. 101

Fig. 6.11: Comparison of the fully developed friction factors as a function of Reynolds number at different heat fluxes for vertical upward and downward flow. The heat flux of 0 kW/m^2 was for isothermal flow. 102

Fig. 7.1: Comparison of isothermal friction factors as a function of Reynolds number using the original and empty flow-calming sections with a square-edged inlet and contraction ratios, CR , of (a) 11 and (b) 33, and also with a re-entrant inlet for contraction ratios of (c) 11 and (d) 33. ... 105

Fig. 7.2: Comparison of the fully developed Colburn j -factors as a function of Reynolds number for the original and empty flow-calming sections at a heat flux of 8 kW/m^2 for (a) square-edged with a contraction ratio of 11, (b) square-edged with a contraction ratio of 33, (c) re-entrant with a contraction ratio of 11 and a (d) re-entrant with a contraction ratio of 33. 107

Fig. 7.3: Comparison of isothermal friction factors for (a) a square-edged and (b) a re-entrant inlet, as well as diabatic friction factors at a heat flux of 8 kW/m^2 for (c) a square-edged and (d) a re-entrant inlet, as a function of Reynolds number. 109

Fig. 7.4: Comparison of the fully developed Colburn j -factors as a function of Reynolds number for different contraction ratios using (a) square-edged inlet and (b) re-entrant inlet at a heat flux of 8 kW/m^2 111

Fig. 7.5: Comparison of the Reynolds numbers at which the transitional flow regime started (Re_{cr}) and ended (Re_{qt}) as a function of contraction ratio for the different inlet geometries at a heat flux of 8 kW/m^2 . “FD” in the legend indicates hydrodynamic fully developed inlet. 112

Fig. 7.6: Comparison of the Reynolds number at which the transitional flow regime (a) started and (b) ended, as well as the difference between the square-edged and re-entrant inlets at the (c) start

($\Delta Re_{inlets} = Re_{squ} - Re_{ree}$) and (d) end ($\Delta Re_{inlets} = Re_{squ} - Re_{ree}$) of the transitional flow regime, as a function of heat flux..... 113

Fig. 7.7: Schematic representation of the influence of contraction ratio on the fully developed Colburn j -factor as a function of Reynolds number for a square-edged (blue) and a re-entrant (green) inlet..... 114

Fig. 7.8: Schematic diagram of the fluid flow pattern for a square-edged inlet with different contraction ratios..... 115

Fig. 7.9: Schematic diagram of the fluid flow pattern for a re-entrant inlet with different contraction ratios..... 115

List of tables

Table 3.1: Ranges and accuracies of the instrumentation used.	39
Table 3.2: Experimental test matrix for the different inclination angles.	47
Table 3.3: Experimental test matrix for the different flow-calming sections, contraction ratios and inlet types at horizontal orientation. Red indicates heating of the test section while blue identifies part of the flow-calming section without heating	48

Nomenclature

A	Arbitrary point in Fig. 6.2	
A	Area	m^2
B	Arbitrary point in Fig. 6.2	
b	Bulk	
C	Coefficient	
C_f	Fanning friction factor	
C_p	Specific heat at constant pressure	$J/kg.K$
D	Diameter	m
eb	Energy balance error	
F	Force	
f	Friction factor/function	
g	Gravitational acceleration	m/s^2
Gr	Grashof number	
Gr^*	Modified Grashof number	
Gr_θ	Inclined tube Grashof number	
Gr_θ^*	Inclined tube modified Grashof number	
Gz	Graetz number	
h	Heat transfer coefficient	$W/m^2.^\circ C$
I	Current	A
i	Data point index	
j	Colburn j -factor	
k	Thermal conductivity	$W/m.K$
L	Length	m
L_h	Hydrodynamic entrance length	m
L_t	Thermal entrance length	m
\dot{m}	Mass flow rate	kg/s
n	Constant	
Nu	Nusselt number	
P	Pressure	Pa
Pr	Prandtl number	
PT	Pressure tap	
P_w	Tube wall parameter	
\dot{Q}	Heat transfer rate	W
\dot{q}	Heat flux	W/m^2
r	Radius	m
R	Thermal resistance	$^\circ C/W$

Ra	Rayleigh number	
Ra_{θ}	Inclined tube Rayleigh number	
Ra_{θ}^*	Inclined tube modified Rayleigh number	
Re	Reynolds number	
Ri	Richardson number	
T	Temperature	°C or K
T	Thermocouples	
t	Tube thickness	m
TG	Transition gradient	
u	Velocity in axial direction	m/s
V	Velocity	m/s
V	Voltage	V
W	Width	m
x	Distance from tube inlet	m

Greek letters

α	Thermal diffusivity	m/s
θ	Inclination angle	°
β	Coefficient of thermal expansion	1/K
μ	Dynamic viscosity	kg/m.s
ν	Kinematic viscosity	m ² /s
ρ	Density	kg/m ³
τ	Shear stress	N/m ²

Superscripts

n	Constant
-----	----------

Subscripts

avg	Average
b	Bulk/bottom
cor	Correlation
cp	Constant property
cr	Critical
e	Exit
exp	Experiment
f	Fluid/friction factor
$grav$	Gravity
i	Inlet/inner/data point index

<i>iw</i>	Inner wall
<i>j</i>	Colburn <i>j</i> -factor
<i>m</i>	Mean
<i>Nu</i>	Nusselt number
<i>o</i>	Outer
<i>offset</i>	Offset at no flow conditions
<i>ow</i>	Outer wall
ΔP	Pressure drop
<i>qt</i>	Quasi-turbulent
<i>ree</i>	Re-entrant
<i>squ</i>	Square-edged
<i>t</i>	top
<i>T</i>	Turbulent
<i>vp</i>	Variable property
<i>w</i>	Wall

Abbreviations (also used as Italic subscripts)

CFD	Computational Fluid Dynamics
DAQ	Data Acquisition System
DC	Direct Current
FC	Forced Convection
FCD/MCD	Boundary between FCD and MCD regions
FCD	Forced Convection Developing
FD	Fully Developed
MC	Mixed Convection
MCD	Mixed Convection Developing
MCD/FD	Boundary between MCD and FD regions
QT	Quasi-turbulent

1. Introduction

1.1. Background

Thermal and cooling systems optimizations have been receiving great attention in industries. One of the most important components in thermal and cooling systems is the heat exchanger, which is used to transfer heat from one system to another depending on the application. A typical example of a thermal system is the boiler where heat is transferred to the working fluid, such as steam to drive different systems in the industries. On the other hand, a chiller unit is another example of a cooling system use to remove heat from a fluid to the environment. Hence, the design and optimization of an efficient heat exchanger is of paramount importance to the energy industries. The choice of heat exchangers operating conditions such as configuration/orientation, type of flow, flow regimes and inlet type/geometry are crucial to achieving high efficiency at low running cost. As most heat exchangers are designed to operate at horizontal or vertical orientations, inclined tube heat exchangers are sometimes used because of their wide range of applications [1-8], such as in air-conditioning and refrigeration systems, solar energy collectors, electronic cooling equipment, automotive vehicles to aeroplanes in the transport industry, and power generation plants operated by fossil fuels, nuclear fuel or concentrated solar power.

Depending on the application, most heat exchangers operates either in the laminar or turbulent flow regimes, and can sometimes be forced to operate in the transitional flow regime (in-between the laminar and turbulent regions) due to design constraints, system upgrades, fouling or even changes in operating conditions that lead to lower mass flow rates. However, for laminar convective flow through a tube, the flow can be either forced convection or mixed convection. With mixed convection, the density differences in the radial direction lead to buoyancy effects in the fluid. To be able to distinguish between forced convection and mixed convection is very important, because the Nusselt numbers of the different conditions vary significantly. Everts and Meyer [9] developed flow regime maps that can be used to determine whether forced or mixed convection conditions exist in horizontal tubes with a constant heat flux boundary condition. For vertical flow, Metais and Eckert [10] developed a flow regime map for both constant heat flux and constant surface temperature boundary conditions.

For forced convection heat transfer in circular tubes, most heat transfer textbooks [11-16] reported that for a constant heat flux boundary condition, the fully developed laminar Nusselt number is constant at 4.36, and independent of Reynolds number or Prandtl number. This Nusselt number of 4.36 was derived analytically, assuming constant fluid properties (density, viscosity, thermal conductivity and specific heat). In actual practice, the fluid properties change with temperature along the tube length or due to changes in mass flow rates and/or heating.

Metais and Eckert [10] considered the flow as forced convection when the Nusselt numbers were within 10% of 4.36. Hallman [17] obtained a Nusselt number of 4.62 at a low Rayleigh number of approximately 25 for vertical upward flow in circular tube. Meyer and Everts [18] recently obtained forced convection conditions with an average laminar Nusselt number of approximately 4.75 at a low heat flux of about 1 kW/m^2 and a Reynolds number of 941. In general, it was concluded that it is very challenging to experimentally obtain forced convection heat transfer with Nusselt number of 4.36, especially at higher heat fluxes and higher Reynolds numbers in the laminar flow regime, as well as the entire transitional flow regime [18]. However, Sudo *et al.* [19] performed forced convection experiments in vertical narrow rectangular channels and found that the effect of buoyancy was negligible on the flow direction (upward and downward flow) for Reynolds number higher than 700.

In vertical tubes, the buoyancy forces (free convection) acts either in the same direction (*assisting flow*) as the inertia forces or in the opposite direction to the inertia forces (*opposing flow*) [11]. In horizontal tubes, textbook laminar forced convection conditions that will ensure a Nusselt number of 4.36 for a constant heat flux, almost never occur as has been shown by Meyer and Everts [18]. It only happens when the heat fluxes are very small, and/or the tube diameters are small, and/or the fluid viscosities are high. Normally the Nusselt numbers in horizontal tubes heated at a constant heat flux are much higher than 4.36 [18, 20, 21]. The reason is that the buoyancy forces act in a perpendicular (radial) direction to the inertia forces, producing secondary flow that significantly enhances the heat transfer, especially in the laminar flow regime.

However, in inclined tubes a combination of the heat transfer and fluid flow characteristics of horizontal and vertical tubes exist. Thus, to fundamentally understand the differences between the flow in horizontal and vertical tubes (in both upward and downward directions) it is important to investigate it in the different flow regimes at different inclination angles, from vertical downward to vertical upward. Inclination buoyancy leads to mixed convection heat transfer, caused by the fluid density differences due to the temperature gradients between the fluid near the heated wall and the cooler fluid near the centreline. This results in increased heat transfer coefficients compared to forced convection heat transfer coefficients. Iqbal and Stachiewicz [22] performed one of the early investigations on mixed convection heat transfer in inclined tubes. It was observed that an increase in inclination angle led to an increase in the fully developed laminar heat transfer coefficients.

Most mixed convection heat transfer analyses for inclined tubes in literature [23-31] showed that inclination buoyancy has a significant effect on the laminar heat transfer, depending on the flow direction. In general, the laminar Nusselt numbers decreased with increase in inclination angle for upward flow. This is because the components of the gravitational (buoyancy) forces changed in the axial and circumferential direction, causing a change in Grashof numbers and thus mixed convection heat transfer. As expected, it was also found that the heat transfer increased with increasing heat flux for all inclination angles, due to the increase in the Grashof number.

To account for inclination angle effects, Vliet [32] and Fuji and Imura [33] replaced the gravitational acceleration, g , in the buoyancy force term of the Grashof number, with the buoyancy force component parallel to the vertical surface. Rani *et al.* [34] developed a unified correlation for predicting natural convection heat transfer in inclined tubes. A modified Grashof number in terms of the modified characteristic length, which is a function of inclination angle, diameter and length, was used instead of the diameter or length only. However, their modified Grashof number correlation did not account for the components of the buoyancy force normal and parallel to the axis of the fluid flow. Furthermore, the aforementioned studies focused on the effect of inclination buoyancy in the laminar flow regime only, without extending the focus to the transitional flow regime.

Good progress has been made in recent years on the experimental analysis of heat transfer and pressure drop in the transitional flow regime of smooth horizontal tubes with a constant heat flux boundary condition [9, 21, 35-44]. These works focused on the influence of heating, mixed convection and inlet geometries/configurations on heat transfer and pressure drop of developing and fully developed flow in smooth horizontal tubes. Others [45-51] investigated transitional flow in horizontal tubes with a constant wall temperature boundary condition for both cooling and heating conditions. However, no work has been conducted that concentrates specifically on the transitional flow regime in inclined tubes.

Ghajar and his co-workers were the pioneers of the work on the effect of inlet disturbances on the heat transfer and pressure drop characteristics in the transitional flow regime of smooth horizontal tubes. Three different inlet configurations were investigated namely: square-edged, re-entrant and bell-mouth. To ensure a uniform upstream flow to the different inlet geometries, a flow-calming section was attached prior to the inlet section. Some of these works can be found in [35, 37-39, 52-56] and summarized in the text book of Cengel and Ghajar [11]. The experiments were conducted at different constant heat fluxes. In general, the heat transfer and pressure drop characteristics, as well as the boundaries of the transitional flow regime, were significantly affected by the inlet geometries.

Meyer and his co-workers were the second group of researchers that worked on the characteristic behaviour of heat transfer and pressure drop in the transitional flow regime of smooth and enhanced tubes, focussing on inlet geometry effects [41, 42, 48, 50], buoyancy effects [18, 21, 57], inclination angles [57], enhancement with twisted tape inserts [41, 58, 59] and annular flow [47, 49]. These analyses involved both cooling and heating conditions under constant wall temperature and constant heat flux boundary conditions, mostly with flow-calming sections and different inlet contraction ratios

Flow-calming sections are mostly used in convection heat transfer experiments, especially involving the transitional flow regime, to minimize the effect of inlet disturbances on the heat transfer and pressure drop characteristics in the different flow regimes. Furthermore, flow-calming

sections also replicate the heat exchanger inlet header and/or plenums. Different flow-calming section contents have been used in the literature and their effects on the transitional flow regime with different inlet geometries have not yet received attention. Furthermore, these flow-calming sections had different contraction ratios to the test section, similar to the different heat exchanger inlet header/plenum sizes found in many practical applications. Different flow-calming section diameters with a constant test section diameter would lead to different inlet disturbances, especially with square-edged and re-entrant inlets.

1.2. Problem statement

Under normal circumstances, fully developed forced convection conditions in the laminar and transitional flow regimes with a constant heat flux boundary condition are challenging to obtain experimentally. Although it is possible to obtain it in zero gravity conditions, small diameter tubes and by using small heat fluxes, the uncertainties are usually high due to the small temperature differences between the wall and fluid. However, it is vital for our fundamental understanding of internal forced convection heat transfer that accurate experimental results with low uncertainties are available in literature. Furthermore, how the Reynolds number boundaries of the transitional flow regime behave for pure forced convection conditions without the influence buoyancy is not known.

Laminar mixed convection Nusselt number correlations as a function of Rayleigh number (or Grashof number) have been developed for upward flow at different inclination angles of 0° , 30° , 45° , 60° and 90° . However, up to now, there is no single laminar Nusselt number and friction factor correlation that exist for both upward and downward flow at all inclination angles. There is little or no sufficient information available in literature on the method of quantifying the effect of buoyancy/mixed convection/Grashof number on the heat transfer and pressure drop characteristics in the transitional flow regime of inclined tubes.

Correlations to predict the Reynolds number boundaries of the transitional flow regime as well as the heat transfer coefficients and friction factors in the transitional flow regime during mixed convection conditions are available in the literature. Although most of these correlations distinguish between the different inlet geometries, they do not account for the different contraction ratios. This can change the characteristic behaviour of the entire transitional flow regime and led to inaccurate predictions.

1.3. Aim

The purpose of this study was to experimentally investigate the effect of tube inclination, heating and inlet contraction ratios on the single-phase heat transfer and pressure drop characteristics of the laminar and transitional flow regimes for pure forced and mixed convection conditions.

1.4. Objectives

The main objectives of this study were:

- i. to design, construct and commission an experimental set-up that can determine the heat transfer coefficients and friction factors from the experimental measurements. The flow regime should be in the laminar, transitional and turbulent flow regimes at different inclination angles and different heat fluxes. The experimental set-up must be able to accommodate a smooth circular tube with different types of inlets and flow-calming section of different diameters.
- ii. to verify that the experimental set-up produces accurate results by conducting measurements in the laminar and turbulent flow regimes with the test section tube in horizontal and vertical orientations during forced and mixed convection conditions and comparing the results with literature.
- iii. to determine the effect of different inclination angles and flow directions on the heat transfer coefficients and friction factors in the laminar and transitional flow regime of a smooth circular tube with square-edged inlet.
- iv. to distinguish in Objective (iii), between the heat transfer in the fully developed and developing flow.
- v. to investigate the effect of other heat fluxes on Objective (iii).
- vi. to develop empirical equations with which Objectives (iii) – (vi) can be quantified.
- vii. to experimentally determine the Nusselt numbers and friction factors for fully developed forced convection conditions, not only in the laminar flow regime, but also in the transitional flow regime.
- viii. to develop correlations to predict the boundaries of the transitional flow regime for pure forced convection condition at different rate of heating.
- ix. to investigate the effect of flow-calming section contents and inlet contraction ratios together with different inlet geometries (square-edged and re-entrant) on the heat transfer and pressure drop characteristics in the transitional flow regime.
- x. to compare the transitional flow heat transfer and pressure drop with a contraction ratio of one using a hydrodynamical fully developed and 90° bend inlets and also compare them with Objective (ix).

These objectives were met using the results of physical measurements of temperatures, pressure drops and mass flow rates in a tube whose orientation and inclination angles could be changed.

1.5. Scope of work

The scope of this research covers the characteristic behaviour of single-phase heat transfer and pressure drop within a smooth inclined circular tube in the laminar and transitional flow regimes. Forced and mixed convection heat transfer in the laminar and transitional flow regimes were investigated. Influence of inlet disturbances on the transitional flow regime was also investigated.

using different inlet contraction ratios and different inlet geometries. It considers the developing and fully developed flows using water as working fluid with a Prandtl numbers of approximately 3 to 8.1. The test section was a smooth circular copper tube with internal diameter of 5.1 mm and a length of 4.6 m. It was rotated at different inclination angle increments from vertically downward (-90°) to vertically upward ($+90^\circ$) flows. The Reynolds numbers range considered was from 400 to 6 000 covering the laminar, transitional and turbulent flow regimes. Constant wall heat flux boundary condition was used by applying different heat fluxes from 1 to 8 kW/m² to the test section.

Square-edged and re-entrant inlets with flow-calming sections of different diameters to achieve different inlet contraction ratios from 1 to 33 were used. Furthermore, a fully developed and 90° bend inlets were used for comparison purposes. The tube wall temperatures were measured at 21 stations along the tube length from inlet to outlet covering the developing and fully developed parts of the test section. Pressure drop measurements were taken in the fully developed part of the test section over a wide range of mass flow rates. A new experimental set-up was design and built purposely to achieve these requirements with a test bench that allows for different inclination angle of the test section and accommodate different flow-calming sections and different inlet geometries.

1.6. Original outcomes

The work in this thesis was published in three articles and the original contributions of these articles with relevant chapters were as follows:

Chapter 5, Meyer *et al.* [57]

- i. buoyancy effects were negligible for vertical upward and downward flows for Reynolds numbers higher than 1 000;
- ii. inclined tube Grashof/Rayleigh numbers were defined to account for the effect of inclination buoyancy on the heat transfer and pressure drop;
- iii. correlations to predict the fully developed average laminar Nusselt number and friction factor for inclined tubes;
- iv. influence of tube inclination angle on the boundaries of transitional flow regime;
- v. transition gradients increase with inclination angle.

Chapter 6, Bashir *et al.* [60]

- i. fully developed laminar forced convection Nusselt numbers were not constant at 4.36, for a constant heat flux boundary condition, but were a function of Reynolds number and independent of Grashof number;
- ii. forced convection was independent of flow direction for Reynolds numbers higher than 600;
- iii. correlations to predict fully developed laminar forced convection Nusselt number for a constant heat flux boundary condition;

- iv. transition occurred at the same mass flow rate and the transitional flow Reynolds numbers increased with heating for forced convection condition;
- v. width of the transitional flow regime in the fully developed region remained constant for all heat fluxes and for forced convection conditions.

Chapter 7, Bashir *et al.* [43]

- i. influence of flow-calming section contents on the transitional flow regime;
- ii. comparison between square-edged, re-entrant, hydrodynamically fully developed and 90° inlets;
- iii. inlet contraction ratios affect the boundaries of the transitional flow regime with square-edged and re-entrant inlets;
- iv. relationship between inlet contraction ratios and heat flux.

1.7. Layout of thesis

The overall thesis consists of eight chapters; Chapter 2 focuses on the fundamentals and literature study on forced and mixed convection heat transfer and pressure drop in the laminar and transitional flow regimes of horizontal, inclined and vertical tubes with different inlet disturbances. Chapter 3 explains the complete experimental set-up and procedure, data reduction method and the results of uncertainty analysis. Chapter 4 discusses the validation of results of the experimental set-up in Chapter 3. Chapter 5 focuses on the mixed convection heat transfer and pressure drop in the laminar and transitional flow regime at different inclination angles. Chapter 6 covers the forced convection heat transfer and pressure drop in the laminar and transitional flow regime with different heat fluxes at vertical inclination of the test section. Chapter 7 investigates the effect of flow-calming section contents and inlet contraction ratios on the transitional flow regime using different inlet geometries, which include the square-edged, re-entrant, hydrodynamically fully developed and 90° bend inlets. Chapter 8 concludes the thesis with some suggested recommendations for further works.

2. Literature review

2.1. Introduction

The state-of-the-art literature on the heat transfer and pressure drop in the laminar and transitional flow regimes is discussed in this chapter with a view to identifying the gaps in the literature. The chapter starts off with a brief introduction on the fundamental concepts and correlations associated with the conventional convective heat transfer and pressure drop in horizontal, inclined, and vertical tubes for the different flow regimes. Developing and fully developed flows for pure forced and mixed convection conditions are briefly discussed. Transitional flow work of Professor Afshin Ghajar and that of Professor Josua Meyer are briefly discussed with emphasis on the inlet and buoyancy effects on the transitional flow regime.

2.2. Dimensionless parameters

For the purpose of analysis and understanding convection heat transfer and internal flow fluid friction within a smooth circular tube, the following non-dimensional parameters are used in describing these characteristics.

2.2.1. Reynolds number

This is the ratio of inertia forces to viscous forces. It is the flow modulus represented as a function of mean fluid velocity, hydraulic diameter of the tube, and kinematic viscosity of the fluid defined as $\nu = \mu/\rho$. It was developed by Osborn Reynolds [61] and was used to differentiate the flow regimes from laminar to turbulent flow regimes. Hence, the Reynolds number for a circular tube is given as [62]:

$$Re = \frac{uD_i}{\nu} \quad 2.1$$

For low Reynolds numbers, the viscous forces are much higher than the inertia forces and therefore suppress the random fluctuations caused by the inertia forces. This type of flow is termed as laminar flow. Furthermore, for high Reynolds numbers, the inertia forces are much higher than the viscous forces and are therefore large enough to cause fluctuations in the fluid. This type of flow is termed as turbulent flow and the flow between the laminar and turbulent flow is known as the transitional flow.

2.2.2. Prandtl number

This is the ratio of momentum diffusivity to thermal diffusivity of the fluid. It gives the fluid property modulus in relation to velocity boundary layers and thermal boundary layers. Thus, the Prandtl number is defined as [14]:

$$Pr = \frac{\nu}{\alpha} = \frac{\mu c_p}{k} \quad 2.2$$

For water, the Prandtl numbers typically ranged between 3 to 8.

2.2.3. Graetz number

This is used to differentiate between the thermally developing flow and fully developed flow in the laminar flow regime and is represented as a function of Reynolds number, Prandtl number and distance from the tube inlet as [11]:

$$Gz = RePr \frac{D_i}{x} \quad 2.3$$

2.2.4. Nusselt number

For a fluid in motion, the heat transfer through the fluid is by convection while for motionless fluid, the heat transfer is by conduction. Thus, the Nusselt number describes the heat transfer enhancements due to the fluid motion (convection effects) and it is the ratio of convective conductance to the molecular thermal conductance [63]. For a circular tube, the Nusselt number is represented in terms of convective heat transfer coefficient, thermal conductivity and the hydraulic diameter of the tube as [14]:

$$Nu = \frac{hD_i}{k} \quad 2.4$$

2.2.5. Colburn j -factor

The Colburn j -factor expresses the heat transfer coefficients while taking into account the variation of fluid Prandtl numbers within the fluid flow and is given as [12]:

$$j = \frac{Nu}{Re Pr^{1/3}} \quad 2.5$$

2.2.6. Grashof number

This is the ratio of buoyancy forces to viscous forces. It is used to describe the natural convection effects on the heat transfer and is given as [13]:

$$Gr = \frac{g\beta(T_w - T_b)D_i^3}{\nu^2} \quad 2.6$$

When using a constant heat flux boundary condition, a modified Grashof number can be used because the temperature differences used to determine the Grashof numbers are not normally known while the heat flux is. The modified Grashof number in terms of heat flux is defined as the product of the Nusselt number and the Grashof number:

$$Gr^* = GrNu = \frac{g\beta\dot{q}D_i^4}{\nu^2k} \quad 2.7$$

2.2.7. Rayleigh number

This is used to quantify the effect of buoyancy, especially in vertical and inclined tubes with assisting or opposing flow heat transfer. The Rayleigh number is used to determine whether the heat transfer is dominated by forced or mixed convection. It is the product of Grashof number and Prandtl number [13]:

$$Ra = GrPr \quad 2.8$$

and the modified Rayleigh number in terms of heat flux is given as:

$$Ra^* = Gr^*Pr \quad 2.9$$

2.2.8. Richardson number

This is the ratio of buoyancy forces to viscous forces. It is used to predict the relative magnitude of buoyancy effects in relation to forced convection effects [64]:

$$Ri = \frac{Gr}{Re^2} \quad 2.10$$

The Richardson number was derived based on boundary layer correlations over a heated flat plate for vertical upward flow. When $Ri \ll 1$, forced convection dominates the flow and when $Ri \gg 1$,

the flow can be dominated by natural convection. For $Ri \approx 1$, the flow is expected to be mixed convection where both natural and forced convection effects are significant [64].

2.2.9. Fanning and Darcy friction factors

The Fanning friction factor is the ratio of the wall friction force (wall shear stress) to the inertial force [63] and is given as:

$$C_f = \frac{2\tau_w}{\rho u^2} \quad 2.11$$

The friction factor can also be represented in terms of the Darcy friction factor, f , which is four times the Fanning friction factor ($f = 4C_f$). The Darcy friction factor is used throughout this analysis. Hence, the Darcy friction factor is related to the pressure drop which is directly related to the pumping power requirements of the system and is defined as [11]:

$$f = \frac{2\Delta PD}{L\rho u^2} \quad 2.12$$

2.3. Transitional flow nomenclature

As the focus of this work is mainly on the transitional flow regime, some nomenclatures used to describe the general characteristics of the entire transitional flow regime, as developed by Ghajar and Tam [38] and Everts and Meyer [21], are briefly discussed in this section. These nomenclatures and correlations are used to differentiate the flow regimes as well as for comparison purposes in this study.

Furthermore, Everts and Meyer [21] recently divided the transitional flow regime into two flow regimes namely; transitional flow regime and quasi-turbulent flow regime (previously known as the low-Reynolds-number-end regime), making a total of four flow regimes for flow in tubes from low to high Reynolds numbers. Fig. 2.1 shows a schematic representation of these flow regimes and the nomenclatures used to describe and differentiate them.

2.3.1. Start of the transitional flow regime, Re_{cr}

The start of the transitional flow regime is the Reynolds number at which the laminar flow regime ended and corresponds to the first abrupt change of the heat transfer coefficients and friction factors from the laminar flow regime [20, 35]. As shown in Fig. 2.1, the Reynolds number at the start of the transitional flow regime, Re_{cr} , was defined as [21]:

$$Re = Re_{cr} \text{ when: } \left(\frac{dj}{dRe} \right)_{i-2:i} = 0 \quad 2.13$$

where $i-2:i$ means that any given point i , dj/dRe was determined from the three data points at $Re(i-2)$, $Re(i-1)$ and $Re(i)$ for increasing Reynolds numbers.

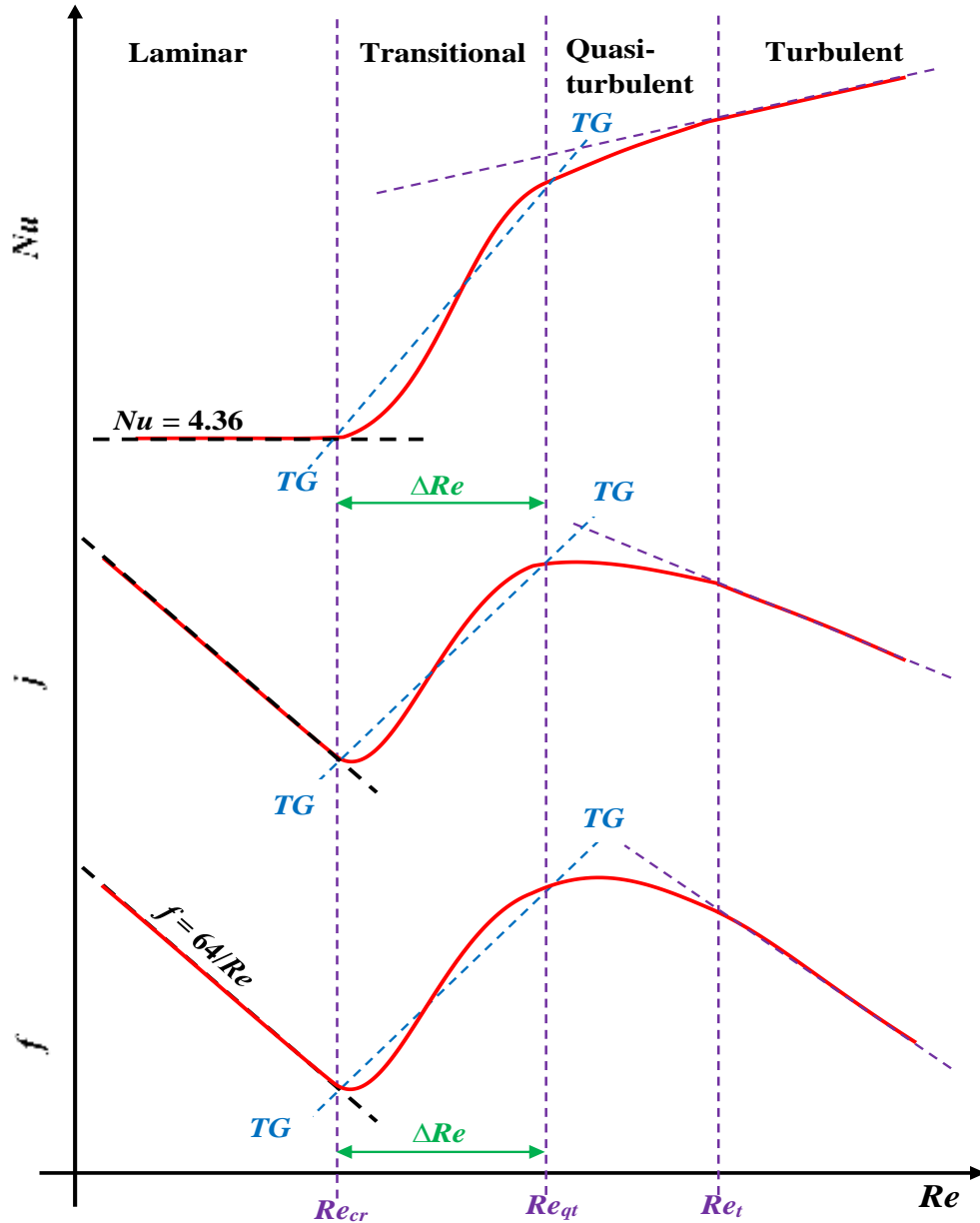


Fig. 2.1: Schematic representation of the different flow regimes in terms of the Nusselt number, Colburn j -factor, and friction factor as a function of Reynolds number. Adapted from Everts [65] and Everts and Meyer [21, 40].

2.3.2. Start of the quasi-turbulent flow regime, Re_{qt}

The start of the quasi-turbulent flow regime is the Reynolds number at which the transitional flow regime ended, Re_{qt} , and was defined as [21]:

$$Re = Re_{qt} \text{ when: } \left(\frac{d^2 Nu}{dRe^2} \right)_{i:i+2} \geq -0.00015 \quad 2.14$$

where $i:i+2$ means that at any given point i , the dNu/dRe was determined from the three data points at $Re(i)$, $Re(i+1)$ and $Re(i+2)$ for increasing Reynolds numbers (while Eq. 2.13 used the results at the previous two Reynolds numbers).

2.3.3. Width of the transitional flow regime, ΔRe

The width of the transitional flow regime, ΔRe , was defined by Everts and Meyer [21] as the difference between the Reynolds numbers at the start and end of the transitional flow regime:

$$\Delta Re = Re_{qt} - Re_{cr} \quad 2.15$$

The width of the transitional flow regime gives a good indication of the Reynolds number range of the entire transitional flow regime.

2.3.4. Transition gradient, TG

The transition gradients represent a trend of how the heat transfer coefficients and friction factors change in the transitional flow regime. The transition gradient of the Colburn j -factors, TG_j , represented by the diagonal dashed blue line from Re_{cr} to Re_{qt} in Fig. 2.1 was defined as:

$$TG_j = \frac{j_{qt} - j_{cr}}{Re_{qt} - Re_{cr}} \quad 2.16$$

where j_{cr} and j_{qt} were the Colburn j -factors at the start and end of the transitional flow regime, respectively. Furthermore, the transition gradient of the Nusselt numbers, TG_{Nu} , and that of the friction factors, TG_f , as shown in Fig. 2.1 were defined as:

$$TG_{Nu} = \frac{Nu_{qt} - Nu_{cr}}{Re_{qt} - Re_{cr}} \quad 2.17$$

$$TG_f = \frac{f_{qt} - f_{cr}}{Re_{qt} - Re_{cr}} \quad 2.18$$

2.3.5. Start of the turbulent flow regime, Re_t

The start of the turbulent flow regime is the Reynolds numbers at which the quasi-turbulent flow regime ended and where the heat transfer coefficients and friction factors first reached the well-known fully turbulent flow correlations [35]. Everts and Meyer [21] defined the start of the turbulent flow regime, Re_t , as:

$$Re = Re_t \text{ when: } \left(\frac{dNu}{dRe}\right)_{QT} = \left(\frac{dNu}{dRe}\right)_T \quad 2.19$$

where

$$\left(\frac{dNu}{dRe}\right)_{QT} = 0.7054Re^{-0.534} \quad 2.20$$

$$\left(\frac{dNu}{dRe}\right)_T = 0.0352Re^{-0.2} \quad 2.21$$

2.4. Developing and fully developed flows in tubes

For fluid flow through a circular tube with uniform temperatures, the velocity boundary layer develops along the tube length from the inlet, due to friction between the fluid layer in contact and the tube wall. This boundary layer grows in the flow direction up to a point where the thickness of the boundary layer is equal to the radius of the tube and thus, the boundary layers meet at the center-line of the tube. The region from the tube inlet to where the velocity boundary layers meet is known as the hydrodynamic entrance region, and the flow in that region is known as hydrodynamically developing flow [11]. Furthermore, the region beyond the hydrodynamic entrance region is known as the hydrodynamically fully developed region. The mean velocity profile in the fully developed region for laminar flow, defined in Eq. 2.22, is parabolic and remains constant along the tube length (for constant fluid properties), as shown with green colour in Fig. 2.2. The maximum velocity occurs the center-line and the minimum velocity occurs at the tube wall. In the turbulent flow regime (not shown), the velocity profile is somewhat blunt [11].

$$u(r) = 2u_m \left(1 - \frac{r^2}{(D/2)^2} \right)$$

2.22

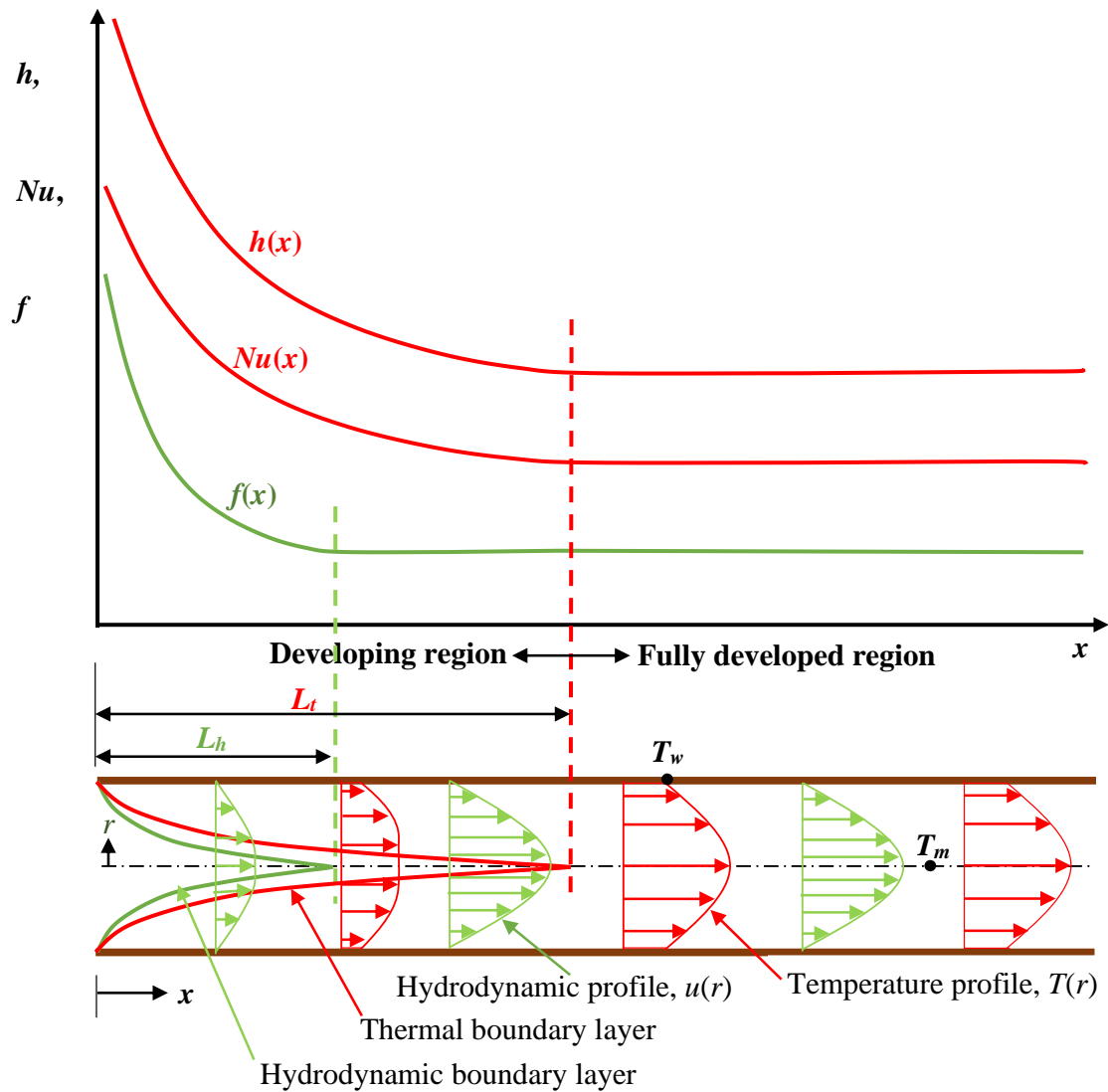


Fig. 2.2: Schematic representation of the heat transfer coefficients, friction factors, velocity and temperature profiles for laminar flow in tubes [11].

The friction factor is a function of wall shear stress, which is related to the slope of the velocity profile. Thus, as the velocity profile remains constant in the hydrodynamically fully developed region, the friction factor also remains constant (solid green line in Fig. 2.2).

However, when a fluid with a uniform temperature flows through a circular tube with different wall temperature, such as a tube heated with a constant heat flux, the fluid adjacent to the wall will assume the wall temperature. This will generate a temperature difference across the tube cross-section between the fluid near the center-line of the tube and the fluid near the tube wall and thus the development of the thermal boundary layer (red lines in Fig. 2.2). Again, the thickness of the thermal boundary layer increases in the flow direction from the tube inlet until they meet at the center of the tube, and this region is known as thermal entrance region. The region beyond the thermal entrance region is known as the thermally fully developed region. When the flow is both hydrodynamically fully developed and thermally fully developed, then the flow is said to be fully developed [11].

The lengths from the tube inlet to the points where the flow becomes hydrodynamically fully developed and thermally fully developed are known as the hydrodynamic entrance length, L_h , and thermal entrance length, L_t . For laminar flow;

$$L_h = 0.05ReD_i \quad 2.23$$

$$L_t = 0.05RePrD_i \quad 2.24$$

Recently, Meyer and Everts [18] found that the thermal entrance length, L_t , for forced convection simultaneously hydrodynamically and thermally developing flow is much longer than $L_t = 0.05RePrD_i$ and therefore proposed $L_t = 0.12RePrD_i$ as more appropriate. For turbulent flow, both the hydrodynamic entrance length and thermal entrance length are approximately taken as 10 diameters ($10D_i$).

In the thermally fully developed region, the dimensionless temperature profile $(T_w - T)/(T_w - T_m)$ remains unchanged and is independent of x , thus the derivative of $(T_w - T)/(T_w - T_m)$ with respect to r must also be independent of x [11]. Mathematically;

$$\frac{\partial}{\partial r} \left(\frac{T_w - T}{T_w - T_m} \right) \Big|_{r=D_i/2} = \frac{-(\partial T / \partial r)|_{r=D_i/2}}{T_w - T_m} \neq f(x) \quad 2.25$$

For a constant heat flux boundary condition, the heat flux to the tube wall can be defined as [11]:

$$\dot{q} = h(x)(T_w - T_m) = k \frac{\partial T}{\partial r} \Big|_{r=D_i/2} \rightarrow h(x) = \frac{k(\partial T / \partial r)|_{r=D_i/2}}{T_w - T_m} \quad 2.26$$

Eq. 2.25 confirmed that for constant properties, the local heat transfer coefficient in Eq. 2.26 remains unchanged and is independent of x in the fully developed region. Hence, both the local heat transfer coefficients and friction factors remain constant in the fully developed region as shown in Fig. 2.2. Although the dimensionless temperature profile remains constant in the thermally fully developed region, the temperature profile may vary along the tube length, as expected, when the heat flux to the tube wall remains constant. This is unlike the velocity profile, which is constant along the tube length for a constant fluid property.

From Eq. 2.26, it follows that for a constant heat flux boundary condition, the thermal conductivity increases due to the increase in fluid temperatures along the tube length and therefore causes the local heat transfer coefficient to increase in the flow direction, assuming that $(T_w - T_m)$ remains constant in the fully developed region. However, to account for the changes in thermal conductivity along the tube length, the local heat transfer coefficient is expressed in terms of the Nusselt number as:

$$Nu = \frac{hD_i}{k} = \frac{D_i(\partial T / \partial r)|_{r=D_i/2}}{T_w - T_m} \quad 2.27$$

Since the tube radius is constant and $(T_w - T_m)$ along the tube length is constant in the fully developed region, the Nusselt number in Eq. 2.27 is constant along the tube length (Fig. 2.2). However, it will be shown (Chapter 6) that for forced convection with a constant heat flux boundary condition, the temperature profile varies along the tube length due to variable fluid properties and thus caused the Nusselt numbers to vary for $Re > 1\,000$.

2.5. Forced convection heat transfer

Internal forced convection occurs when the fluid is forced to flow through a duct or tube by an external means such as pump or fan [11]. For pure forced convection heat transfer, the fluid velocity is expected to suppress the buoyancy effects that can cause mixed convection within the fluid flow. For fluid flow in tubes, the flow can either be laminar, transitional, quasi-turbulent or turbulent flow.

2.5.1. Laminar flow

Laminar flow can either be developing or fully developed flow along the tube length. For fully developed laminar flow, the fluid particles move in a straight line with a constant axial velocity and the velocity profile in the tube (indicated by green curves in Fig. 2.2) remains constant along the tube length. For developing flow, the local laminar Nusselt numbers decrease along the tube length due to the increasing thermal boundary layer (entrance effect) until the Nusselt numbers became constant (fully developed flow) as shown in Fig. 2.2. The laminar forced convection heat transfer characteristics depend on the thermal conditions on the tube wall. For a constant wall

temperature boundary condition, the theoretical laminar Nusselt number is constant at 3.66, while for a constant heat flux boundary condition, the Nusselt number is constant at 4.36, and are both independent of Reynolds number, Prandtl number and axial location. The local peripheral wall temperatures during forced convection are expected to be uniform and the fluid temperature decrease toward the center of the tube due to convection heat transfer. Thus, the temperature profile in the tube (indicated by red curves in Fig. 2.2) remains constant along the tube length for constant fluid properties. This study contradicts (by making use of experimental measurements) the classical heat transfer theory for forced convection conditions in a circular tube for laminar fully developed flow with a constant heat flux boundary condition, that the Nusselt number is 4.36 for all Reynolds numbers and Prandtl numbers. It will be shown that this is correct only for Reynolds numbers between approximately 600 and 1 000. At higher Reynolds numbers, the Nusselt numbers increased with increasing Reynolds number by approximately 26% up to the critical Reynolds number. However, it is confirmed that the friction factors for fully developed forced convection laminar flows were indeed $64/Re$ (even for diabatic conditions with variable fluid properties).

According Ghajar and Tam [35], flow in horizontal tubes can be considered as forced convection when the ratio of the heat transfer coefficients at the top and bottom of the tube is greater than 0.8. Meyer and Everts [18] found that for ratios up to 0.9 buoyancy effects were still significant and therefore recommends that the ratio should be greater than 0.9 when water is used as the test fluid.

2.5.1.1. Fluid properties

Although the derivation of the Nusselt number of 4.36 during forced convection conditions was obtained for a constant heat flux boundary condition and constant properties, this is not the case in actual practice. The fluid properties change with temperature along the tube length. However, the properties can also change because of changes in mass flow rates and/or heat flux. Due to the challenge of conducting forced convection experiments, especially in the laminar flow regime, several numerical analyses focused on the effects of changes in fluid properties on the forced convection heat transfer and pressure drop characteristics in smooth tubes [66].

Nonino *et al.* [67] performed a numerical analysis on laminar forced convection developing flow for different horizontal channels including a circular tube with a constant wall temperature boundary condition. It was found that the change in viscosity with temperature along the channel length significantly affected the laminar forced convection heat transfer coefficients, while the other fluid properties were assumed to be constant. This is similar to the findings of Nouar [68], that the heat transfer coefficients were affected by a decrease in viscosity due to an increase in temperature along the tube length. Zhai *et al.* [69] investigated the effect of axial conduction due to the change in fluid properties on the laminar forced convection heat transfer coefficients. It was found that varying fluid properties had a greater influence on the velocity profile in the developing region, while the temperature profile was more affected in the fully developed region.

Correlations such as Eq. 2.28 [66] can therefore be used to account for changes in the fluid properties:

$$\frac{Nu_{vp}}{Nu_{cp}} = \left(\frac{\mu_b}{\mu_w}\right)^n \quad 2.28$$

The variable property Nusselt number, Nu_{vp} , in Eq. 2.28 is a function of the constant property Nusselt number, $Nu_{cp} = 4.36$, viscosity ratio (μ_b/μ_w), and n . Depending on the heating or cooling conditions with liquids or gases, different values of n were obtained based on regression analysis of some experimental data. For laminar fully developed flow with heating, Deissler [70] and Shannon and Depew [71] recommended $n = 0.14$ for liquids. From Eq. 2.28, it followed that the variable property Nusselt number, Nu_{vp} , increased with increasing heat flux due to the increase in viscosity ratio.

Herwig [72] numerically investigated the effect of different fluid properties, other than viscosity only, to correct the constant property Nusselt number. Eq. 2.29 is a more sophisticated correlation that takes into consideration more fluid properties:

$$\frac{Nu_{vp}}{Nu_{cp}} = \left(\frac{\mu_w}{\mu_b}\right)^{-0.107} \left(\frac{\rho_w}{\rho_b}\right)^{0.34 - \frac{0.128}{Pr}} \left(\frac{k_w}{k_b}\right)^{0.245} \left(\frac{c_{pw}}{c_{pb}}\right)^{0.255} \quad 2.29$$

Eq. 2.29 shows the variable property Nusselt number, Nu_{vp} , as a function of the constant property Nusselt number, Nu_{cp} , and the ratios of viscosity, density, thermal conductivity and specific heat at the wall and bulk temperatures, respectively. Hence, Eq. 2.29 also followed a similar pattern than Eq. 2.28, where the Nusselt numbers increased with heat flux due to the increasing viscosity ratio (μ_b/μ_w). A similar approach was also followed by Koppel and Smith [73].

Zhao *et al.* [74] recently developed a new correlation for the variable property Nusselt number, Nu_{vp} , numerically, with properties evaluated at the bulk fluid temperatures. This was to account for property-temperature sensitivities, especially at higher bulk fluid temperatures, and for different fluids. However, because the correlation was a function of heat flux, the Nusselt numbers changed with heat flux. This is not necessarily the case for pure forced convection, as will be shown in this study.

The effects of variable fluid properties on the forced convection heat transfer coefficients were also investigated by many researchers for micro-convective applications [75-77]. It was found that the effect of fluid properties on the forced convection heat transfer coefficients were significant. However, there is little experimental data available to validate and investigate the effects of the

fluid properties, not only on laminar flow, but also on transitional flow forced convection heat transfer and pressure drop characteristics.

2.5.2. Transitional flow

The flow in the transitional flow regime alternates between the laminar and turbulent flow regimes, and the Nusselt numbers increase from the forced convection laminar Nusselt number of 4.36 to the turbulent Nusselt numbers. Huber and Walter [78] studied forced convection in the transitional flow regime of a co-current flow vertical heat exchanger between Reynolds numbers of 4 000 and 10 000. However, transition in tubes occurs much earlier than a Reynolds number of 4 000 depending on the rate of heating and inlet geometry [18, 35, 43]. Therefore, they also considered part of the quasi-turbulent and turbulent flow regimes as the transitional flow regime. Due to difficulty in conducting forced convection experiments especially in horizontal tubes, there is little information in literature on the characteristic behaviour of the pure forced convection heat transfer in the transitional flow regime, where transition starts at a Nusselt number 4.36 and buoyancy effects are insignificant. Wei [79] recently identified six different flow and heat transfer regimes in the absence of buoyancy effects (forced convection) from the laminar to turbulent flow regimes of smooth horizontal plane-channel. It was concluded that with the assumption of no buoyancy or entrance effects, it was difficult to analytically predict the transitional flow heat transfer coefficients from the governing equations. Furthermore, for pure forced convection conditions, the effect of flow direction and tube orientation on the laminar and transitional heat transfer characteristics were not investigated in literature.

2.5.3. Quasi-turbulent and turbulent flow

In the quasi-turbulent and turbulent flow regimes, forced convection heat transfer coefficients depends on the thermal conductivity as well as the eddy diffusivity, which is a function Reynolds number and Prandtl number. In general, turbulent flow is mostly dominated by forced convection heat transfer as the turbulent and chaotic behaviour of the fluid flow suppresses the buoyancy effects.

2.6. Mixed convection heat transfer

When a fluid flows inside a tube (internal) or over a surface (external) by natural means such as the buoyancy effect, the heat exchange between the wall and the fluid is by natural or free convection. For a combined natural and forced convection effect, the heat exchange is called mixed convection. For flow in tubes, mixed convection heat transfer is mainly due to buoyancy forces caused by the fluid density differences due to the temperature gradients between the fluid near the heated wall and the cooler fluid near the centreline. These generally enhances the heat transfer compared to forced convection heat transfer. In general, the behaviour of mixed convection heat transfer in tubes depends on the tube orientation, flow direction and flow regime. This section reviews different works on mixed convection heat transfer and pressure drop in horizontal (Fig.

2.3(a)), inclined (Fig. 2.3(b)) and vertical (Fig. 2.3(c)) tubes for both laminar and transitional flow regime in order to identify gaps in the literature.

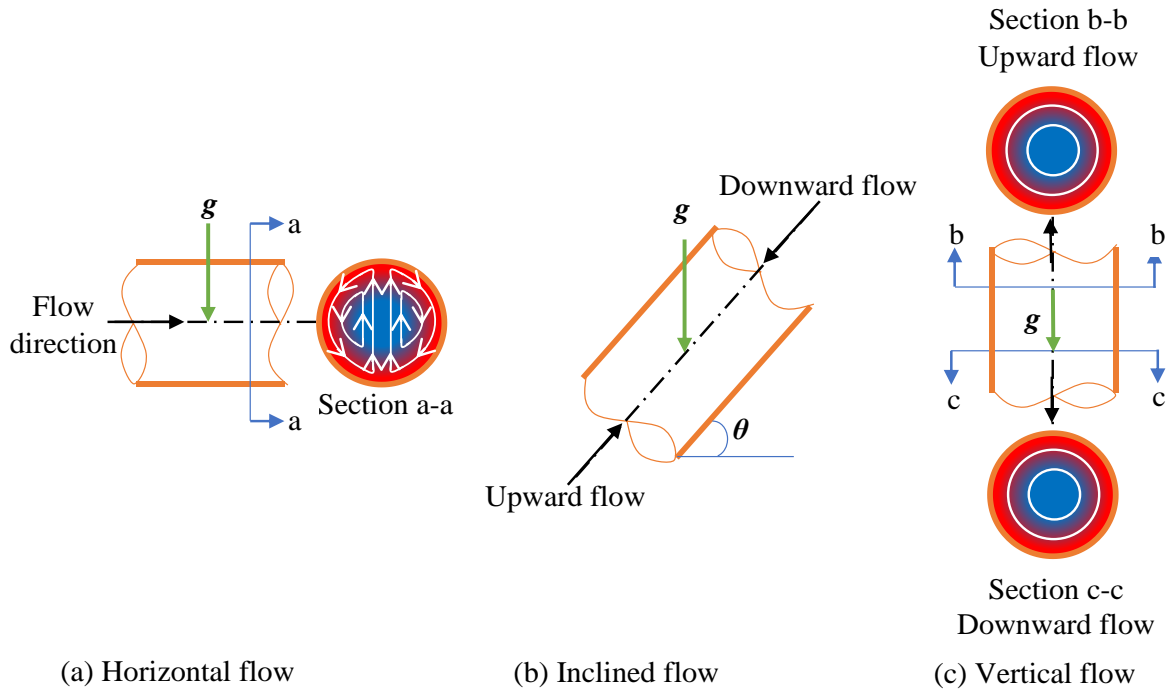


Fig. 2.3: Schematic representation of buoyancy effects on the fluid flow and heat transfer in (a) horizontal, (b) inclined, and (c) vertical tubes for both upward and downward flows.

2.6.1. Laminar flow: Horizontal tubes

Mixed convection heat transfer in horizontal tubes is caused by the buoyancy forces which act in the radial direction to the inertia forces, generating a secondary flow within the flow. The fluid with a higher temperature (lower density) near the tube wall circulates upward, while the fluid with a lower temperature (higher density) near the centerline circulates downward in the direction of gravity (Section a-a in Fig. 2.3(a)). These counter-circulations enhance the heat transfer and significantly increase the laminar Nusselt numbers [20]. Hence, for mixed convection conditions, the laminar Nusselt numbers are easily 180%-520% higher than 4.36 [21, 55].

Laminar mixed convection in horizontal tubes has been investigated since the 1950s to date and a review on these works can be found in book chapters by Aung [80] and Raithby and Hollands [81]. It was concluded that for fully developed flow with constant heat flux boundary condition, the heat flux applied to the tube wall produces a temperature gradient and causes density differences and thus, buoyancy effects due to gravitational forces. These lead to mixed convection and heat transfer enhancement depending on the heat flux and tube diameter.

Other researchers investigated the effect of buoyancy, not only in the fully developed region, but also in the developing region. McComas and Eckert [82] performed experiments with air and found that the local Nusselt numbers from the tube inlet first decreased along the tube length and then increased until a constant value is reached due to buoyancy effects. Similar results were obtained by Shannon and Depew [83] and Barozzi *et al.* [26] when using water as the working fluid. For higher Grashof numbers, Hong *et al.* [84] and Cheng and Ou [85] found that the local Nusselt numbers decreased in the flow direction and then became constant. However, for lower Grashof numbers, Cheng and Ou [85] found that the local Nusselt numbers decreased in the axial direction due to the entrance effect until a minimum value was reached where the buoyancy effects started becoming significant and overcome the entrance effects. This led to an increase in the local Nusselt numbers to a constant value. Cheng and Ou [85] classified the three regions formed along the tube length due to the entrance and buoyancy effects as the Leveque solution region, intermediate region and the region where the local Nusselt numbers became constant. Meyer and Everts [18] obtained a similar result where the three regions formed along the tube length and their boundaries were quantified and defined as the Forced Convection Developing (FCD), Mixed Convection Developing (MCD) and Fully Developed (FD) regions. It was found that for mixed convection heat transfer, both the FCD/MCD and MCD/FD boundaries occurred earlier (in terms of axial position) with increasing buoyancy effects (Grashof numbers) due to the increase in heating or tube diameter. Furthermore, the MCD/FD boundary (thermal entrance length) for mixed convection condition was found to be much shorter than that of forced convection condition. A revised thermal entrance length for mixed convection heat transfer was developed as a function of Grashof number and Graetz number.

Tam and Ghajar [20], Tam *et al.* [56], Olivier and Meyer [48] and Everts and Meyer [40] reported that the fully developed laminar friction factors in horizontal tubes are significantly affected by the buoyancy effects for mixed convection conditions. The magnitude of the friction factors is normally higher than the isothermal friction factors predicted by the Poiseuille correlation ($64/Re$). To account for the buoyancy effects, Tam and Ghajar [20] and Tam *et al.* [56] developed a laminar friction factor correlation for mixed convection heat transfer in horizontal tubes.

2.6.2. Laminar flow: Vertical tubes

Mixed convection heat transfer in vertical tubes differ from that of horizontal tubes. In vertical tubes, as the flow is either vertically upward or vertically downward, the buoyancy forces (natural convection) acts either in the same direction (*assisting flow*) as the inertia forces, or in opposite direction to the inertia forces (*opposing flow*) [11]. Fig. 2.3(c) shows the schematic representation of the buoyancy effects in vertical tubes for both upward assisting flow and downward opposing flow.

One of the early researches on laminar mixed convective heat transfer in vertical tubes was conducted by Eckert and Diaguila [86] in 1954. In 1989, Jackson *et al.* [87] reviewed different

theoretical and experimental works on the forced and mixed convection heat transfer for laminar and turbulent flows in vertical tubes.

Mohammed [88] experimentally investigated the effect of flow direction on laminar mixed convection heat transfer under a uniform heat flux boundary condition in vertical tubes. It was found that the wall temperatures for buoyancy opposing flow were higher than for assisting flow, thus the Nusselt number would be lower for the opposed flow. Comparing the results with horizontal tubes [89], the opposed flow surface temperatures for vertical tubes were higher than that of the horizontal tubes. Furthermore, Mohammed and Salman [90] developed a correlation for the average laminar Nusselt number for opposing and assisting air flow in the developing region of a vertical circular tube. For opposed flow, the Nusselt numbers were Reynolds number and Grashof number dependent. The analysis was for Reynolds numbers between 400 and 1 600.

For fully developed flow in vertical heated tubes, Kakac *et al.* [63] defined the heat transfer coefficients as a function of Rayleigh number. It was found that for buoyancy assisting flow, the laminar Nusselt number increased as the Rayleigh number increased and was always higher than the pure forced convection Nusselt number of 4.36 and lower for the case of buoyancy opposing flows. For developing flow, similar to horizontal tubes, the thermal entrance length was significantly affected by the buoyancy effects and thus, the thermal entrance length decreased with an increase in Rayleigh number (Grashof number/buoyancy effects).

In general, for laminar mixed convection flow with a constant heat flux boundary condition and vertical upward assisting buoyancy flow, the Nusselt numbers can be higher than the forced convection Nusselt number while for vertical downward opposing buoyancy flow, the Nusselt numbers can be lower than the forced convection Nusselt [63]. These mostly occurred at lower Reynolds numbers where the buoyancy forces became more significant and suppressed the inertia forces, thus, dominating the heat transfer. For higher laminar Reynolds numbers, the inertia forces can suppress the buoyancy effects and the heat transfer can be forced convection as will be shown in this study.

2.6.3. Laminar flow: Inclined tubes

Similar to vertical tubes, mixed convection heat transfer in inclined tubes is a function of buoyancy assisting or opposing flow, but the heat transfer and fluid flow characteristics are different due to the inclination effects. In inclined tubes, the components of the gravitational (buoyancy) forces changed in the axial and circumferential direction, causing a change in Grashof numbers and thus mixed convection heat transfer as shown in Fig. 2.3(b). Iqbal and Stachiewicz [22] found that an increase in inclination angle led to an increase in the fully developed laminar heat transfer coefficients. Barozzi *et al.* [26] found a slight decrease in heat transfer rates for an increase in inclination angle from 0° to $+60^\circ$ for upward flows.

Most mixed convection heat transfer analyses for inclined tubes in literature [23-31] showed that inclination buoyancy has a significant effect on the laminar heat transfer, depending on the flow direction. Tian *et al.* [91] used flow visualizations to investigate the effect of buoyancy on laminar mixed convection heat transfer in inclined narrow rectangular channels with asymmetrical heating. They considered upward developing flow near vertical inclination angles between $+60^\circ$ to $+90^\circ$. It was found that transverse flow and buoyancy forces normal to the tube wall were the main contributing factors to mixed convection and heat transfer enhancement within the channel. A modified Grashof number correlation in terms of inclination angle, to account for buoyancy forces, in narrow rectangular channels was also developed in their part II article [92]. Correlations to predict the heat transfer coefficients for inclined tubes were developed in literature [23, 24, 28]. Most of these correlations were for specific angles (either 0° , 30° , 45° , 60° or 90°) in the either upward or downward flow directions. Up to now, there exists no correlation to predict either the heat transfer coefficients or friction factors for all inclination angles and for all flow directions.

Although significant work has been done on flow through inclined tubes during phase change [1-3, 5-8, 93-95], very little has been done on the expected simpler case of single-phase flow through inclined tubes in the laminar flow regime.

2.6.4. Transitional flow: Horizontal tubes

The heat transfer and pressure drop characteristics in the transitional flow regime of horizontal circular tubes has been mainly investigated by two group of researchers headed by Professor Afshin Ghajar from Oklahoma State University and Professor Josua Meyer from University of Pretoria. Professor Afshin Ghajar and his co-workers were the first to investigate transitional flow in horizontal tubes for a constant heat flux boundary condition since the 1990s. Professor Josua Meyer and his co-workers continued with the work on transitional flow to date, using both constant heat flux and constant wall temperature boundary conditions as well as annular flow. These works were reviewed concurrently together with other works in the transitional flow regime in this section. In general, transition in tubes is a function of flow type (axial position), rate of heating, working fluid, inlet geometry, tube configuration and orientation.

2.6.4.1. Developing and fully developed flows in smooth tubes

Transition from laminar to turbulent flow tubes usually occurs along the length of the tube when the Reynolds number is above the critical Reynolds number. Nishi *et al.* [96] reviewed different works on transition from laminar to turbulent regions along the tube length and found that depending on the fluid velocity, transition occurred gradually along the tube length until fully developed turbulence is achieved. Kalinin and Yarkho [97] and Everts and Meyer [21] found that the wall temperatures and mass flow rates fluctuate along the tube length when the flow is in the transition region.

Ghajar and co-workers focused on the local heat transfer results (at $x/D_i = 192$) in the fully developed region as well as the pressure drop measurements along the length of the tube [20, 35, 38, 52-54, 56, 98]. As the wall and fluid temperatures increased along the tube length, the Reynolds numbers at the start and end of the transitional flow regime increased due to decrease in fluid viscosity. Hence, the Reynolds numbers at which the transitional flow regime started increased linearly along the tube length [38].

Meyer and co-workers focused on both local and average heat transfer results in both the developing and fully developed regions [18, 21, 41, 42, 48, 50, 57-59]. Everts and Meyer [21] studied the heat transfer and pressure drop characteristics of transitional flow in the developing and fully developed regions using long horizontal tubes. The test section tubes were much longer than any other test section used previously in the literature, with a maximum length-to-diameter ratio of (x/D_i) of 1 373. Transition along the length of the tube was divided into three regions; in region 1, buoyancy effects were negligible and the width of the transitional flow regime decreased along the tube length. In region 2, buoyancy effects started developing and the width of the transitional flow regime decreased with both increase in buoyancy and axial location. In the third region, the flow became fully developed and the width of the transitional flow regime was independent of axial location, but it decreased with increasing buoyancy effects [21].

Similar to Ghajar and Madon [53] and Tam *et al.* [56], Everts and Meyer [40] investigated the isothermal and diabatic friction factors of developing and fully developed flows in smooth horizontal tubes. It was found that both the critical Reynolds numbers at the start and end of the transitional flow regime, and the transition gradients of the friction factors increased along the tube length.

2.6.4.2. Heating and buoyancy effects

For both developing and fully developed flows, heating caused the viscosity of the fluid to decrease and the Reynolds numbers to increase. For horizontal tubes, heating also generated buoyancy effects (mixed convection) due to density differences within the fluid flow and changed the transitional flow characteristics. Ghajar and co-workers used different mixtures of ethylene glycol and water in their experiments with relatively large tube diameters (up to 15.8 mm), which gave high Prandtl numbers (up to 160) and high Rayleigh numbers (up to 10^6). However, Meyer and co-workers used water as the working fluid with low Prandtl numbers (up to 7) and relatively small tube diameters (up to 19 mm). Therefore, a wide range of Rayleigh numbers (Grashof numbers) were covered in literature for the analysis of the effect of heating and buoyancy (mixed convection) on transitional flow through smooth horizontal tubes.

Ghajar and Tam [35] found that the Reynolds number at which the transitional flow regime started and ended increased with increase in heat flux. Everts and Meyer [9, 21, 40] investigated mixed convection heat transfer and pressure drop in smooth horizontal tubes in the laminar, transitional, quasi-turbulent and turbulent flow regimes using two different approaches. Firstly, they compared

different tube diameters, because the Grashof number, and thus buoyancy effect, is proportional to D_i^3 . Similar to Ghajar and Tam [20, 35], different heat fluxes were used in the second approach. It was found that when the buoyancy effects were increased by either the tube diameter or heat flux, both the Reynolds numbers at which the transitional flow regime started and ended, as well as the width of the transitional flow regime and transition gradient were affected. Therefore, buoyancy effects significantly affected both the heat transfer and pressure drop characteristics of the transitional flow regime.

A third approach that can be used to investigate mixed convection heat transfer without varying the heat flux or tube diameter, is to change the inclination angle of the test section. As will be shown in this study (Chapter 5), different levels of buoyancy (represented by the Grashof numbers) can be generated by changing the inclination angles of a test section.

2.6.4.3. Mini- and micro-tubes

According to Kandlikar *et al.* [99], a tube can be considered as micro-tube when the tube diameter is less than 200 μm and as a mini-tube when the tube diameter ranged between 200 μm to 3 μm . Ghajar *et al.* [54] performed experiments with mini- and micro-tubes and examined the effect on the transitional flow friction factors for isothermal flow conditions. The friction factor results showed that as the tube diameter was decreased from 283 μm to 667 μm , the start of the transitional flow regime was delayed from Reynolds number of 1 500 to 2 200, while the end of the transitional flow regime was relatively constant at a Reynolds number of 4 000 and 3 000 for tube diameters higher than 732 μm and between 737 μm to 667 μm , respectively. Decreasing the tube diameters further from 667 μm to 337 μm caused both the start and end of the transitional flow regime to be delayed. However, for tube diameters greater than 1 373 μm , the isothermal friction factors were independent of tube diameter.

The effect of heating on the friction factors were also investigated by Tam *et al.* [100] in mini-tubes and by Tam *et al.* [56] in micro-tubes. They found that the critical Reynolds numbers at the start of the transitional flow regime increased with increase in heat flux, while the end of transitional flow Reynolds numbers remained relatively constant. Dirker *et al.* [42] compared three different rectangular micro-channels with hydraulic diameters of 0.57, 0.85 and 1.05 mm, using three different inlet geometries. It was found that for a constant heat flux boundary condition, the start and end of the transitional flow regime were not significantly affected by the channel diameter to length ratio of these channel diameters.

2.6.4.4. Enhanced tubes

Tam *et al.* [98] used internal micro-fin tubes for heat transfer enhancements to investigate the effect on heat transfer and pressure drop in all the flow regimes. The laminar isothermal friction factors were higher than for smooth tubes ($64/Re$) and the width of the transitional flow regime was greater than for smooth tubes. This is due to the presence of micro-fins that increased the

surface roughness of the tube. As the spiral angle increased, the drag on the surface of the tube increased and caused the friction factors in the transitional and turbulent flow regimes to increase. For diabatic friction factors, Tam *et al.* [98] found that the start of the transitional flow regime was a function of inlet geometry and spiral angle, while the end of the transitional flow regime was only a function of spiral angle.

Meyer and Olivier [50, 51] compared two different enhanced tubes with two smooth tubes of the same diameters using four different inlet geometries. The first tube had an outer diameter of 15.9 mm with 25 fins and a helix angle 18° , while the second tube had an outer diameter of 19.1 mm with 35 fins and a helix angle of 27° . The relative roughness of the two tubes were kept approximately the same. The following conclusions were made: (a) the isothermal friction factors of the enhanced tubes were higher than for smooth tubes in the laminar and transitional flow regimes; (b) as the helix angle increased, the magnitude of the isothermal friction factors increased and the Reynolds numbers at the end of the transitional flow regime decreased; (c) a secondary transition occurred between Reynolds number 3 000 and 10 000 for both the isothermal and diabatic friction factors, as well as the heat transfer results; (d) the heat transfer in the turbulent flow regime increased with increase in helix angles and was higher than smooth tubes; (e) correlations to predict the transitional flow Reynolds numbers for enhanced tubes were developed.

Meyer and Abolarin [41] and Abolarin *et al.* [58, 59] used different types of twisted tape inserts for heat transfer enhancements and investigated the heat transfer and pressure drop characteristics of the transitional flow regime. Twisted tape inserts generated more turbulence within the flow and increased mixing and thus, caused the heat transfer and pressure drop to increase. Meyer and Abolarin [41] found that when the twist ratio was decreased, transition occurred earlier and the width of the transitional flow regime decreased. Abolarin *et al.* [58] also used alternating clockwise and counter clockwise twisted tape inserts that were connected longitudinally with different connection angles. The boundaries of the transitional flow regime were significantly affected by the connection angles and it caused transition to occur at lower Reynolds numbers due to increased disturbances. Abolarin *et al.* [59] compared peripheral u-cut twisted tape inserts of different depth ratios with and without ring inserts. It was found that when the depth ratio of the peripheral cuts increased, transition occurred earlier. When ring inserts were used, transition occurred earlier than without the rings on the peripheral u-cut twisted tape inserts. It was concluded that as the ring space ratio increased, transition was delayed. For all the different types of twisted tapes used [41, 58, 59], correlations to predict the heat transfer and pressure drop in the laminar, transitional and turbulent flow regimes were developed.

Others [101-104] used corrugated tubes and wire coil inserts for the enhancement to investigate the heat transfer characteristics of the laminar and transitional regimes.

2.6.4.5. Nanofluids

Osman *et al.* [105] conducted experiments using aluminium oxide-water nano-fluids with volume concentrations of 0.3, 0.5 and 1% as the working fluid in a horizontal rectangular channel. Heat transfer and pressure drop characteristics in the transitional flow regime were investigated for a constant heat flux boundary condition, between Reynolds numbers of 200 and 7 000. It was found that an increase in volume concentration delayed transition and increased the heat transfer coefficients in the transitional and turbulent flow regimes. Furthermore, the pressure drop increased with an increase in volume concentration in all the flow regimes. Meyer *et al.* [44] used three different concentrations of multi-walled carbon nanotubes (MWCNT) to investigate the effects on the heat transfer coefficients and friction factors in the transitional flow regime. Similar to Osman [105], transition was also delayed with increase in nanofluid concentration. Thus, when the volume concentration of the nanofluid was increased, the viscosities of the nanofluid increased which caused the critical Reynolds numbers to decrease.

2.6.4.6. Annuli

Ndenguma *et al.* [47, 49] investigated the heat transfer and pressure drop characteristics of the transitional flow regime in a concentric annular passage for heating and cooling conditions. The effects of longitudinal wall temperatures on the inner wall of the annular passage were investigated for a simultaneously hydrodynamically and thermally developing flow [47]. It was found that for mixed convection conditions, the degree of uniformity of the longitudinal wall temperature significantly affected the boundaries of the transitional flow regime and led to increased heat transfer coefficients and friction factors. Ndenguma *et al.* [49] also compared different annular dimensions for approximately uniform wall temperature on the inner wall of the annular passage. An annular geometric parameter was proposed, which is a function of annular diameter ratio and hydraulic diameter. For both the heating and cooling conditions, the width of the transitional flow regime decreased with increase in annular geometric parameter.

2.6.5. Transitional flow: Vertical and inclined tubes

Most of the transitional flow work in vertical tubes in the literature focused on the start of the transitional flow regime for either natural or mixed convection heat transfer. Galanis and Behzadmehr [106] reviewed different works on mixed convection in vertical ducts and reported that the increase in heating can cause transition from laminar to turbulent flow to occur at Reynolds numbers lower than 2 000 in vertical tubes. Scheele *et al.* [107] used a dye to study the effect of natural convection on transition from laminar flow to a disturbed flow along the length of a vertical tube. It was found that for upward flow, the growth of small disturbances along the length of the tube caused instabilities within the flow that led to transition, while for downward flow, transition occurred suddenly because of the separation of flow at the wall. Behzadmehr *et al.* [108] showed an instability in the flow at the start of the transitional flow regime caused by the buoyancy effects at different Reynolds numbers in vertical tubes. Their transitional flow work concentrated on the

start of transition along the length of the tube at low Reynolds numbers of 1 000, 1 300 and 1 600 only, not the entire transitional flow regime. Hence, the heat transfer and pressure drop characteristics of the transitional flow regime from laminar to turbulent flow regimes need to be investigated for both vertical upward and downward flow directions. Up to now, there is little information in the literature on the characteristic behaviour of single-phase mixed convection heat transfer and pressure drop in the transitional flow regime of inclined tubes. As discussed in Section 2.6.4.2, for horizontal tubes, buoyancy effects (due to heating or increase in tube diameter) significantly affected the boundaries of the transitional flow regime, as well as the transition gradients. However, in inclined tubes the behaviour of buoyancy force is more complicated than in horizontal and vertical tubes and thus, can change the characteristic behaviour of the transitional flow regime.

2.7. Effects of inlet disturbances on transitional flow

2.7.1. Inlet geometry

Ghajar and co-workers [35, 37-39, 52-56] were the pioneers of the work on the effect of inlet disturbances on the heat transfer and pressure drop characteristics of the transitional flow regime of smooth horizontal tubes. Three different inlet configurations were investigated namely: square-edged, re-entrant and bell-mouth as shown in Fig. 2.4. Meyer and Oliver [48, 50, 51] investigated another inlet geometry known as the hydrodynamically fully developed inlet (Fig. 2.4(d)) in addition to the three inlets investigated by Ghajar and co-workers. To ensure a uniform upstream flow to the different inlet geometries, a flow-calming section was attached prior to the inlet sections. The flow-calming section replicate the heat exchanger inlet header and/or plenums found in many practical applications.

For the re-entrant inlet geometry (Fig. 2.4(a)) the test section was slid one diameter into the inlet section, as found typically in the headers of shell and tube heat exchangers. For the square-edged inlet (Fig. 2.4(b)), which is found in most heat exchangers, there was a sudden contraction at the inlet section to the test section. These two inlets (Fig. 2.4(a)) and (Fig. 2.4 (b)) were associated with flow disturbances and eddy formation at the inlet of the test section as the diameter of the inlets were larger than the test section diameter (contraction ratio of larger than one). To avoid the formation of eddies at the inlet of the test section, the bell-mouth inlet (Fig. 2.4(c)) consisted of a smooth and gradual contraction from the flow-calming section diameter to the test section diameter. The hydrodynamically fully developed inlet (Fig. 2.4(d)) also consisted of a smooth entrance with the same diameter as the test section (contraction ratio of one).

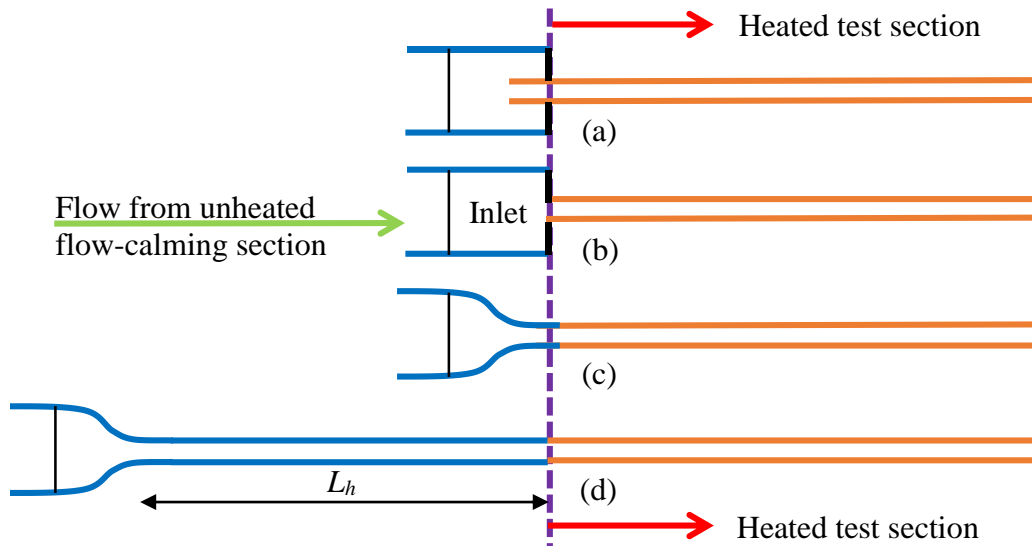


Fig. 2.4: Schematic representation of the different inlet geometries: (a) re-entrant, (b) square-edged, (c) bell-mouth, and (d) hydrodynamically fully developed. Adapted from Everts [65].

For the heat transfer analysis, Ghajar and Tam [35] found that the re-entrant inlet (Fig. 2.4(b)) generated the greatest disturbances at the inlet and therefore led to an earlier transition than the other inlets. The bell-mouth inlet generated the least disturbances and therefore delayed transition the most. In general, the smoother the inlet, the longer transition is delayed. Other studies [20, 48, 53, 56] found similar results for the friction factors with different inlet geometries in the transitional flow regime.

However, because it was found that the heat transfer and pressure drop characteristics of the transitional flow regime of horizontal tubes were significantly affected by the inlet geometry, different correlations for the heat transfer coefficients, friction factors, as well as the transitional flow Reynolds numbers were developed for the different inlet geometries. Some of these correlations can be found in [18, 20, 35, 38, 48, 50, 51, 53, 56].

2.7.1. Inlet contraction ratios

Ghajar and co-workers used a similar flow-calming section diameter (with a contraction of 10) throughout their experiments for the different inlet geometries. The influence of different inlet contraction ratios on each inlet geometry was thus not investigated. Changing the contraction ratio could change the magnitude of upstream flow disturbances in the flow-calming and inlet sections.

Dirker *et al.* [42] investigated the effect of three different inlet contraction ratios (5, 6.25 and 10) on transitional flow with a bell-mouth inlet and one contraction ratio each for the sudden contraction and swirl inlets. It was found that for the bell-mouth inlet, transition was delayed as the contraction ratio decreased from 10 to 5. Meyer *et al.* [41] conducted experiments using a flow-calming section with a large contraction ratio of approximately 58, to avoid any effects of the inlet header geometry. It can be expected that the use of different or lower inlet contraction ratios, typically found in many practical settings, might influence the flow asymmetry and affect the behaviour and boundaries of the transitional flow regime.

Other researchers also investigated the influence of inlet geometries and disturbances not only in the transitional flow regime, but also in the laminar and turbulent flow regimes. Mohammed [109] investigated the effect of different levels of hydrodynamically fully developed flow on the laminar heat transfer coefficients. The flow-calming sections had the same tube diameter as the test section (contraction ratio of one) but was unheated, while the test section was heated at a constant heat flux. This generated different velocity distributions in the hydrodynamic entrance region and suppressed the inlet effects. In practice, heat exchangers can have different inlet headers that are usually larger than the tubes (higher contraction ratios) which affects the heat transfer and pressure drop characteristics. A bell-mouth inlet with a contraction ratio of 3 was also investigated. The local Nusselt numbers for the bell-mouth inlet were found to be higher than for the other inlets. This is similar to the findings of Tam and Ghajar [52] where the local heat transfer coefficients were significantly affected by the bell-mouth inlet when compared to the square-edged and re-entrant inlets, especially in the transitional flow regime.

Nagendra [110] studied the influence of inlet turbulence on the mixed convection heat transfer in the transitional and turbulent flow regimes of a smooth horizontal tube. The inlet disturbances were introduced by placing an inlet probe near the inlet. It was found that the inlet disturbances caused transition to occur earlier, but had no influence in the turbulent flow regime. However, for $ReRa(D_i/L)$ larger than 10^6 , it was found that the inlet disturbances had no influence on any of the flow regimes. Mori *et al.* [111] also found that the level of the inlet turbulence significantly affected the critical Reynolds numbers and the disturbances changed with Rayleigh number. For large $ReRa$, the inlet disturbances had no influence.

Al-Arabi [112] investigated the influence of inlet disturbances on heat transfer in the turbulent flow regime using four different inlet configurations (fully developed with long flow-calming section, bell-mouth, square-edged and bend inlet geometries). Heat transfer correlations for turbulent flow were developed as a function of Reynolds number, Prandtl number or axial position, depending on the type of inlet or inlet turbulence.

2.7.2. Flow-calming section contents

Tam and Ghajar [52] investigated different turbulence levels in the flow-calming section with a bell-mouth inlet geometry by placing different screens upstream of the bell-mouth inlet. It was found that for finer screens, the turbulence at the bell-mouth inlet was less, which caused an unusual behaviour of the local heat transfer coefficients. Different flow-calming section contents have been used in the literature such as plastic straws, honey comb, acrylic plates and different sizes of screens, mostly arranged in a circular tube with a diameter larger than the test section. However, there is little information on the influence of these contents on the heat transfer and pressure drop characteristics of the transitional flow regime with different inlet geometries.

2.7.3. Multiple circular tubes

Meyer *et al.* [41] conducted experiments with multiple circular tubes heated at constant heat fluxes. The purpose was to investigate the influence of flow maldistribution at the inlet of multiple tubes, as well as tube protrusion in relation to the adjacent tubes, on the heat transfer and pressure drop characteristics in the laminar, transitional and turbulent flow regimes. It was found that as the pitch ratio increased, the critical Reynolds numbers and transition gradients of the side tubes decreased due to decrease in flow asymmetry. For a square-edged inlet, transition in the centre tube was delayed compared to a single tube. Furthermore, a protrusion of the centre tube increased the asymmetry of the flow in the side tubes and therefore increased their critical Reynolds numbers and transition gradients.

2.8. Summary and conclusions

This chapter reviewed some of the fundamentals of convective heat transfer and pressure drop in the laminar, transitional, quasi-turbulent and turbulent flow regimes. Previous works on fluid flow in horizontal, inclined and vertical tubes for pure forced and mixed convection conditions were also reviewed.

Previous studies reported that it was challenging to perform forced convection experiments in horizontal tubes with low uncertainties, due to presence of buoyancy effects. There are thus still gaps in the literature on forced convection heat transfer and pressure drop. It will be shown in Chapter 4 that forced convection conditions can be achieved with the tube in a vertically upward or downward orientation at higher laminar Reynolds numbers. The laminar Nusselt number of 4.36 during forced convection conditions for a constant heat flux boundary condition was derived based on constant fluid properties; however, in actual practice, the fluid properties changed with temperature along the tube length. The effects of variable fluid properties on the heat transfer coefficients and friction factors were investigated numerically. Furthermore, there is little information available in literature on the characteristics behaviour of the transitional flow regime for pure forced convection conditions.

It has been found that extensive research has been done on the mixed convection heat transfer in inclined tubes for both upward and downward flows in the laminar flow regime. However, there are still gaps in the literature on the method of quantifying the effect of buoyancy/mixed convection/Grashof number on the heat transfer and pressure drop characteristics in the transitional flow regime of inclined tubes. Furthermore, most of the available laminar Nusselt number correlations as a function Rayleigh number/Grashof number were for specific angles (either 0°, 30°, 45°, 60° or 90°). Up to now, no general correlations for heat transfer coefficients or friction factors for all inclination angles are available.

Correlations to predict the Reynolds number boundaries of the transitional flow regime as well as the heat transfer coefficients and friction factors in the transitional flow regime during mixed convection conditions are available in literature. Although most of these correlations distinguish between the different inlet geometries, they do not account for the different contraction ratios. Changing the contraction ratio could change the magnitude of upstream flow disturbances in the flow-calming and inlet sections and thus, significantly affects the boundaries of the transitional flow regime. Also, the influence of flow-calming section contents on the transitional flow regime with different inlet geometries have not yet receive attention.

In general, it can be concluded that there are several gaps in the forced and mixed convection literature, especially for inclined tubes. It is vital for our fundamental understanding of internal forced convection heat transfer that accurate experimental results with low uncertainties are available in literature. Heat transfer and pressure drop correlations for all inclination angles, as well as information on the characteristic behaviour of the entire transitional flow regime of inclined tubes are required. Furthermore, the effect of flow-calming section contents and contraction ratios together with different inlet geometries on the heat transfer and pressure drop characteristics in the transitional flow regime needs to be investigated.

3. Experimental set-up and data reduction

3.1. Introduction

This chapter discusses the experimental set-up used to conduct all the single-phase heat transfer and pressure drop experiments at different inclination angles, heat fluxes, inlet geometries using different flow-calming sections. It gives an overview of the equipment, material, instrumentation and the test section used in the experimental set-up. The experimental procedure as well as the data reduction method are discussed and an uncertainty analysis of the results are presented.

3.2. Experimental set-up

Fig. 3.1 shows the experimental set-up used to conduct the experiments for this study. Water was circulated from a 500 ℓ storage tank through the flow meters, a flow-calming section, the test section, and then back to the storage tank for cooling and recirculation. A chiller unit was coupled to the storage tank to cool down the heated water and maintain the water at a constant temperature.

A 420 ℓ /hr magnetic gear pump was used to circulate the water through the test section. The pump was connected to the experimental set-up using a rubber hose to prevent transmitting vibrations from the pump to the test section. The pump was controlled from a personal computer and the flow rate was changed by adjusting the voltage signal sent through a Labview program. A pressure relief valve was used to bypass the water back to the storage tank when the pressure exceeded the system pressure threshold value. A water bypass line was used to increase the backpressure to avoid flow pulsations in the test section which might influence the transitional flow characteristics [113]. A pressure gauge was used prior to the flow-calming section to monitor the pressure of the system.

The mass flow rate of the water to the test section was measured using two Coriolis flow meters with different capacities. These flow meters had an accuracy of $\pm 0.05\%$ of the full scale and a maximum flow rate of 330 ℓ /hr and 108 ℓ /hr respectively. The flow meter with a higher flow rate (330 ℓ /hr) was used for measurements in the quasi-turbulent and turbulent flow regimes, while the smaller flow meter (108 ℓ /hr) was used for measurements in the laminar to quasi-turbulent flow regimes. The mixer design of Bakker *et al.* [114] with alternating right and left hand twisted helical plates, was used for both the inlet and exit mixers. The inlet Pt100 probe was installed inside a soft Nylon mesh downstream of the inlet mixer. The outlet Pt100 probe was installed downstream of the outlet mixer with the water stream passing along the probe in an axial direction [65].

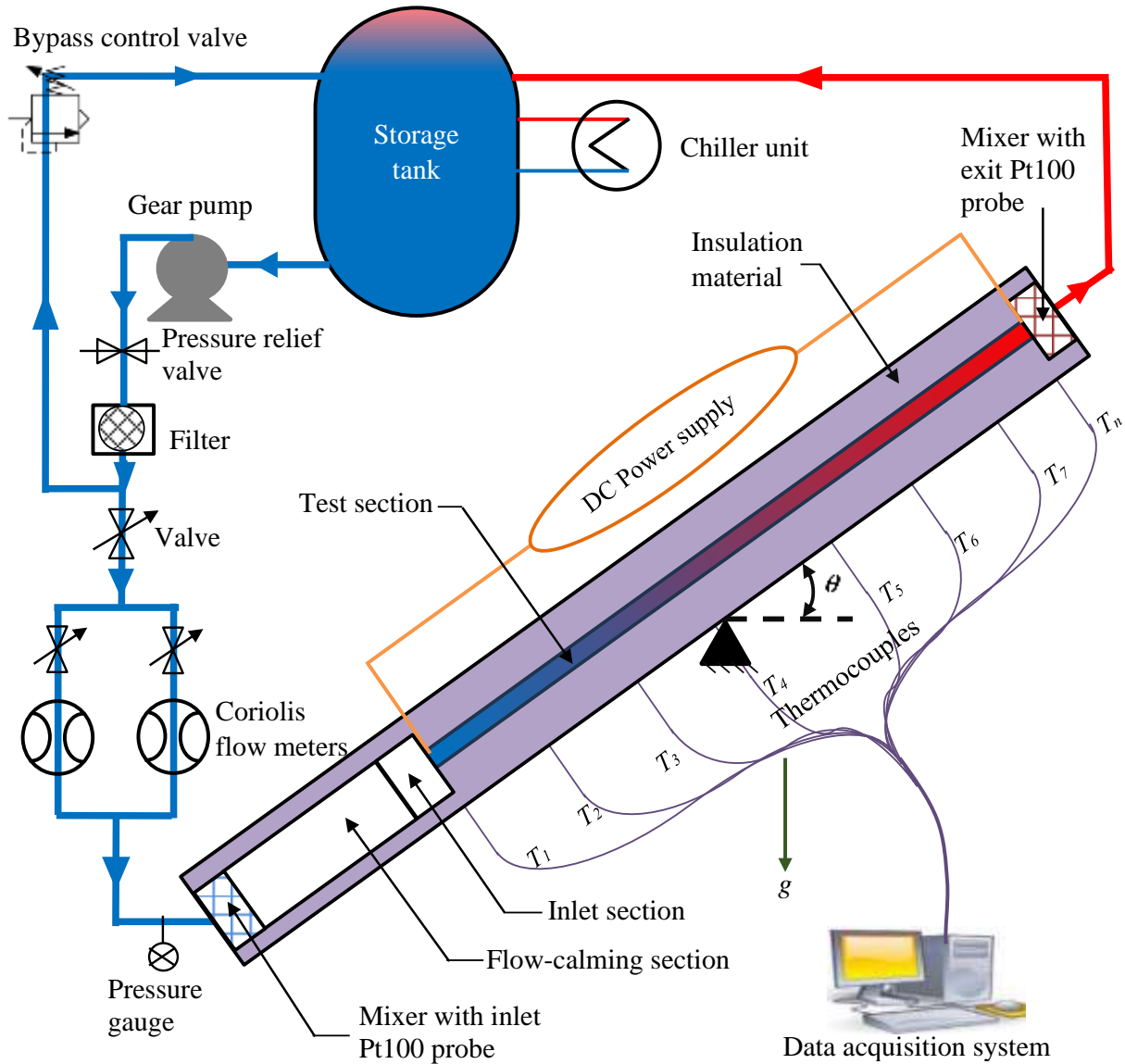


Fig. 3.1: Schematic layout of the experimental set-up.

3.2.1. Flow-calming section and inlet section

A flow-calming section (Fig. 3.2(a) and (b)) was installed prior to the test section to ensure a uniform inlet velocity distribution to the test section. A similar design to Ghajar and Tam [35] and Tam *et al.* [56] was used in Fig. 3.2(a), except that the same tube diameter was used for both the flow-calming and inlet sections to avoid any vortex occurrence caused by diameter differences. Furthermore, the contraction ratio (ratio of the inner diameter of the flow-calming section to the inner diameter of the test section) was 33 for Fig. 3.2(a); while Ghajar and Tam [35] used a contraction ratio of 10. The flow-calming section in Fig. 3.2(a) was made of clear acrylic tube with an outer diameter and length of 180 mm and 616 mm, respectively. Three air bleed valves were located at the top of the tube to remove trapped air.

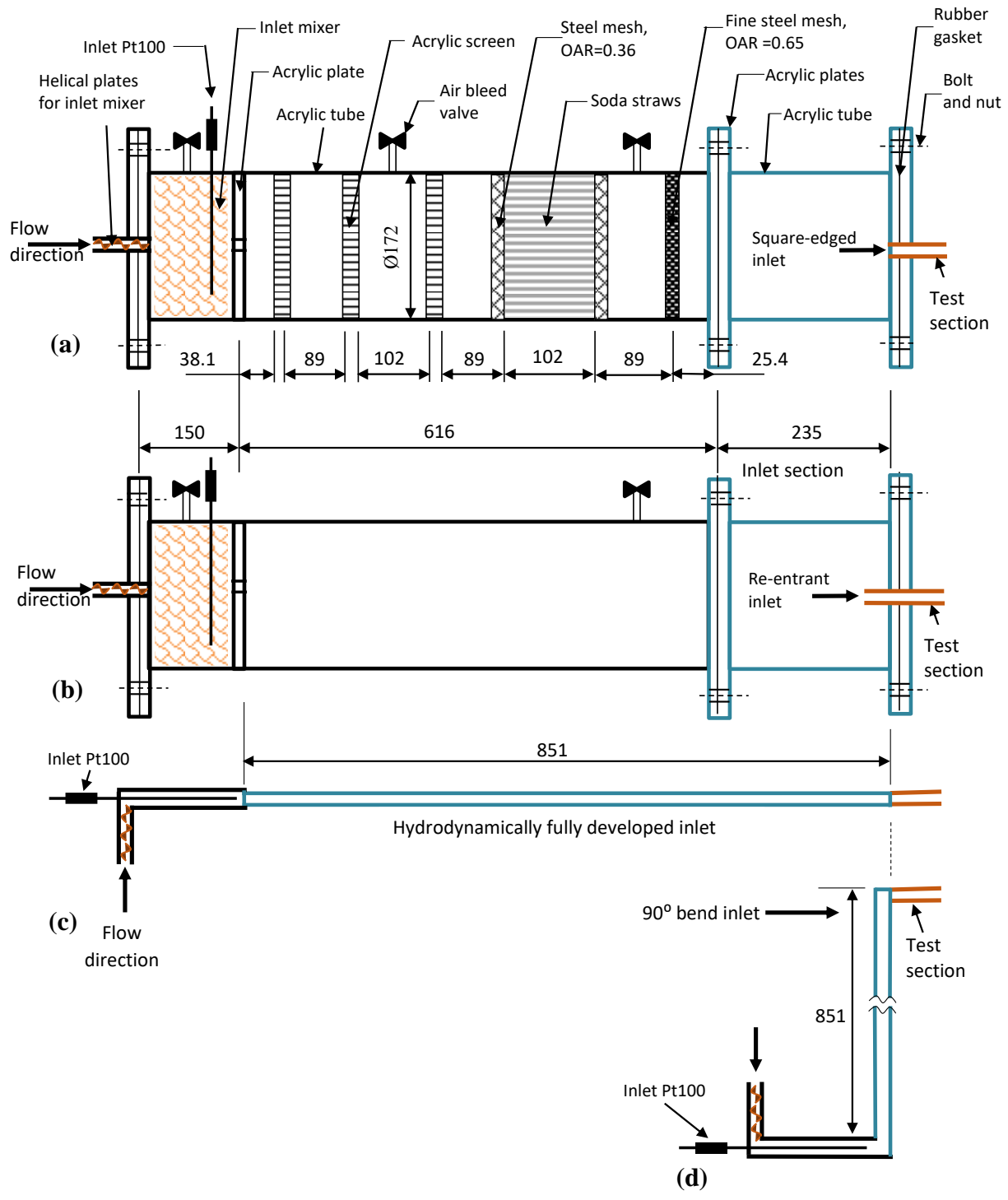


Fig. 3.2: Schematic representation of the inlet mixer with (a) the original flow-calming section with a square-edged inlet, (b) the empty flow-calming section a re-entrant inlet, (c) the hydrodynamically fully developed inlet and (d) the 90° bend inlet. (All dimensions given in mm).

Three perforated acrylic plastic plates, separated 89 mm and 102 mm from each other, were placed 38.1 mm from the inlet of the flow-calming section. Each acrylic plate contained 73 holes, with a diameter of 11 mm. This was followed by tightly packed plastic straws with a diameter of 6 mm, length of 102 mm and open area ratio (OAR) of 0.92. The plastic straws were located 89 mm from the acrylic plates and were placed in-between galvanized steel wire mesh screens with an open area ratio of 0.55. Another fine steel wire mesh screen with an open area ratio of 0.45 was located approximately 25.4 mm before the outlet of the flow-calming section. The inlet section consisted of acrylic tube with a length of 235 mm and inner diameter of 172 mm. A square-edged inlet was used for the forced and mixed convection analysis in Chapter 5 and 6 at different inclination angles with flow-calming section in Fig. 3.2(a).

The effect of flow-calming section contents and contraction ratios on the transitional flow regime are investigated in Chapter 7 using various flow-calming sections of different diameters. For this analysis, Fig. 3.2(a) was considered as the original flow-calming section and the purpose was to ensure that the flow inlet condition at the test section inlet was uniform and undisturbed. Fig. 3.2(b) contains a schematic representation of an empty flow-calming section (except for the inlet mixer) to investigate the effect and significance of the flow-calming section contents on the heat transfer and pressure drop characteristics. Although Fig. 3.2(a) is shown with a square-edged inlet and Fig. 3.2(b) with a re-entrant inlet (test section slid one diameter into the inlet section), both types of inlets were tested on both flow-calming sections. A hydrodynamically fully developed inlet (Fig. 3.2(c)) and a 90° bend inlet (Fig. 3.2(d)) were also investigated. Four different contraction ratios (5, 11, 15 and 33) were investigated by changing the flow-calming section diameter.

The inlet section containing either the square-edged inlet (Fig. 3.2 (a)) or the re-entrant inlet (Fig. 3.2 (b)) was located between the flow-calming section and test section. Both the hydrodynamically fully developed inlet (Fig. 3.2(c)) and 90° bend inlet (Fig. 3.2(d)) had the same diameter as the test section (contraction ratio of one) and an isothermal hydrodynamic length equal to the other flow-calming and inlet section length (851 mm). This ensured that the flow in cases Fig. 3.2(c) and Fig. 3.2(d) was fully developed. Based on $L_t = 0.05ReD_i$ and a Reynolds number of 2 500, a length of $125D_i$ is required. The length of $167D_i$ (851 mm) in Fig. 3.2(c) and Fig. 3.2(d) therefore ensured hydrodynamic fully developed flow at the inlet of the test section.

3.2.2. Test section

Fig. 3.3 is a schematic representation of the test section, indicating the two pressure tap locations, thermocouple stations, as well as the flow directions for the different inclination angles. The test section was made from a smooth hard drawn copper tube with measured inner and outer diameters of 5.1 mm and 6.3 mm, respectively. The test section had a total measured length of 4.6 m and therefore a maximum length-to-diameter ratio (x/D_i) of 886. The average surface roughness of the test section was measured to be approximately 0.206 μm using a Mitutoyo SurfTest SJ-210 surface

roughness tester with a diamond stylus. The relative surface roughness was therefore 4.1×10^{-5} , and for all practical purposes, the tube can be considered as smooth.

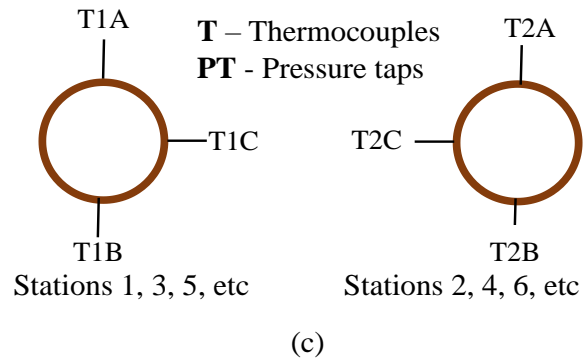
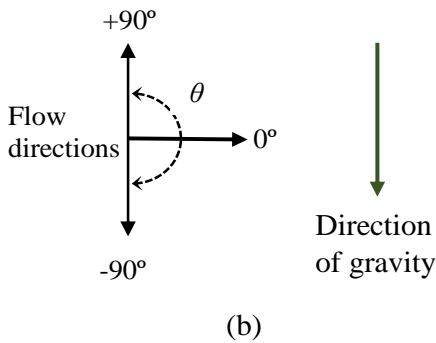
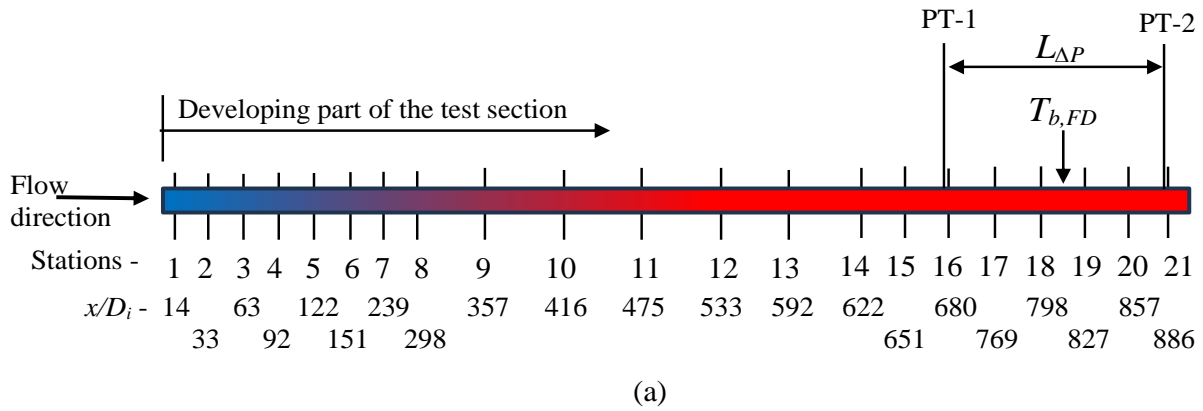


Fig. 3.3: Schematic representation of (a) the test section indicating the pressure taps (PT) and thermocouple stations (T), (b) the flow directions and (c) a cross section of the test section tube that shows the thermocouple positions per station.

The wall temperatures were measured at 21 thermocouple stations. As shown in Fig. 3.3(a), the thermocouple stations were located at closer intervals near the inlet and in the fully developed part to capture enough data in the developing and fully developed regions. T-type thermocouples with a diameter of 0.25 mm were used. Due to the small diameter of the test section, three thermocouples were used at each station (Fig. 3.3(c)). One thermocouple at the top and bottom of the tube and another thermocouple alternating at the side between 90° (for station 1, 3, 5, etc.) and 270° (for station 2, 4, 6, etc.). The thermocouples were soldered to the outer surface of the tube by drilling a 0.4 mm depression and inserting a flux and solder. Heat was applied to the tube and once the solder melted, the thermocouple was inserted and the tube was allowed to cool down.

The theoretical thermal entrance length, L_t , for forced convection was calculated to be 3.2 m (based on $L_t = 0.05RePrD_i$ with a Reynolds number of 2 100 and a Prandtl number of 6). Therefore, conservatively the last 1.4 m of the test section always had fully developed flow and was considered as the “fully developed” part of the test section. This part was used to obtain the fully developed pressure drop and heat transfer results. For the temperature measurements the last six stations (stations 16 to 21) were used. Two pressure tap stations (PT-1 and PT-2 with length $L_{\Delta P} = 1$ m apart) were located within the fully developed region and corresponded closely to the last six temperature measuring stations.

To ensure that the pressure taps did not cause any flow obstructions within the test section, a 0.5 mm diameter hole was drilled through each pressure tap. This hole was less than 10% of the inner diameter of the tube, as suggested by Rayle [115]. The holes were properly de-burred to avoid any local increase in pressure due to presence of burrs that might have formed during the drilling process. A differential pressure transducer with an interchangeable diaphragm was connected to the pressure taps using a Nylon tube. Two different diaphragms were used for the high and low pressure drop measurements. The ranges and accuracies of all the instruments used, are summarised in Table 3.1.

Table 3.1: Ranges and accuracies of the instrumentation used.

Instruments	Range	Accuracy
EA-PS 8080-60 2U Laboratory DC power supply	0 – 1 500 W	3 W
RS PRO LCD Inclinometer	0 – 360°	0.2°
Omega Pt100 probes	0 – 100°C	0.06°C
Omega Thermocouples	–200 – 350°C	0.1°C
Validyne differential Pressure transducers	0 – 3.5 kPa 0 – 14 kPa	8.75 Pa 35 Pa
Emerson Elite Coriolis flow meters		
CMFS010	0 – 108 ℓ/hr	0.054 ℓ/hr
CMFS015	0 – 330 ℓ/hr	0.165 ℓ/hr

For a constant heat flux boundary condition, two T-type constantan heating wires with a diameter of 0.38 mm, were tightly coiled around the test section (skipping the thermocouple junctions) [65] and connected in parallel to a DC power supply. The two heating wires were connected in opposite polarities to avoid electromagnetic interferences due to the applied currents [113].

3.2.3. Test bench

A 6 m long test bench was designed and built to accommodate the test section together with the flow-calming and mixing sections. This test bench was placed on a rigid frame with a height of 3 m. Damping pads were used to avoid vibration from the floor and the equipment to the test section. The test bench was pivoted at the centre and supported at both ends so that it can be orientated at different inclination angles, θ , from -90° downward to $+90^\circ$ upward. Tension cables were used to ensure that the test bench remained straight and rigid at all inclination angles. A digital inclinometer attached to the test bench was used to measure and set the required inclination angle.

3.2.4. Insulation

The flow-calming section, inlet section, test section, mixers and tubes were insulated to prevent heat transfer to the environment using Armaflex® insulation material with a thermal conductivity of 0.034 W/m.K. The thickness of the insulation around the test section was 60 mm and the maximum heat loss was estimated with one-dimensional heat transfer calculations (taking into consideration the average measured wall and outside insulation temperature measurements and insulation resistance) to be less than 2%.

3.3. Experimental procedure

Steady-state conditions were reached approximately two hours after the first start-up of a day. Steady-state conditions were assumed once there were no significant changes in the mass flow rate, temperature, and the pressure drop readings. The experiments were conducted by starting with the highest mass flow rate and then decreasing the mass flow rates by adjusting the pump speed in the Labview program. To minimize flow pulsations, the bypass and supply valves were continuously adjusted such that the pump can operate at higher mass flow rates. The heat flux was set from the DC power supply by applying the required voltage and current signals.

Measurements were taken at greater mass flow rate intervals in the laminar and turbulent flow regimes, but at closer intervals near and within the transitional flow regime. After each Reynolds number increment, approximately 5-10 minutes in the quasi-turbulent and turbulent flow regimes and 15-20 minutes in the laminar flow regime, were required to reach steady-state. In the transitional flow regime, fluctuations in temperature, mass flow rate, pressure drop and energy balance were observed, therefore more time (approximately 20–30 minutes) was required to reach steady-state. Once steady-state was achieved, 400 data points were logged at a frequency of 20 Hz. These data points were then averaged to obtain one data point. The data logged included the inlet and exit temperatures, wall temperatures, ambient temperatures, mass flow rates and pressure drops. The temperature of the water in the storage tank was also monitored to ensure a constant inlet temperature.

The above procedure was repeated for different inclination angles. The inclination angle was increased at smaller increments from -90° (vertically downward) to $+90^\circ$ (vertically upward). The horizontal angle was defined as 0° as shown in Fig. 3.3(b). Once the test bench was set to the required inclination angle, a strong locking mechanism was used to ensure that the inclination angle did not change during experiments. For experiments with different flow-calming sections, the procedure was repeated at horizontal orientation only. All the data obtained were saved and used in a separate program for the analysis.

3.4. Data reduction

Over the tube with measured length, L , the fluid temperatures, $T(x)$, at any axial position, x , were determined from the measured inlet, T_i , and exit, T_e , fluid temperatures as obtained from the two Pt100 probes located at the inlet and outlet of the test section:

$$T(x) = T_i + \frac{(T_e - T_i)x}{L} \quad 3.1$$

Thus, linear temperature profiles were assumed for the temperatures, because constant heat fluxes were applied to the test section. The bulk temperature for the *fully developed* part of the test section ($T_{b,FD}$ in Fig. 3.3) was determined at the measured distance $x = 3.92$ m from the inlet, as shown in Fig. 3.3(a). This corresponded to the centre of the two pressure taps. Depending on what was required (fully developed bulk values or local values) these temperatures were also used to determine all the fluid properties (densities, ρ , viscosities, μ , Prandtl numbers, Pr , specific heat values, C_p , and volume expansion coefficients, β) using the correlations of Popiel and Wojtkowiak [116] for water.

The single-phase pressure drops were estimated using a similar approach to previous work [117-122]. The friction pressure drops, ΔP_f , used to calculate the friction factors were obtained as follows:

$$\Delta P_f = \Delta P_{exp} - \Delta P_{grav} \quad 3.2$$

ΔP_{exp} , was the measured pressure drops, $\Delta P_{measured}$, obtained from the differential pressure transducers at different inclination angles that were corrected by the pressure offset, ΔP_{offset} at no flow condition to account for the vertical height ($L_{\Delta P} \sin \theta$ in Fig. 3.3) pressure difference between the pressure taps at isothermal conditions:

$$\Delta P_{exp} = \Delta P_{measured} + \Delta P_{offset} \quad 3.3$$

When heat was applied at different inclination angles, the gravitational pressure drops, ΔP_{grav} in Eq. 3.2, were due to density difference with and without heating (due to temperature gradients) and were defined as the difference between the pressure at the reference inlet fluid temperature before heating (isothermal) and the average pressure within the heated test section (between the pressure taps):

$$\Delta P_{grav} = \rho_{b,FD} g L_{\Delta P} \sin\theta - \rho_i g L_{\Delta P} \sin\theta = (\rho_{b,FD} - \rho_i) g L_{\Delta P} \sin\theta \quad 3.4$$

where $\rho_{b,FD}$ and ρ_i were the bulk density obtained from the temperature at the bulk fully developed, b,FD station in Fig. 3.3(a) and the density at the inlet (before the fluid is heated in the test section), respectively. At the maximum heat flux of 8 kW/m² and the lowest Reynolds number of 2 100, the fluid density changed from 997 to 988 kg/m³ along the tube length for the +90° inclination angle. This change in density was sufficient to change the gravitational and frictional pressure drops, especially at low Reynolds numbers, where the pressure drop was low. At these conditions, the frictional pressure drop (Eq. 3.2) may change up to ±135%.

The gravitational acceleration, g , was taken as 9.81 m/s² and $L_{\Delta P}$ was the distance between the two pressure taps (PT-1 and PT-2 in Fig. 3.3) which was 1.0 m. The inclination angles, θ , were measured from the horizontal plane and upward fluid flows were defined as having a positive value for, θ , while downward flows were defined as having negative signs. Thus, for vertical upward and downward flows, inclination angles of $\theta = +90^\circ$ and $\theta = -90^\circ$ were used respectively, while $\theta = 0^\circ$ was used for horizontal flow.

The friction factors, f , were obtained from the calculated frictional pressure drops, ΔP_f , as follows:

$$f = \frac{2\Delta P_f D_i}{L_{\Delta P} \rho_{b,FD} V_{avg}^2} = \frac{\Delta P_f \rho_{b,FD} \pi^2 D_i^5}{8L_{\Delta P} \dot{m}^2} \quad 3.5$$

The local or bulk fully developed Reynolds numbers were calculated from the measured mass flow rates:

$$Re = \frac{4\dot{m}}{\pi D_i \mu} \quad 3.6$$

with the viscosities, μ , determined at the local mean fluid temperature, $T(x)$, or at the bulk fully developed, b,FD temperature station as shown in Fig. 3.3(a).

The heat transfer rates, \dot{Q}_f , to the fluid were determined from the measured mass flow rates, \dot{m} , and the difference between the measured inlet and exit fluid temperatures:

$$\dot{Q}_f = \dot{m}C_p(T_e - T_i) \quad 3.7$$

The energy balance error, eb , was used to compare the measured heat transfer to the water, \dot{Q}_f , with the electrical energy supplied, $\dot{Q} = I\Delta V$, and is given as:

$$eb = \left[\frac{\dot{Q} - \dot{Q}_f}{\dot{Q}} \right] \times 100 \quad 3.8$$

where I and ΔV were the measured currents and voltage drops.

The heat flux, \dot{q}_f , was calculated as follows:

$$\dot{q}_f = \frac{\dot{Q}_f}{\pi D_i L} \quad 3.9$$

The heat transfer rate to the fluid, \dot{Q}_f , was used to determine the heat flux rather than the electrical power supplied, \dot{Q} , as the electrical power supplied was always a little larger than the heat transfer rate to the water, \dot{Q}_f , because of the heat losses from the test section. These heat losses were on average 2.5% and corresponded well to the theoretical determined heat losses (taking into consideration the resistance of the insulation material, average measured wall temperatures and the measured temperatures on the outside of the insulation wall).

The local heat transfer coefficients at any axial point, x , from the tube inlet were determined as:

$$h = \frac{\dot{q}_f}{T_{iw} - T(x)} \quad 3.10$$

where $T(x)$ was obtained from Eq. 3.1 and T_{iw} was the inner wall temperature obtained by taking into consideration the tube thermal resistance, R_w , as:

$$T_{iw} = T_{ow} - \dot{Q}_f R_w \quad 3.11$$

The outside wall temperatures, T_{ow} , were the average of the three thermocouple measurements at each station. The tube thermal resistance, R_w , was determined as:

$$R_w = \frac{\ln(D_o/D_i)}{2\pi k_w L} \quad 3.12$$

where D_o (6.3 mm) and D_i (5.1 mm) were the measured tube outer and inner diameters and k_w the thermal conductivity of the copper tube, which was 401 W/m.K [11].

These calculations showed that the temperature differences between the inside and outside walls were negligible and much smaller than the errors of the thermocouple measurements. Although these differences were taken into consideration in this study, for all practical purposes it could be assumed that the inner wall temperatures were equal to the measured outside wall temperatures.

From the local heat transfer coefficients, the local Nusselt numbers were calculated as:

$$Nu = \frac{hD_i}{k} \quad 3.13$$

The average Nusselt numbers of the fully developed part of the test section from $x = 3.47$ m (station 16 in Fig. 3.3) to $x = 4.52$ m (station 21) were obtained from calculating the averages of the local Nusselt numbers at the last six measuring stations.

Also determined were the Colburn j -factors:

$$j = \frac{Nu}{RePr^{\frac{1}{3}}} \quad 3.14$$

and the Grashof number, Gr , as:

$$Gr = \frac{g\beta\rho^2(T_w - T(x))D_i^3}{\mu^2} \quad 3.15$$

as well as the modified Grashof number, Gr^* , in terms of heat flux:

$$Gr^* = \frac{g\beta\rho^2\dot{q}_f D_i^4}{k\mu^2} \quad 3.16$$

The Rayleigh number, Ra , was determined from the product of the Grashof number and Prandtl number:

$$Ra = GrPr \quad 3.17$$

The average values of the Grashof numbers and Rayleigh numbers over the fully developed part of the test section were determined by averaging the last six values.

The Reynolds number at the start of the transitional flow regime, Re_{cr} , was obtained as prescribed by Everts and Meyer [21]:

$$Re = Re_{cr} \text{ when: } \left(\frac{dj}{dRe} \right)_{i-2:i} = 0 \quad 3.18$$

where $i-2:i$ means that at any given point i , dj/dRe was determined from the three data points at $Re(i-2)$, $Re(i-1)$ and $Re(i)$ for increasing Reynolds numbers. The Reynolds number at the end of the transitional flow regime, Re_{qt} , were defined as [21]:

$$Re = Re_{qt} \text{ when: } \left(\frac{d^2Nu}{dRe^2} \right)_{i:i+2} \geq -0.00015 \quad 3.19$$

where $i:i+2$ means that at any given point i , the dNu/dRe was determined from the three data points at $Re(i)$, $Re(i+1)$ and $Re(i+2)$ for increasing Reynolds numbers (while Eq. 3.18 used the results at the previous two Reynolds numbers).

The width of the transitional flow regime, ΔRe , and the transition gradient of the Colburn j -factors, TG_j , as recently defined by Everts and Meyer [21], were calculated using the Reynolds numbers and Colburn j -factors at the start and end of the transitional flow regime:

$$\Delta Re = Re_{qt} - Re_{cr} \quad 3.20$$

$$TG_j = \frac{j_{qt} - j_{cr}}{Re_{qt} - Re_{cr}} \quad 3.21$$

3.5. Experimental test matrix

Table 3.2 summarizes the matrix of experiments captured at various inclination angles between -90° to $+90^\circ$. A total of 1 288 mass flow rate measurements, 83 720 temperature measurements and 1 288 pressure drop measurements were conducted at 15 different inclination angles. In general, heat fluxes of 4, 6 and 8 kW/m² were used at all the different inclination angles, except for an additional case where a very small heat flux of 280 W/m² was used for forced convection

validation purposes. Furthermore, heat fluxes of 1 and 2 kW/m² were used for the horizontal and vertical orientations, only for forced convection comparison purposes. The last row of values in Table 3.2 was for isothermal flow conditions; thus, no heat was applied and the results were used for the isothermal pressure drop validation and comparison.

Furthermore, Table 3.3 summarizes the experiments that were conducted using different flow-calming sections, contraction ratios and inlet types. As the focus of this study was on transitional flow, experiments were only conducted between Reynolds numbers of 1 000 and 6 000. This ensured that the entire transitional flow regime was covered, as well as sufficient parts of the laminar and quasi-turbulent flow regimes for continuity, without getting too high water outlet temperatures (laminar flow) or high heat transfer coefficient uncertainties (turbulent flow). A total of 1 538 mass flow rate measurements, 99 970 temperature measurements and 1 538 pressure drop measurements were conducted. “Original” in Table 3.3 refers to the flow-calming section with full contents (such as shown in Fig. 3.2(a)) while “Empty” refers to the flow-calming section without contents inside (such as shown in Fig. 3.2(b)).

In general, from Table 3.2 and Table 3.3, a total of 2 679 mass flow rate measurements, 174 135 temperature measurements, 2 679 pressure drop measurements and 15 inclination angles were conducted for this study. It should be noted that the database (summarized in Table 3.2) collected for this study is approximately at least one to two orders of magnitude larger than that of previous studies for (vertical and inclined tubes) that varied from 36 [23] – 4 200 [123] temperature measurements, 5 [124] – 44 [125] pressure drop measurements, 2 [27] – 98 [24] mass flow rate measurements and 4 [23, 24, 26, 27] inclination angles. It can therefore be expected that with this big data base, it will be possible to generate much more phenomena than what was identified previously.

Table 3.2: Experimental test matrix for the different inclination angles.

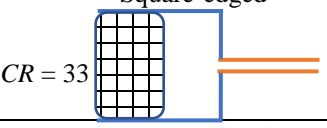
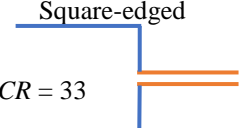
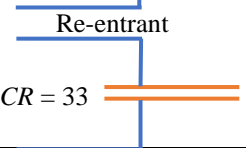
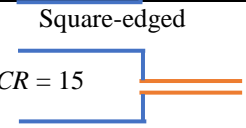
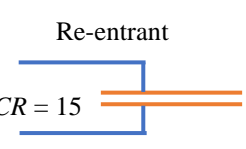
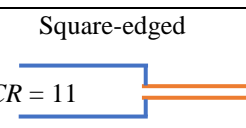
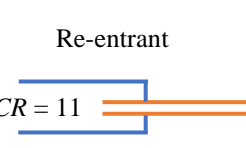
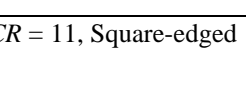
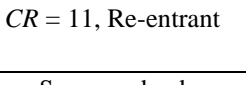
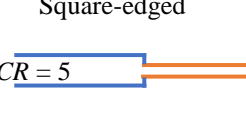
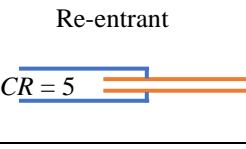
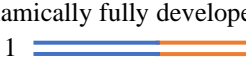

Inclination angle	Heat flux [kW/m ²]	Reynolds number range	Inclined tube Grashof number	Mass flow rate measurements	Temperature measurements ^a	Pressure drop measurements
+90°	1	250 – 2 922	$167 \leq Gr \leq 2\,036$	37	2 405	37
	2	375 – 2 049	$484 \leq Gr \leq 6\,382$	19	1 235	19
	4	1 086 – 5 892	$406 \leq Gr \leq 12\,719$	38	2 470	38
	6	1 571 – 5 778	$748 \leq Gr \leq 20\,139$	36	2 340	36
	8	2 153 – 5 985	$1\,077 \leq Gr \leq 24\,426$	36	2 340	36
+89°	6	1 495	335	1	65	1
+85°	6	1 484 – 5 708	65 – 1 613	35	2 275	35
+80°	6	1 507 – 443	134 – 2 735	32	2 080	32
+60°	4	1 084 – 5 588	215 – 4 875	39	2 535	39
	6	1 452 – 5 977	353 – 8 100	37	2 405	37
	8	1 928 – 5 822	540 – 9 982	38	2 470	38
+30°	4	1 106 – 5 818	371 – 7 058	39	2 535	39
	6	1 488 – 5 881	589 – 11 900	38	2 470	38
	8	1 950 – 5 859	972 – 15 906	36	2 340	36
0°	0.28 ^b	256 – 720	161 – 180	6	390	6
	1	919 – 2 771	176 – 895	23		23
	4	1 057 – 6 078	404 – 8 011	38	1 495	38
	6	1 451 – 6 082	677 – 14 235	36	2 340	36
	8	1 946 – 5 886	1 116 – 18 040	34	2 210	34
-30°	4	1 091 – 5 892	352 – 6 802	34	2 210	34
	6	1 423 – 5 709	646 – 12 678	35	2 275	35
	8	1 986 – 5 558	998 – 15 129	32	2 080	32
-60°	4	1 094 – 5 509	224 – 4 350	35	2 275	35
	6	1 512 – 5 616	359 – 7 361	34	2 210	34
	8	2 004 – 5 859	561 – 9 762	31	2 015	31
-80°	6	1 511 – 5 163	147 – 2 611	32	2 080	32
-85°	6	1 504 – 5 977	62 – 1 472	35	2 275	35
-87°	6	1 500	938	1	65	1
-88°	6	1 498	648	1	65	1
-89°	6	1 497	335	1	65	1
-90°	1	453 – 1 508	$554 \leq Gr \leq 1\,174$	14	910	14
	2	337 – 2 052	$881 \leq Gr \leq 8\,170$	18	1 170	18
	4	1 092 – 6 097	$397 \leq Gr \leq 12\,309$	37	2 405	37
	6	1 576 – 5 874	$777 \leq Gr \leq 21\,343$	37	2 405	37
	8	2 150 – 5 887	$1\,145 \leq Gr \leq 23\,602$	33	2 145	33
0°, ±30°, ±60°, ±90°	0 ^c	1 000 – 6 000	-	280	18 200	280
Total				1 288	83 720	1 288

^a Three thermocouples per station and two Pt100 probes (inlet and exit bulk temperatures).

^b Heat flux for forced convection validation experiments.

^c Isothermal experiments for pressure drop validation experiments.

Table 3.3: Experimental test matrix for the different flow-calming sections, contraction ratios and inlet types at horizontal orientation. Red indicates heating of the test section while blue identifies part of the flow-calming section without heating

Calming section	Contraction ratio (CR) and inlet type	Heat flux [kW/m ²]	Reynolds number	Mass flow rate measurements	Temperature measurements	Pressure drop measurements
Original	 Square-edged $CR = 33$	0	1 047 – 6 014	40	2 600	40
		4	1 057 – 6 078	37	2 405	37
		6	1 451 – 6 082	36	2 340	36
		8	1 946 – 5 886	34	2 210	34
Empty	 Square-edged $CR = 33$	0	1 045 – 5 706	39	2 535	39
		4	1 261 – 5 253	34	2 210	34
		6	1 592 – 5 749	33	2 145	33
		8	2 081 – 5 840	32	2 080	32
	 Re-entrant $CR = 33$	0	1 084 – 5 428	44	2 860	44
		4	1 075 – 5 568	35	2 275	35
		6	1 486 – 5 782	32	2 080	32
		8	1 906 – 5 583	30	1 950	30
Empty	 Square-edged $CR = 15$	0	1 015 – 5 259	36	2 340	36
		4	1 219 – 5 691	35	2 275	35
		6	1 546 – 5 868	33	2 145	33
		8	2 017 – 5 848	32	2 080	32
	 Re-entrant $CR = 15$	0	1 131 – 5 223	36	2 340	36
		4	1 220 – 5 433	34	2 210	34
		6	1 551 – 5 814	34	2 210	34
		8	2 061 – 5 913	33	2 145	33
Empty	 Square-edged $CR = 11$	0	1 098 – 5 705	37	2 405	37
		4	1 211 – 5 676	35	2 275	35
		6	1 451 – 5 899	34	2 210	34
		8	1 977 – 5 915	33	2 145	33
	 Re-entrant $CR = 11$	0	1 038 – 5 121	38	2 470	38
		4	1 211 – 5 717	34	2 210	34
		6	1 475 – 5 655	35	2 275	35
		8	2 059 – 5 884	33	2 145	33
Original	 $CR = 11$, Square-edged	0	1 026 – 5 032	36	2 340	36
		8	2 065 – 5 900	34	2 210	34
	 $CR = 11$, Re-entrant	0	1 131 – 5 428	37	2 405	37
		8	2 019 – 5 859	30	1 950	30
Empty	 Square-edged $CR = 5$	0	1 079 – 4 853	33	2 145	33
		4	1 092 – 5 354	33	2 145	33
		6	1 451 – 5 573	33	2 145	33
		8	2 007 – 5 759	32	2 080	32
	 Re-entrant $CR = 5$	0	1 032 – 5 164	37	2 405	37
		4	1 173 – 5 349	34	2 210	34
		6	1 477 – 5 196	32	2 080	32
		8	2 000 – 5 250	31	2 015	31
Empty hydrodynamically fully developed	 $CR = 1$	0	1 051 – 5 427	41	2 665	41
		8	1 866 – 5 886	36	2 340	36
Empty	 90° bend $CR = 1$	0	1 069 – 5 144	43	2 795	43
		8	1 865 – 5 870	38	2 470	38
Total				1 538	99 970	1 538

3.6. Uncertainties

All uncertainties were estimated within a 95% confidence level as prescribed by Dunn [126]. For the uncertainty analyses of this study, the manufacturer instrumentation errors were used as the fixed errors and two times the standard deviation of 400 data points as the random error. The thermocouples and Pt100 probes were calibrated against a reference thermometer with an accuracy of $\pm 0.03^\circ\text{C}$. The maximum Reynolds number uncertainty was found to be approximately 1.8%. The maximum friction factor uncertainty in the laminar region was 8.5% and it reduced to approximately 2.3% in the turbulent flow regime. In the transitional flow regime, the friction factor uncertainty increased to a maximum of 14%. This was due to fluctuations of the mass flow rates, temperatures and pressure drop measurements within the transitional flow regime [21].

The maximum Nusselt number uncertainties were 2.8%, 13%, and 5.8% respectively in the laminar, transitional and turbulent flow regimes at the maximum heat flux of 8 kW/m^2 . Again, the higher uncertainties in the transitional flow regime were caused by the higher fluctuations in the wall and exit temperature measurements. As the inclination angle increased from horizontal (0°) flow to the maximum inclination angle (vertical flow), the maximum Nusselt number uncertainty in the laminar flow regime decreased slightly to 2.3%. This was due to increase in temperature difference between the fluid and wall temperatures as the inclination angle increased. The uncertainties in the turbulent flow regime at vertical flow followed a similar trend with that of horizontal flow and were approximately the same. As expected in the transitional flow regime, due to the fluctuations of the measurements, the maximum Nusselt number uncertainty for vertical flow was 20%. Furthermore, as the heat flux decreased from 8 kW/m^2 to 1 kW/m^2 , all the uncertainties increased slightly, as expected, due to decrease in temperature difference between the bulk fluid and wall temperatures. At the lowest heat flux of 4 kW/m^2 , for all the inclination angles, the maximum Nusselt number uncertainties were 4.2%, 18%, and 12% respectively, in the laminar, transitional and turbulent flow regimes. All these uncertainties were for the original flow-calming section with the maximum contraction ratio of 33 (Fig. 3.2(a)). For all the contraction ratios (both empty and original flow-calming sections) used in this study, the uncertainties followed a similar trend in each flow regime. Furthermore, the re-entrant and square-edged inlets showed no significant effect on the uncertainties.

Although experiments were conducted at Reynolds numbers up to 6 000, the results showed that for this study, sufficient conclusions could be made for Reynolds numbers up to 4 000. At this Reynolds number the maximum Nusselt number uncertainties at a heat flux of 6 kW/m^2 for the horizontal and vertical inclination angles were 4.4% and 4.8% respectively. It has also been found that the Colburn j -factor uncertainties were for all practical purposes the same as that of the Nusselt number uncertainties.

3.7. Summary, conclusions and recommendations

The complete experimental set-up with flow-calming section and test section, as well as the experimental procedure and data reduction method were described in detail in this chapter. The test section was 4.6 m long and was made from a smooth hard drawn copper tube with measured inner and outer diameters of 5.1 mm and 6.3 mm, respectively. A 6 m long test bench was designed and built to accommodate the test section together with the different flow-calming sections, as well as the different inlet geometries and contraction ratios. The test bench was pivoted at the centre and supported at both ends so that it can be orientated at different inclination angles from vertical downward to vertical upward.

The wall temperatures were measured at 21 thermocouple stations, while the inlet and exit water temperatures were obtained from Pt100 probes placed inside the inlet and exit mixers, respectively. To measure the pressure drops, two pressure tap stations at a distance of 1 m apart were located within the fully developed region and corresponded closely to the last six temperature measuring stations. The flow-calming section, inlet section, test section, mixers and tubes were properly insulated and the maximum heat loss in the test section was estimated to be less than 2%.

Depending on the type of analysis, four different types of inlets namely; square-edged and re-entrant inlet with different inlet contraction ratios (5, 11, 14 and 33), as well as a hydrodynamically fully developed inlet and a 90° bend inlet were investigated. Experiments were conducted at various inclination angles from vertical upward flow (+90°) to vertical downward flow (-90°), with horizontal flow (0°) and several other angles in between. A total of 2 679 mass flow rate measurements, 174 135 temperature measurements and 2 679 pressure drop measurements were conducted using water (Prandtl numbers between 3.5 and 8.1) as the working fluid. The Reynolds number range covered were from 400 to 6 000 at constant heat fluxes varying from 1 to 8 kW/m².

The experimental procedure followed was to ensure steady-state conditions were reached before the data-capturing, by allowing adequate time for the first start-up and also between mass flow rate increments. Steady-state conditions were assumed once there were no significant changes in the mass flow rates, temperatures, pressure drops and the energy balance readings. A strong locking mechanism was used to ensure that the inclination angle did not change during experiments at different inclination angles.

An uncertainty analysis of the results was performed and found that the Reynolds number uncertainty was approximately constant and less than 1.8% in all the flow regimes. For the friction factors, the maximum uncertainties in the laminar, transitional and turbulent flow regimes were 8.5%, 14% and 2.3%, respectively. For the Nusselt numbers and Colburn j -factors, the maximum uncertainties at the lowest heat flux for all the inclination angles were 4.2%, 18%, and 12% respectively, in the laminar, transitional and turbulent flow regimes. As the heat flux increased, the uncertainties in all the flow regimes decreased. The maximum Nusselt number and Colburn j -

factor uncertainty in the laminar flow regime decreased slightly as the inclination angle increased from horizontal to vertical orientation, while in the turbulent flow regime, the uncertainties followed a similar trend for all the inclination angles. For all inlet geometries and contraction ratios (both empty and original flow-calming sections) used in this study, the uncertainties followed a similar trend in each flow regime.

4. Validation

4.1. Introduction

The purpose of this chapter is to validate the experimental set-up and data reduction method used. The heat transfer coefficients and friction factors are validated against well-known correlations published in the literature. Validation experiments were conducted for the smooth tube in a horizontal ($\theta = 0^\circ$ in Fig. 3.1) and vertical ($\theta = 90^\circ$ in Fig. 3.1) orientations with the original flow-calming section (Fig. 3.2(a)). The validation experiments consisted of isothermal friction factors (Section 4.2), local laminar Nusselt numbers for forced (Section 4.3) and mixed (Section 4.4) convection conditions, and the average Nusselt numbers in the turbulent flow regime (Section 4.5).

4.2. Isothermal Pressure drops

The pressure drop validation considered a total of 40 data points for decreasing Reynolds numbers from 6 000 to 1 000, thus spanning over the turbulent, transitional and laminar flow regimes. The laminar and turbulent isothermal friction factors were compared with the Poiseuille [127] ($f = 64/Re$) and Blasius [128] correlations respectively in Fig. 4.1. The fully developed friction factors were determined over the last part of the test section and the Reynolds number was determined at the centre between the two pressure taps (b, FD - station in Fig. 3.3(a)).

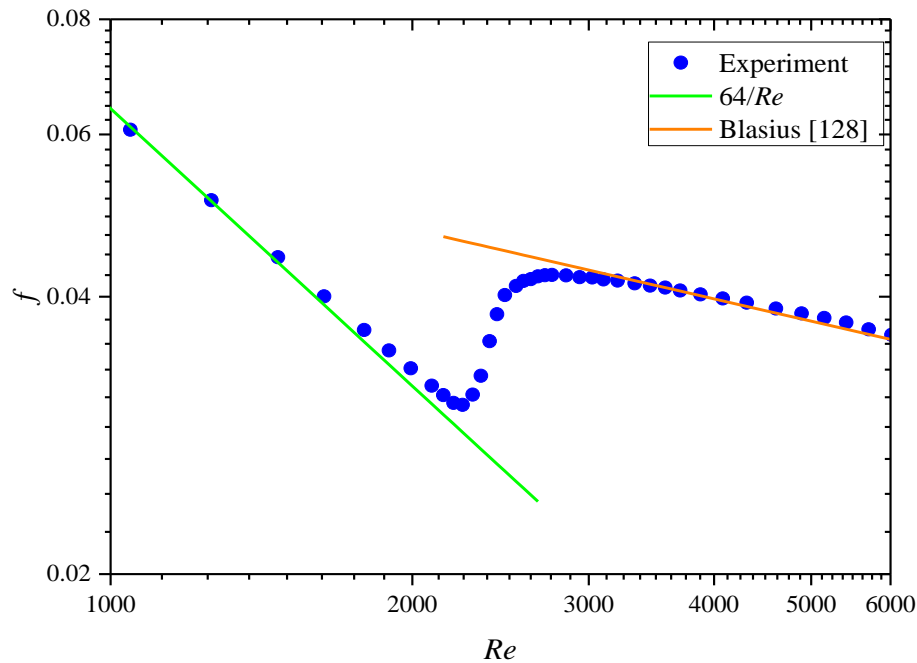


Fig. 4.1: Validation of the fully developed isothermal friction factors for horizontal flow with literature.

The laminar isothermal friction factors compared well with the Poiseuille correlation between Reynolds numbers of 1 000 and 2 200, with an average deviation of 2.7% and a maximum deviation of 5%. In the turbulent flow regime, the experimental data compared well with the Blasius [128] correlation between Reynolds number of 4 000 and 6 000, with an average deviation of 1% and a maximum deviation of 1.7%.

4.3. Laminar forced convection heat transfer

The local laminar Nusselt numbers at a very small heat flux of 280 W/m^2 and a bulk fully developed Reynolds number of 660 (with a corresponding Prandtl number of 5.18) are given in Fig. 4.2. According to the newly developed flow regime map of Everts and Meyer [9], forced convection conditions were expected. Fig. 4.2 indicates that the Nusselt numbers indeed converged to the theoretical value of 4.36 for a constant heat flux boundary condition, which confirmed that the flow was dominated by forced convection. The maximum uncertainty in the fully developed region was 17%.

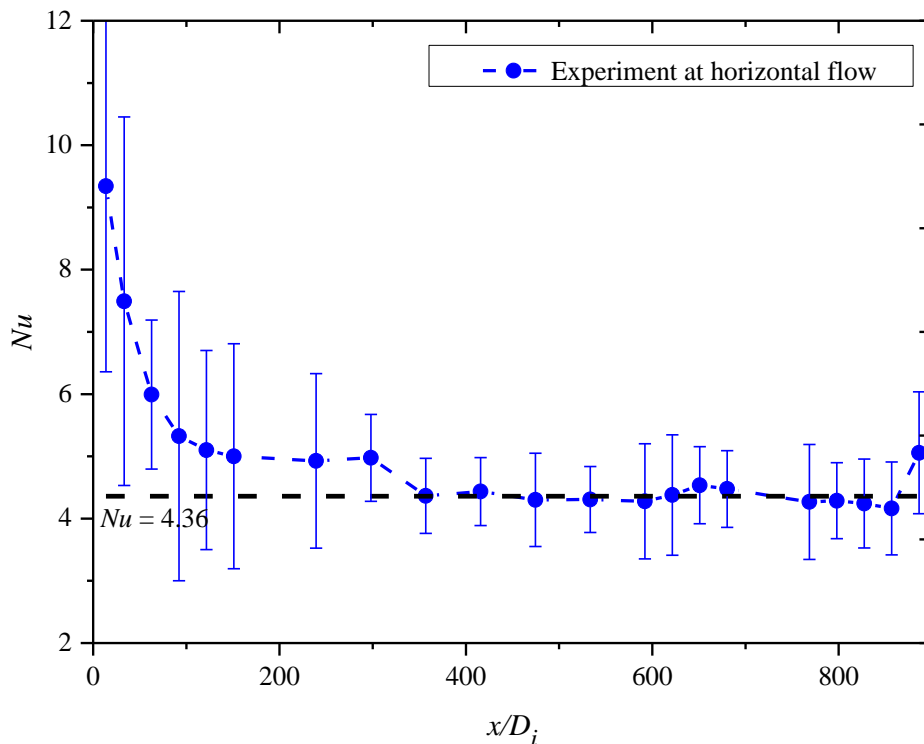


Fig. 4.2: Validation of the local laminar Nusselt numbers as a function of the axial position for forced convection conditions at a heat flux of 280 W/m^2 and bulk fully developed Reynolds number of 660.

The average Nusselt number between $x/D_i = 416$ and $x/D_i = 857$ in Fig. 4.2 was 4.39, which was within 0.7% of the value of 4.36. The last measuring points at $x/D_i = 886$ was excluded as it seemed as if the flow was influenced by the exit mixer. As this was also observed in previous studies [9, 18, 21, 40-42, 44, 47-50], it is recommended for future work that the distance between the last measuring station and the tube outlet/mixer be increased.

According to Meyer and Everts [18] a longer thermal entrance length is required when the flow is simultaneously hydrodynamically and thermally developing (as in this study), therefore a coefficient, C , of 0.12 instead of 0.05 was suggested in the correlation $L_t = CRePrD_i$. For the conditions in Fig. 4.2, the flow was thus expected to be fully developed at $x/D_i = 459$. Fig. 4.2 indicates that the flow was fully developed between $x/D_i = 357$ and $x/D_i = 416$, which was within 10% of $x/D_i = 459$. These results also show that the flow will be fully developed over the last part of the test section, between the two pressure taps PT-1 and PT-2 in Fig. 3.3. This is because the thermal entrance length for forced convection is the longest and it decreased with increasing buoyancy effects (mixed convection) [18] as the inclination angle increased (as will be shown in Chapter 5). Furthermore, it is known [11] that the hydrodynamic entrance length is less than the thermal entrance length for fluids with Prandtl numbers greater than one. It was therefore assumed that once the flow is thermally fully developed, it is also hydrodynamically fully developed.

To verify the start of the fully developed region for the vertical orientations, Fig. 4.3 compares the local Nusselt numbers in Fig. 4.2 at horizontal orientation, with the vertical upward and downward flow orientations. The vertical upward and downward results were at a bulk Reynolds number of 1 050 and a high heat flux of 4 kW/m². The solid black line represents the forced convection correlation of Shah and London [16].

Fig. 4.3 shows that the Nusselt numbers for both vertical and horizontal orientations decreased along the tube length in the developing region, as the thermal boundary layer developed, up to where the Nusselt numbers became relatively constant along the tube length from approximately $x/D_i = 416$, corresponding to the thermal entrance length. The flow was therefore fully developed from $x/D_i = 416$ for all the flow orientations in Fig. 4.3, where all the fully developed local Nusselt numbers were within 4.7% of the constant property Nusselt number of 4.36. The fully developed local Nusselt numbers for the vertical and horizontal flow orientations correlated very well with the correlation of Shah and London [16] with an average deviation of 4% and a maximum deviation of 8%.

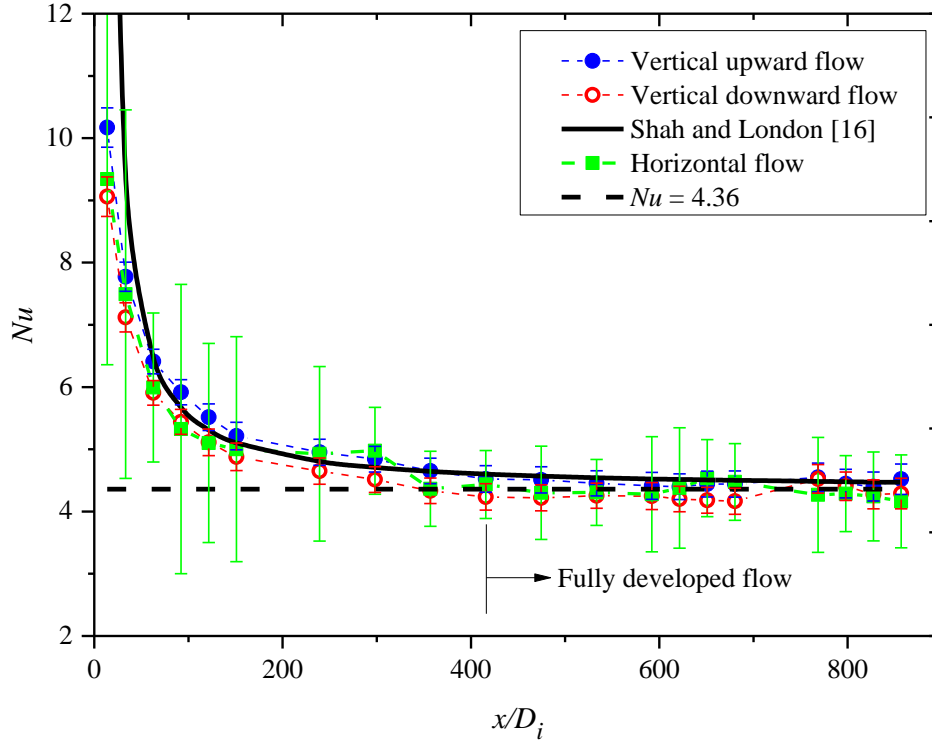


Fig. 4.3: Comparison of local Nusselt numbers as a function of the axial position for vertical and horizontal flow orientations. The horizontal tube is at a bulk Reynolds number of 660 and a very low heat flux of 280 W/m². The flows for vertical upward and vertical downward orientations are at a bulk Reynolds number of approximately 1 050 and a high heat flux of 4 kW/m².

To ensure that the flow in the fully developed region will always be fully developed, Fig. 4.4 compares the local Nusselt numbers along the axial location of the tube at a higher Reynolds number (close to the start of the transitional flow regime) and more heat fluxes than in Fig. 4.3, for both upward and downward flows. As expected, the Nusselt numbers decreased along the tube length and became relatively constant between $416 < x/D_i \leq 475$, indicating that the flow became fully developed. Therefore, Fig. 4.3 and Fig. 4.4 confirmed that for $x/D_i \geq 416$, the flow was fully developed for the horizontal, as well as the vertical upward and downward orientations. The last six thermocouple stations used for the fully developed analysis in this study were within $680 < x/D_i \leq 886$ (much longer than the thermal entrance length).

Fig. 4.3 and Fig. 4.4 show that the Nusselt numbers for horizontal flows, as well as vertical upward and downward flows, were approximately the same. The maximum difference of 8% was found in the developing region at $x/D_i \approx 122$ at a heat flux of 4 kW/m² in Fig. 4.4. However, once the flow was fully developed, the average and maximum differences were only 2% and 4%, respectively. Therefore, it was confirmed that tube orientation and flow direction had no influence on the laminar Nusselt numbers.

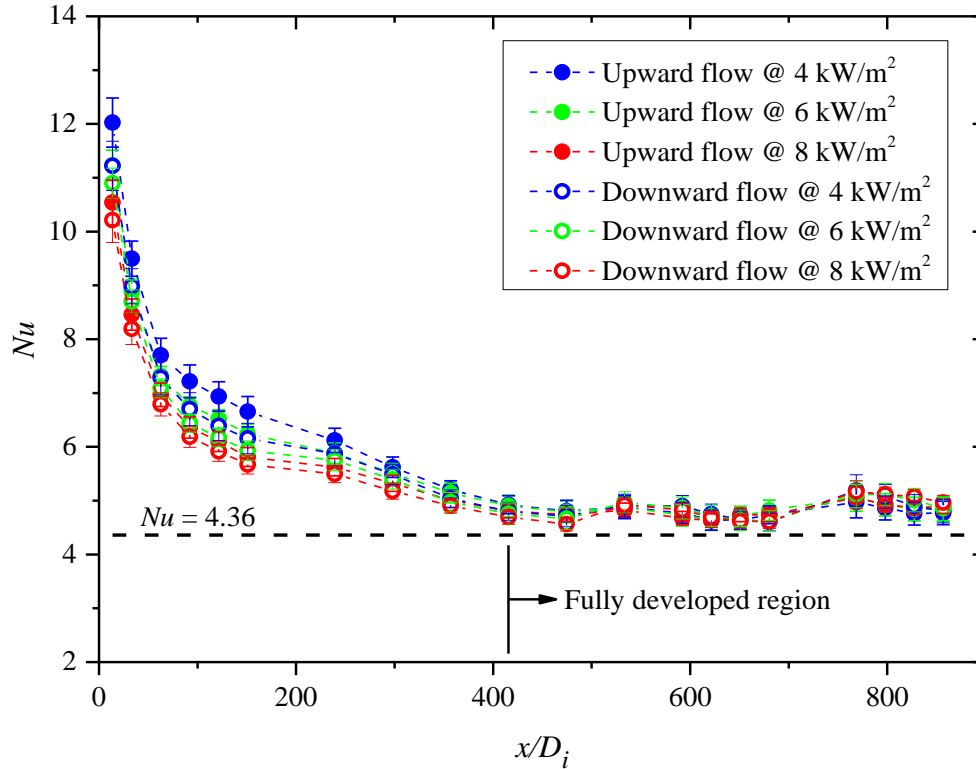


Fig. 4.4: Comparison of local Nusselt numbers as a function of the axial position at higher heat fluxes and a Reynolds number of approximately 2 100 for vertical upward and downward flows.

To investigate the effect of buoyancy on the wall temperatures, Fig. 4.5 compares the average wall temperature differences between the top and bottom of the test section, at the same heating condition, as a function of Reynolds number for vertical upward and horizontal flows. This figure indicates that for horizontal flow at a heat flux of 6 kW/m^2 , the minimum and maximum temperature differences varied between $0.12 - 0.16^\circ\text{C}$. This were greater than the thermocouple uncertainties, thus indicating the presence of buoyancy effects that caused secondary flow and mixed convection. This temperature difference decreased with an increase in Reynolds number for horizontal flow.

However, for the vertical upward flow, the corresponding wall temperature differences were approximately constant and were less than the uncertainty of the temperature measurements. This indicated the absence of buoyancy effects and hence confirmed forced convection heat transfer. This means that all the peripheral wall temperatures at a specific measuring station were approximately equal. Similar results were obtained with other heat fluxes and Reynolds numbers, as well as for downward flow. Because the upward and downward flow results were similar, it confirmed negligible buoyancy effects.

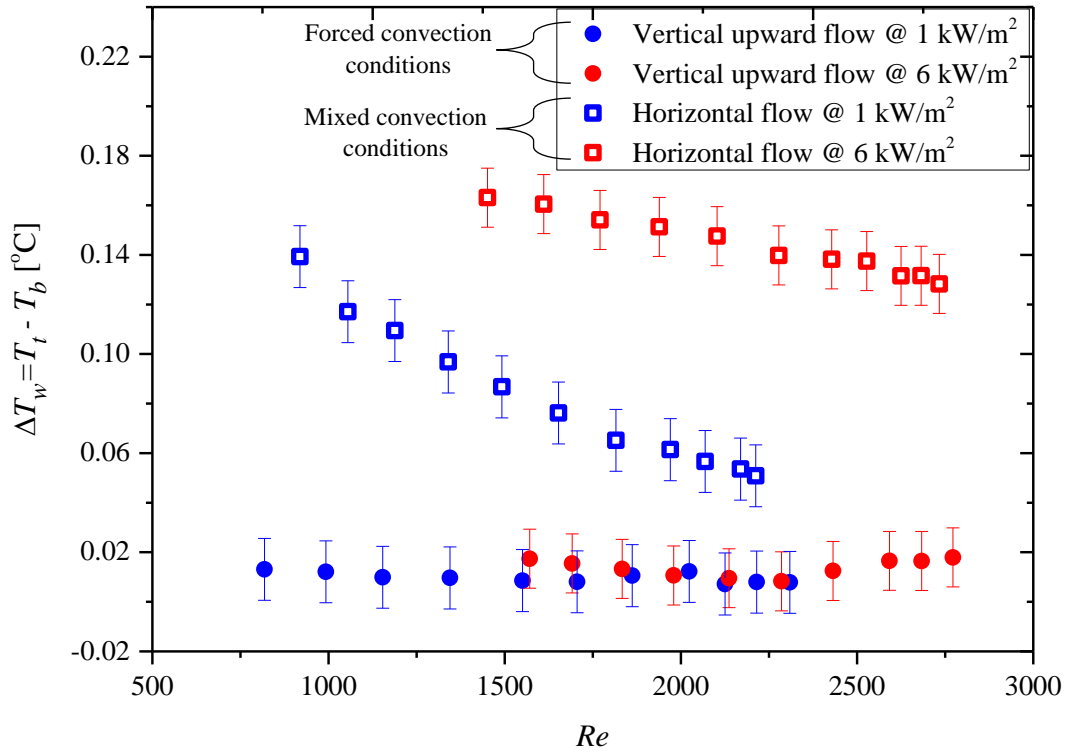


Fig. 4.5: Comparison of the average wall temperature differences between the top and bottom thermocouples for horizontal flow and vertical upward flow as a function of Reynolds number at different heat fluxes.

Furthermore, to confirm that forced convection conditions existed for all the fully developed local laminar heat transfer results of all the vertical upward and downward flows, the results were plotted on the flow regime map of Metais and Eckert [10] in Fig. 4.6. This flow regime map is valid for both vertical upward and downward flows in circular tubes with constant heat flux and constant wall temperature boundary conditions and for $0.01 < PrD_i/L < 1$. Fig. 4.6 show that all the results ($0.01 < PrD_i/L < 0.02$) of both upward and downward flows were within the laminar forced convection region. Again, confirming forced convection heat transfer for laminar vertical flow ($600 \leq Re \leq Re_{cr}$). Comparing the Richardson number, which is the ratio of buoyancy forces to viscous forces (Gr/Re^2), also confirmed forced convection conditions, because all the Richardson numbers were less than 0.1 ($0.0001 \leq Ri \leq 0.01$).

Although the experimental set-up was not developed for Reynolds numbers below approximately 300 (because of the range limitations of the Coriolis mass flow meters), limited experiments were conducted at lower Reynolds numbers. It was found from the heat transfer results that at Reynolds

numbers of 400 and 600, assisting and opposing flows became significant and the Nusselt numbers decreased significantly.

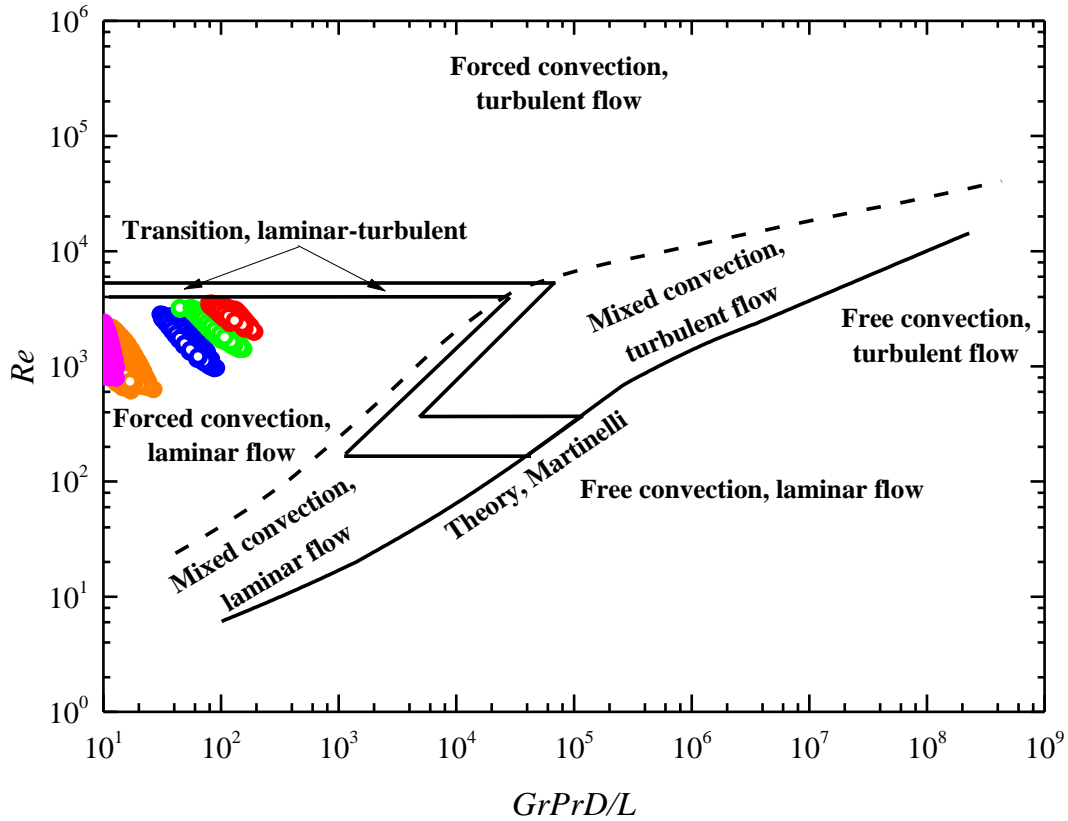


Fig. 4.6: Comparison of the laminar forced convection results on the flow regime map of Metais and Eckert [129] for heat fluxes of 1 kWm^2 (pink), 2 kWm^2 (orange), 4 kWm^2 (blue), 6 kWm^2 (green) and 8 kWm^2 (red) for both vertical upward and downward flow at all the axial locations in the fully developed region ($416 < x/D_i < 857$).

4.4. Laminar mixed convection heat transfer

The local Nusselt numbers at a heat flux of 6 kW/m^2 , bulk Prandtl of 3.29, bulk Reynolds number 1 450, and a modified Grashof number of 109 264, were compared with the correlations of Morcos and Bergles [130] and Meyer and Everts [18] in Fig. 4.7. For all the experiments conducted, the modified Grashof numbers ranged between 2 393 and 119 452, which varied by two orders of magnitude. According to the flow regime map of Everts and Meyer [9], the flow was expected to be dominated by mixed convection. This was confirmed by the measurements, because the Nusselt numbers were much higher than 4.36. For instance, at the highest heat flux of 8 kW/m^2 , the Nusselt numbers increased by 86% from the forced convection Nusselt number of 4.36, to a Nusselt number of 8.1 at horizontal orientation, which indicate a significant heat transfer enhancement due

to buoyancy effects and thus mixed convection. Furthermore, the results also correlated well with the correlation of Meyer and Everts [18] with an average deviation of 4% and maximum deviation of 7%.

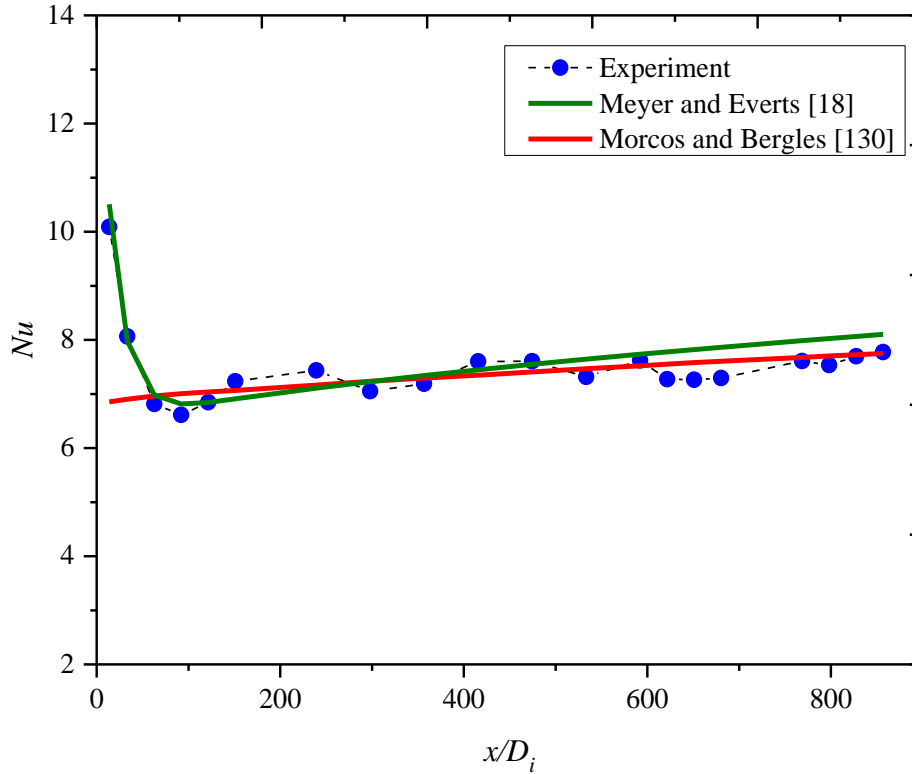


Fig. 4.7: Validation of the local Nusselt numbers as a function of the axial position for mixed convection conditions at a heat flux of 6 kW/m² and bulk Reynolds number of 1 450.

Although the correlation of Morcos and Bergles [130] was developed for tube wall parameters, $P_w = kD_i/(k_w t)$, between 2 and 66, it varied in this study between 0.0133 and 0.0138, which was far outside the specified range for which the correlation was developed. However, the average deviation between the experimental results and the correlation of Morcos and Bergles [130] was 2.6%, and the maximum deviation was only 5%. It therefore seemed as if the correlation of Morcos and Bergles [130] were valid for a much wider range of tube wall parameters than they have specified. This was also found by Meyer and Everts [18].

4.5. Turbulent flow

The average Nusselt number of the fully developed part of the test section in the turbulent flow regime were compared with the correlations of Gnielinski [131] and the newly developed correlations of Meyer *et al.* [132] in Fig. 4.8. The results compared well with the correlations of Gnielinski [131] and Meyer *et al.* [132] with average deviations of 6.1% and 5.6% respectively

and maximum deviations of 13% and 8.6% respectively. Although it is not shown in this thesis, the comparison of the Colburn j -factors with the literature was found to be approximately the same with that of the Nusselt numbers for all the flow regimes. In general, the deviations between the experimental results and literature were larger in the turbulent flow regime than in the laminar flow regimes. This was as expected, because the temperature differences between the wall and fluid decreased with increasing Reynolds numbers, which led to increased uncertainties.

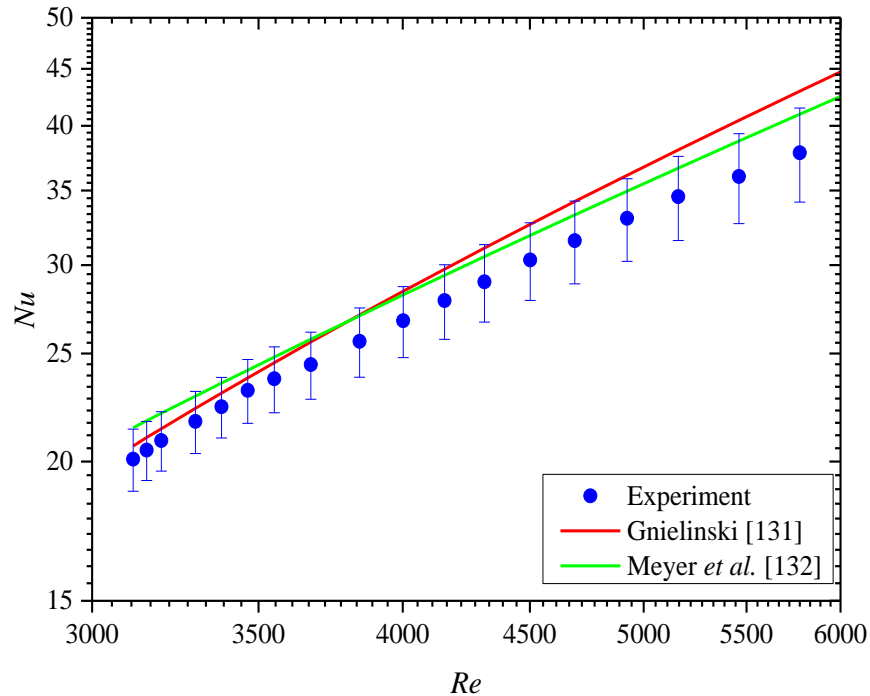


Fig. 4.8: Comparison of the average fully developed turbulent Nusselt numbers as function of Reynolds number with literature. The Nusselt numbers were the average over the fully developed part and the Reynolds number was determined at the b,FD -point identified in Fig. 3.3.

4.6. Conclusions and recommendations

The experimental set-up and data reduction method were validated against the literature in this chapter. The heat transfer coefficients and friction factors were compared against well-known correlations with the test section at horizontal and vertical orientations. The validation included the isothermal friction factors, local laminar Nusselt numbers for forced and mixed convection conditions, as well as the average Nusselt numbers in the turbulent flow regime.

The fully developed laminar isothermal friction factors correlated well with literature between Reynolds numbers of 1 000 and 2 200, with an average deviation of 2.7%. In the turbulent flow regime, the average deviation from literature was 1%.

It was confirmed that at a very small heat flux of 280 W/m^2 and a bulk fully developed Reynolds number of 660 (with a corresponding Prandtl number of 5.18), forced convection conditions dominated the flow in the test section during horizontal orientations. It was also found that at this condition, the flow was fully developed from $x/D_i = 416$ and the average Nusselt number between $x/D_i = 416$ and $x/D_i = 857$ was 4.39, which was within 0.7% of the value of 4.36. Similarly, for all the vertical upward and downward flows, the flow became fully developed from $x/D_i = 416$. At a Reynolds number of 1 050 and a heat flux of 4 kW/m^2 , all the fully developed local Nusselt numbers for the vertical upward and downward flows correlated very well with the literature and were within 4.7% of the constant property Nusselt number of 4.36. Therefore, it was confirmed that forced convection conditions existed for all the fully developed local laminar heat transfer results of all the vertical upward and downward flows, for all the heat fluxes and Reynolds numbers higher than 600.

For the laminar mixed convection heat transfer validations, the results were compared for the test section in a horizontal orientation and the local Nusselt numbers correlated well with the literature with an average deviation of 4%. In the turbulent flow regime, the average Nusselt number of the fully developed part of the test section correlated very well with the literature with an average deviation of 6.1%.

Therefore, the validation experimental results presented in this chapter, compared very well with the literature. It can therefore be concluded that the experimental set-up and data reduction method could produce reliable results.

5. Mixed convection heat transfer and pressure drop

5.1. Introduction

This chapter investigates the effect of inclination angle on the mixed convection heat transfer and pressure drop characteristics. The comparison of heat transfer and pressure drop results were made as function of inclination angle and the results were used to investigate the direct relationship between inclination angle and buoyancy force. The general notation in most graphs in this chapter where inclination angles were used, was that the square (blue) markers represented horizontal flow, while the other inclination angles were represented by solid circle markers for upward flow, and empty circle markers for downward flow. The results were always for fully developed flow (Sections 5.2 and 5.3), except when otherwise stated. Therefore, the Reynolds numbers were always at the b,FD point as shown in Fig. 3.3(a). Local Reynolds numbers were only used in Section 5.4. Most of the results (except where otherwise stated) were given at a heat flux of 6 kW/m^2 as the uncertainties at this heat flux were the lowest. The same trends were observed at the other heat fluxes as well, therefore the same conclusions could be made. Correlations to determine the laminar heat transfer coefficients and friction factors for all inclination angles were also developed.

5.2. Fully developed flow pressure drop

5.2.1. Isothermal friction factors

Fig. 5.1 compares the isothermal fully developed friction factors as a function of Reynolds number for inclination angles from -90° (downward) to $+90^\circ$ (upward). For comparison purposes, the Poiseuille ($64/Re$) [127] and Blasius [128] correlations for laminar and turbulent flow respectively, were also included. As expected, Fig. 5.1 indicates that there were no significant differences between the friction factors obtained at different inclination angles and all the results were within the measurement uncertainties. The start and end of the transitional flow regime were also the same for all inclination angles. In the laminar flow regime, the magnitude of all the friction factors of the different inclination angles were approximately equal and within 5% deviation from $64/Re$. Similarly, in the quasi-turbulent and turbulent flow regimes, the friction factors of the different inclination angles were all within a 1.7% deviation from the Blasius [128] correlation.

Although the uncertainties in the transitional flow regime were higher, due to the mass flow rate and pressure drop fluctuations, there was no significant difference between the friction factors obtained at different inclination angles. This is because the same flow-calming section and inlet geometry were used and there were no temperature differences in the tube that could lead to

buoyancy forces that influence the mechanism of transition. The transitional flow regime started at a Reynolds number of approximately 2 260 for all the inclination angles. These results were as expected, but were necessary for comparison purposes.

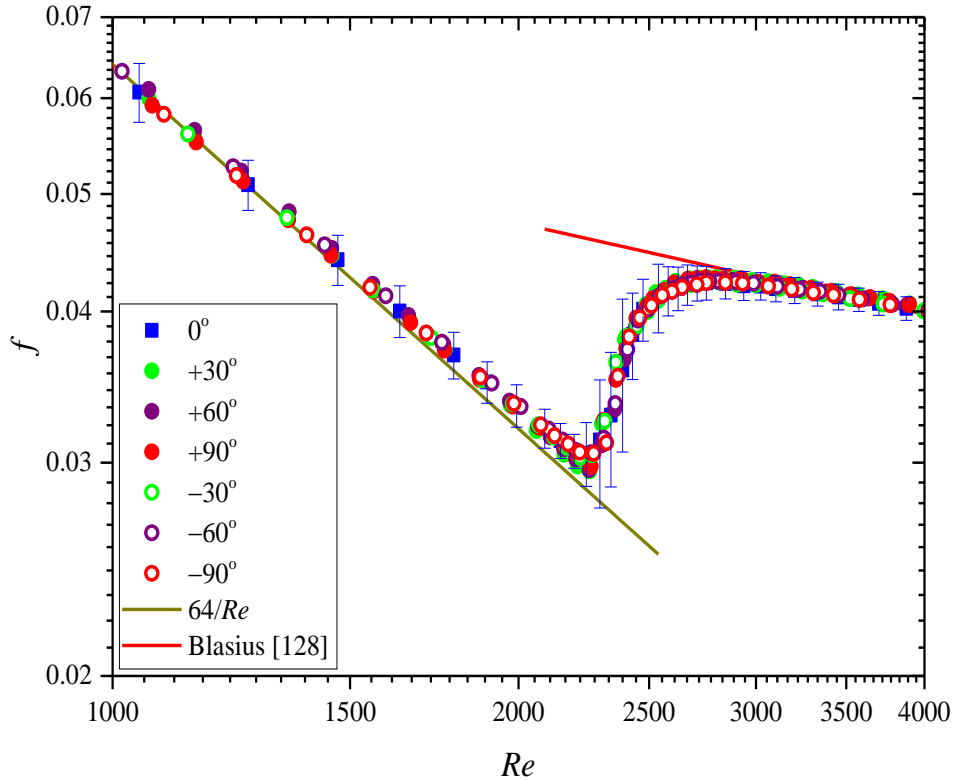


Fig. 5.1: Fully developed isothermal friction factors as a function of Reynolds number for different inclination angles in the upward and downward flow directions.

5.2.2. Diabatic friction factors

Fig. 5.2 shows the friction factors at a heat flux of 6 kW/m² for different inclination angles as a function of Reynolds number. In the laminar flow regime, the friction factors of horizontal flow ($\theta = 0^\circ$) were on average 15% higher than the Poiseuille ($64/Re$) correlation. This corresponds well to findings of Ghajar and Tam [20] and Everts and Meyer [40]. Although the viscosity shear forces on the heated wall decreased with an increase in temperature, secondary flow due to the buoyancy forces led to increased friction factors [40].

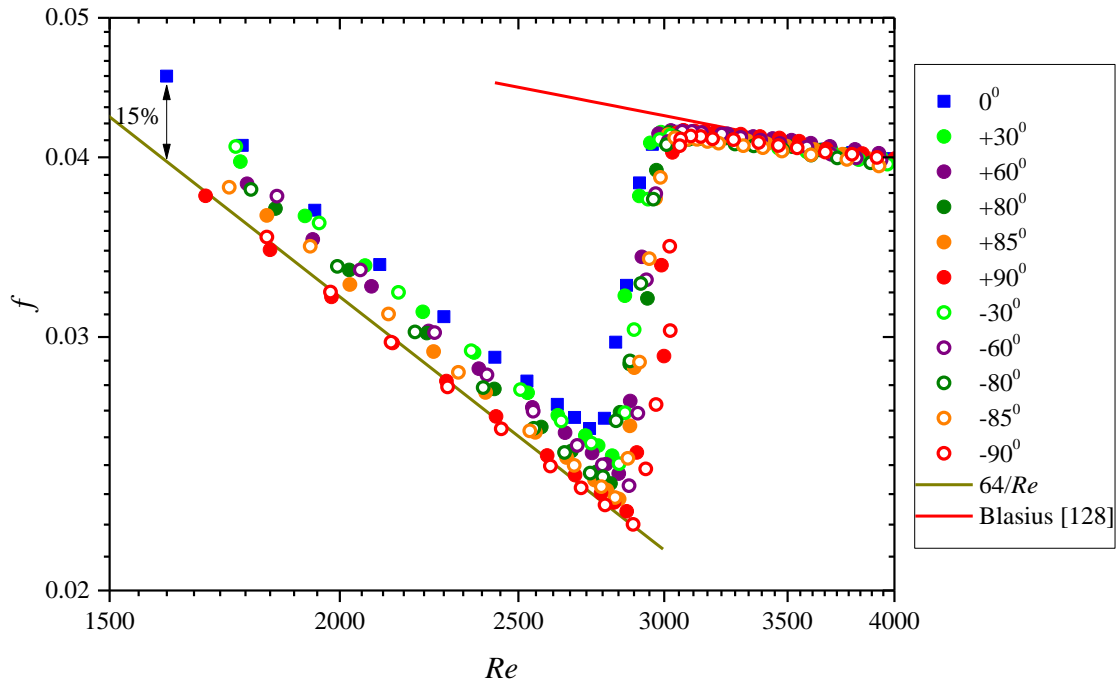


Fig. 5.2: Comparison of fully developed diatomic friction factors as a function of Reynolds number for different inclination angles at a heat flux of 6 kW/m^2 .

Fig. 5.2 also indicates that the laminar friction factors decreased with the absolute value of the inclination angle, $|\theta|$, and that the friction factors were a symmetric function of inclination angle. Thus, the friction factors for an inclination angle of -30° (downward) were the same as for an inclination angle of $+30^\circ$ (upward). The vertical upward and downward flow friction factors were the lowest and corresponded closer to the forced convection friction factors predicted by the Poiseuille correlation ($64/Re$).

In Fig. 5.3(a), the friction factors were given as function of inclination angle for five Reynolds numbers varying from 1 800 – 2 700. For clarification, the y-scale scale for a Reynolds number of 2 600 has been enlarged in Fig. 5.3(b) to more clearly show that the friction factors for a specific angle, such as $+30^\circ$ upward, corresponded very well to the same angle of -30° downward. Furthermore, the friction factors for vertical upward flow ($\theta = +90^\circ$) and vertical downward ($\theta = -90^\circ$) flow converged to the forced convection and isothermal results of $f = 64/Re$. For flow at a specific laminar Reynolds number in a horizontal ($\theta = 0^\circ$) heated tube, the friction factor was significantly higher than the isothermal friction factor.

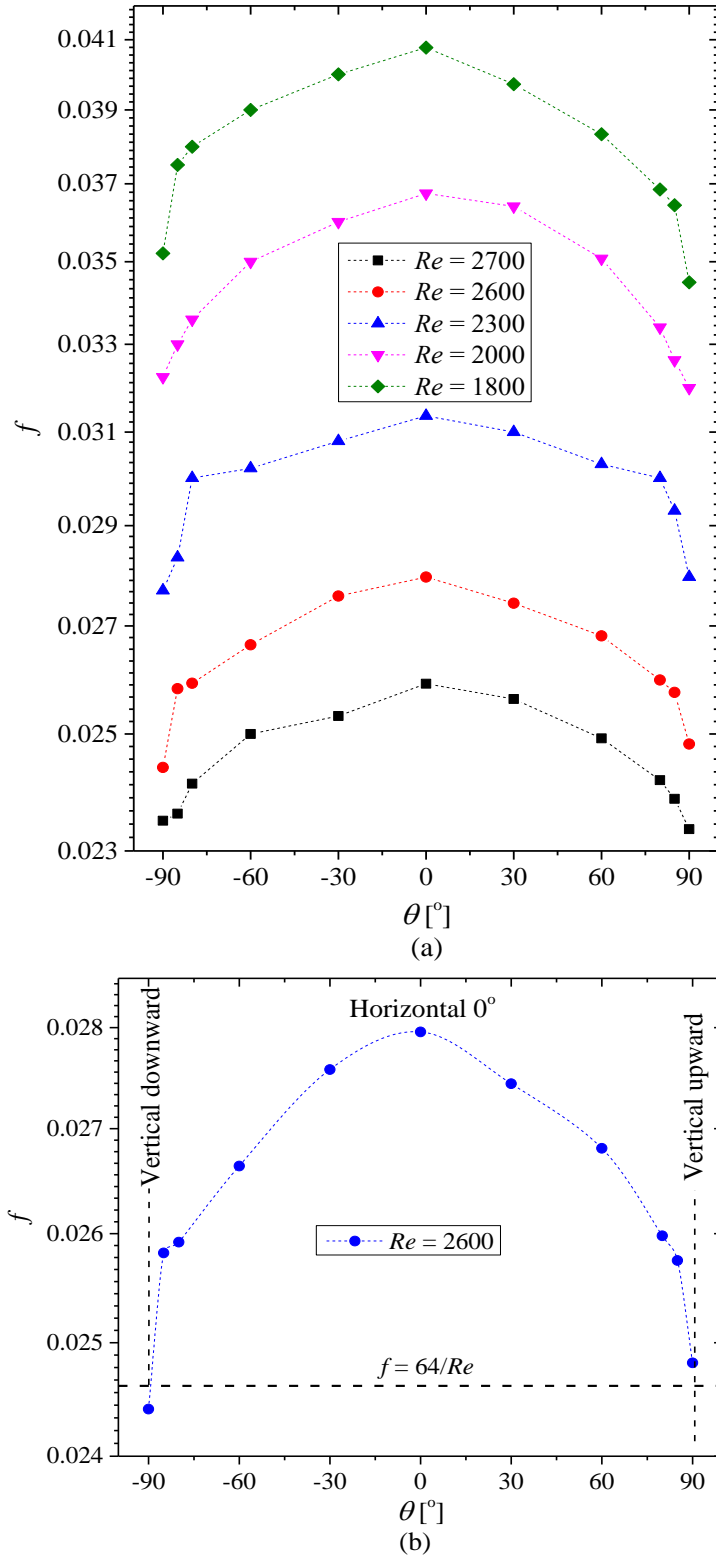


Fig. 5.3: Comparison of fully developed diatomic friction factors at a heat flux of 6 kW/m^2 as a function of inclination angle at (a) different Reynolds numbers and (b) Reynolds number of 2 600.

It can therefore be concluded that buoyancy effects were the greatest for the tube in a horizontal configuration ($\theta = 0^\circ$) and decreased with changes in the inclination angle (either upward or downward inclination angle). Hence, an increase in the absolute value of the inclination angle, $|\theta|$, decreased the buoyancy effects and therefore the laminar friction factors decreased accordingly. Furthermore, for the purposes of this study, vertical flow (upward or downward) could be considered as pure forced convection when the Reynolds number was higher than 600, as shown in Section 4.3. Fig. 5.3 also indicates that the increase in inclination angle from 60° to 90° , led to a greater decrease in friction factors than when the inclination angle was increased from 0° to 30° . Therefore, the decrease in the buoyancy force was more significant near vertical inclination angles than near horizontal inclination angles.

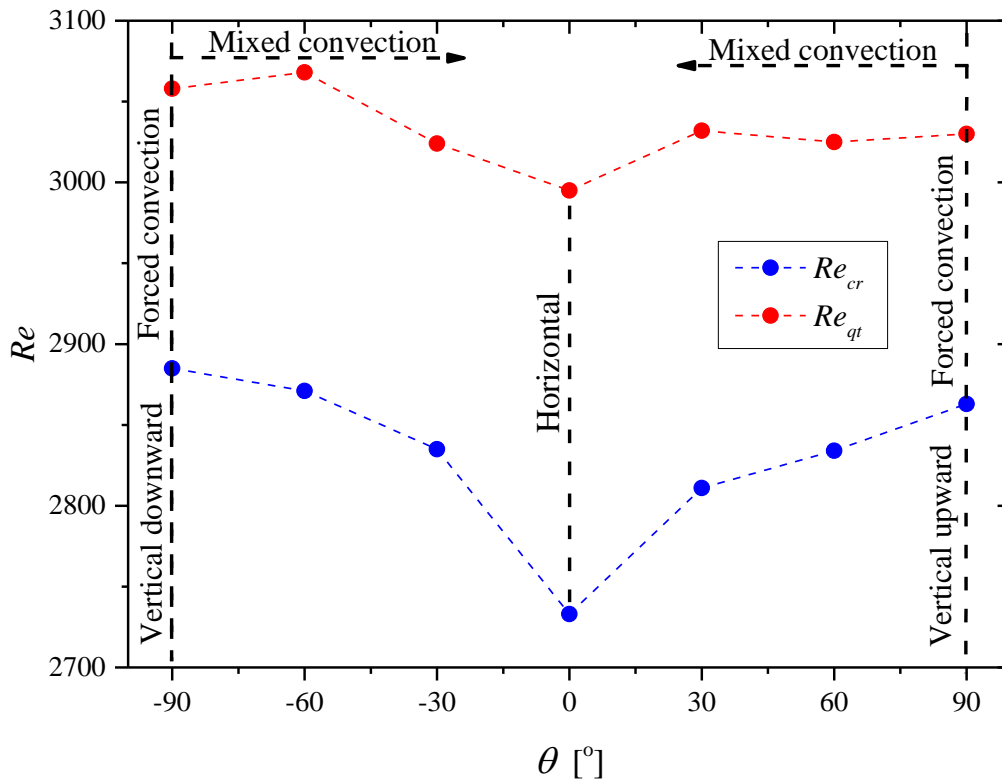


Fig. 5.4: Reynolds numbers at which the transitional flow regime started (Re_{cr}) and ended (Re_{qt}) as a function of inclination angle for the diabatic friction factors in Fig. 5.2 at a heat flux of 6 kW/m^2 .

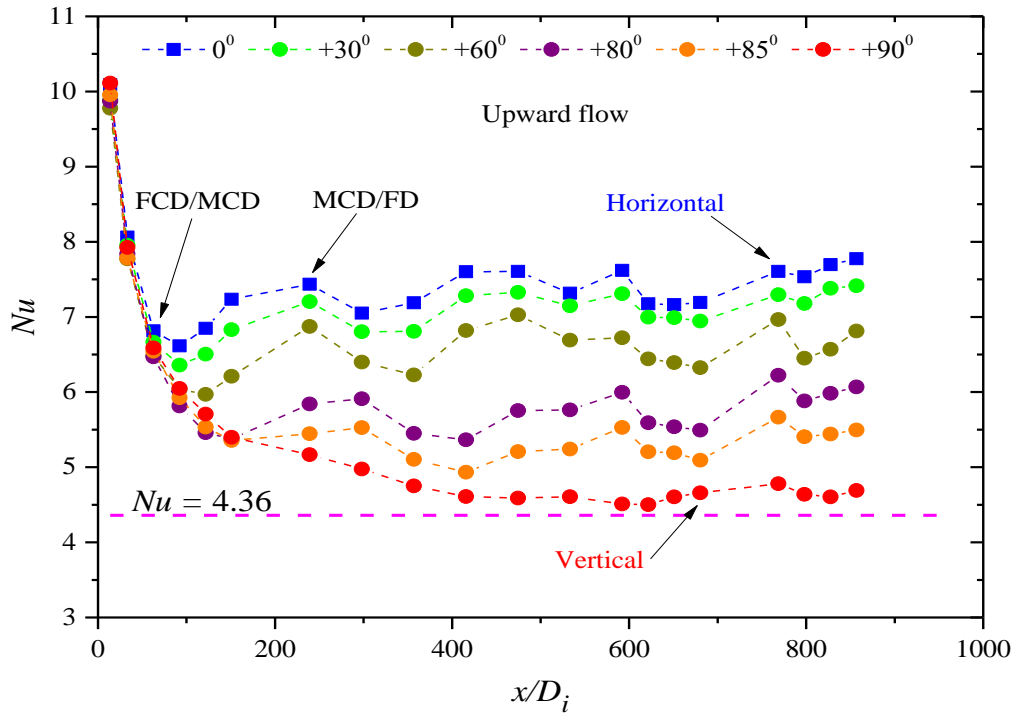
The Reynolds numbers at which the transitional flow regime started (Re_{cr}) and ended (Re_{qt}) in Fig. 5.2 were compared as a function of inclination angle in Fig. 5.4. The transitional flow regime started at a Reynolds number of 2 733 for $\theta = 0^\circ$, but was delayed to a Reynolds number of approximately 2 885 when the inclination angle was increased to vertical upward and downward flow. Although both the Reynolds numbers at which the transitional flow regime started and ended increased with increasing inclination angle, the increase was significantly more for the critical Reynolds numbers (Re_{cr}) and Re_{qt} was considered to be approximately constant. This is because buoyancy effects were greater at the start of the transitional flow regime (near the laminar flow regime where the buoyancy effects were a maximum) than at the end of the transitional flow regime (near the quasi-turbulent flow regime where the buoyancy effects were negligible). This also explains why the differences in friction factors for the different inclination angles in Fig. 5.2 were more at the start of the transitional flow regime than near the end of the transitional flow regime.

5.3. Fully developed flow heat transfer

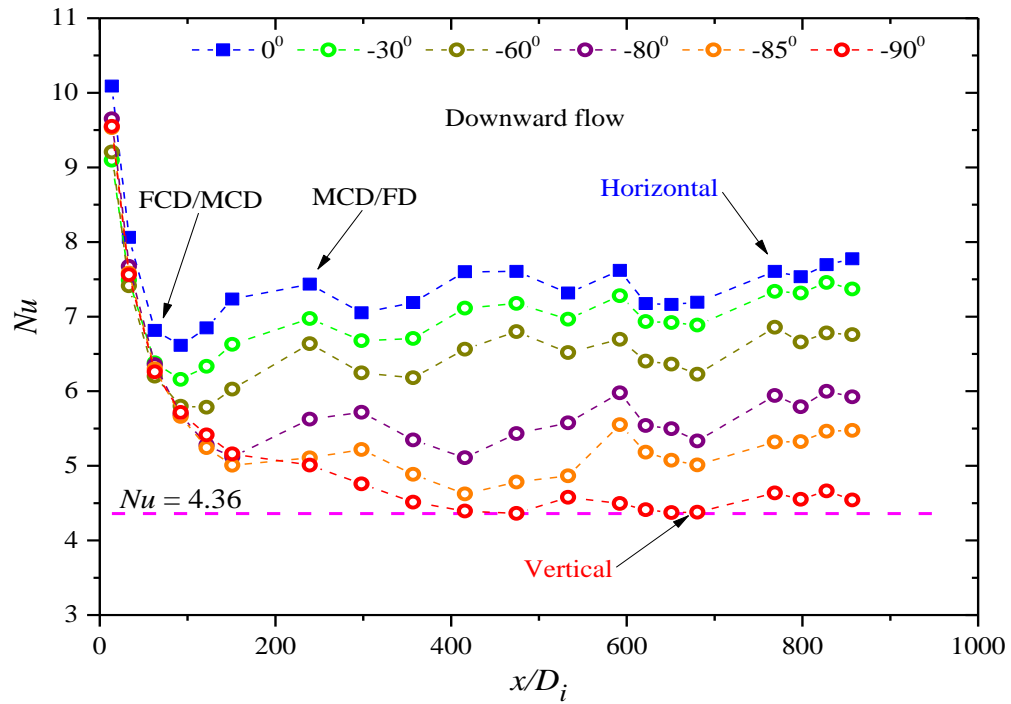
5.3.1. Laminar flow

The local Nusselt numbers at different inclination angles were plotted as a function of axial location at a bulk Reynolds number of 1 600 for upward flow in Fig. 5.5(a) and downward flow in Fig. 5.5(b). The constant property forced convection Nusselt number of 4.36 for a constant heat flux is indicated by the black dotted line. In general, six conclusions can be made from Fig. 5.5:

- i. The flow could be considered as fully developed at $x/D_i \approx 416$. This confirmed that the flow was fully developed between the two pressure taps at $x/D_i = 680$ and $x/D_i = 886$ for the all inclination angles.
- ii. The horizontal ($\theta = 0^\circ$) fully developed Nusselt number was 7.5 on average, which was within 4.8% of the fully developed Nusselt number value of 7.9 predicted using the correlation of Meyer and Everts [18].
- iii. The Nusselt numbers for vertical upward flow ($\theta = +90^\circ$) and vertical downward flow ($\theta = -90^\circ$) converged to the same theoretical forced convection value of 4.36. The Nusselt numbers for vertical upward and downward flow were within 5.7% and 5.3% respectively, of 4.36.
- iv. Similar to the friction factors in Fig. 5.3, the Nusselt numbers decreased with increasing inclination angle. The Nusselt number enhancement for the other inclination angles compared with vertical flow could therefore only be because of mixed convection.



(a)



(b)

Fig. 5.5: Comparison of the local laminar Nusselt numbers as a function of the axial position for different inclination angles at a bulk Reynolds number of approximately 1 600 and a heat flux of 6 kW/m² for (a) upward flow and (b) downward flow.

- v. The three regions (Forced Convection Developing (FCD), Mixed Convection Developing (MCD) and Fully Developed (FD)) which were recently defined by Meyer and Everts [18] for mixed convective laminar flow, were also observed in Fig. 5.5, based on the different inclination angles. For horizontal flow, the laminar Nusselt numbers decreased along the tube length up to $x/D_i = 63$. Between $x/D_i = 63$ and $x/D_i = 239$, buoyancy effects became significant which caused the Nusselt numbers to increase along the tube length due to the increasing thermal boundary layer thickness [18]. The Nusselt numbers became approximately constant after $x/D_i = 239$, which indicated that the flow was fully developed. The FCD/MCD boundary occurred at $x/D_i = 63$ for horizontal flow, but was delayed to $x/D_i = 92$, $x/D_i = 122$ and $x/D_i = 151$ as the inclination angle was increased to 30° , 60° and 80° respectively. This is as expected, because Meyer and Everts [18] found that the FCD/MCD boundary occurred earlier (in terms of axial position) with increasing buoyancy effects and it is known from Fig. 5.3 and Fig. 5.5 that buoyancy effects decreased with increasing inclination angles. The axial position of the MCD/FD boundary also increased with increasing inclination angles, which confirmed that buoyancy effects decreased the thermal entrance length [18]. Furthermore, as indicated by Meyer and Everts [18], buoyancy effects caused the Nusselt numbers in the MCD and FD regions to increase, which explains why the laminar Nusselt numbers in Fig. 5.5 decreased with increasing inclination angle.
- vi. Similar to the friction factors in Fig. 5.3, the Nusselt number results were symmetric around the inclination angle of 0° . Thus, the results of -30° and $+30^\circ$, -60° and $+60^\circ$, etc. were all the same.

To prove the symmetry around the inclination angle of 0° , Fig. 5.6 compares the average fully developed Nusselt numbers as a function of inclination angle at approximately the same bulk fully developed Reynolds numbers (for instance at a Reynolds number of approximately 1 600, the bulk Reynolds number at $\theta = 0^\circ$ was 1 610 and at $\theta = -90^\circ$ was 1 580). This figure indicates that in general the Nusselt numbers increased with decreasing $|\theta|$ due to increased buoyancy effects. At a 30° increment from the vertical orientation (i.e. from 90° to 60°) the Nusselt numbers at a Reynolds number of 1 600 increased by 44%, while for a 30° increment from 30° to 0° , the increase was only 4%. Therefore, similar to the diabatic friction factors in Fig. 5.3, small changes in inclination angle near vertical flows led to significant changes in the buoyancy effects.

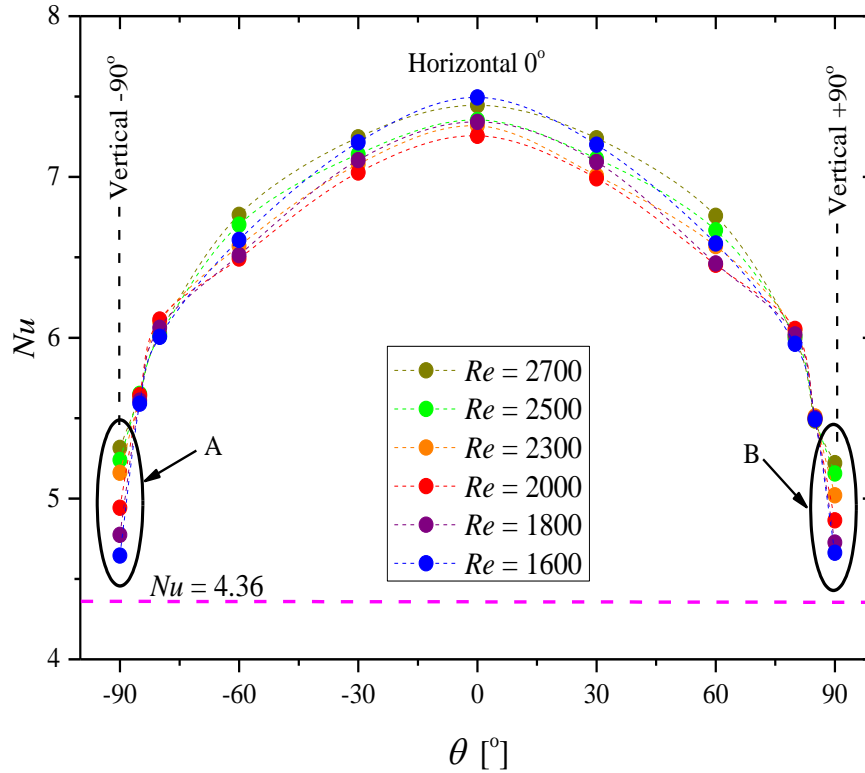


Fig. 5.6: Average Nusselt numbers as a function of inclination angle for fully developed laminar flow at different bulk Reynolds numbers and a heat flux of 6 kW/m².

To clarify the decreasing buoyancy effects with increasing inclination angle, the free body diagrams showing the components of buoyancy forces acting on the fluid flow for different tube orientations are given in Fig. 5.7. For horizontal flow (Fig. 5.7(a)), the buoyancy forces act perpendicular to the flow axis and therefore create the maximum disturbances within the flow, in the form of secondary flow [133]. This distorts the thermal boundary layer by decreasing its thickness and thereby enhancing the heat transfer. As indicated in Fig. 5.7(d), the buoyancy force, F_b , is a maximum when the tube is in a horizontal orientation as $\cos\theta = 1$ for $\theta = 0^\circ$. At inclined angles (Fig. 5.7(b)) the magnitude of the buoyancy force ($F_b \cos\theta$) decreases with $\cos\theta$ and reaches a minimum for vertical upward and downward flow (Fig. 5.7(c)). For vertical flow, the inertia forces dominate the buoyancy forces. A similar behaviour was also observed by Tian *et al.* [91] in a narrow rectangular channel where mixed convection was induced at different inclination angles (near vertical inclination angles between 60° to 90°). For each Reynolds number of the vertical inclination angles ($\pm 90^\circ$), identified as A and B in Fig. 5.6, the Nusselt number increased as function of Reynolds number. This increase was more significant for vertical flow than at other inclination angles. As will be shown in Chapter 6, for Reynolds number higher than approximately

1 000, the laminar heat transfer coefficients in vertical tubes were a function of Reynolds number and independent of flow direction, buoyancy and heat flux.

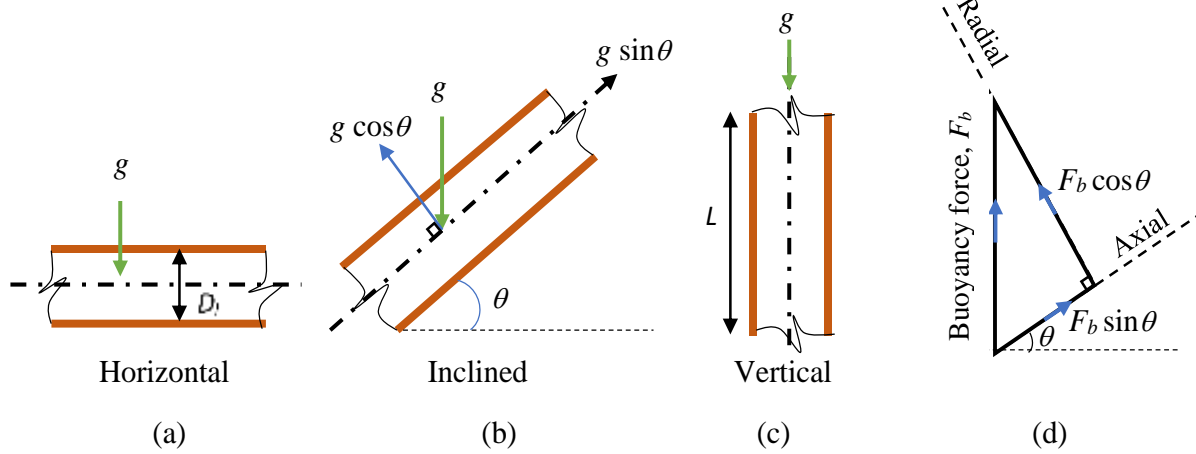


Fig. 5.7: Components of the buoyancy force for different tube orientations.

5.3.2. Laminar Nusselt number and friction factor correlations

A mixed convection Nusselt number correlation can be expressed as the sum of a forced convection part, Nu_{FC} , plus a mixed convection part, Nu_{MC} , that enhances the heat transfer:

$$Nu = Nu_{FC}(Re) + Nu_{MC}(Pr, Gr, Re) \quad 5.1$$

The forced convection Nusselt number correlation (Eq. 6.5) developed in Section 6.2 was used for the forced convection part.

To find an appropriate correction for the mixed convection part, more experiments were conducted at finer inclination angle increments near vertical upward and downward flow, because more changes were observed at these angles. Fig. 5.8 compares the average fully developed Nusselt numbers at a Reynolds number of 1 600 for different inclination angles with a cosine curve. This figure indicates that the expected correction of $\cos\theta$ (that is $Nu(\theta) = Nu_{FC} + (Nu - Nu_{FC})\cos\theta$) to account for mixed convection heat transfer is insufficient, especially for $60^\circ < \theta < 89^\circ$ (as well as $-60^\circ < \theta < -89^\circ$).

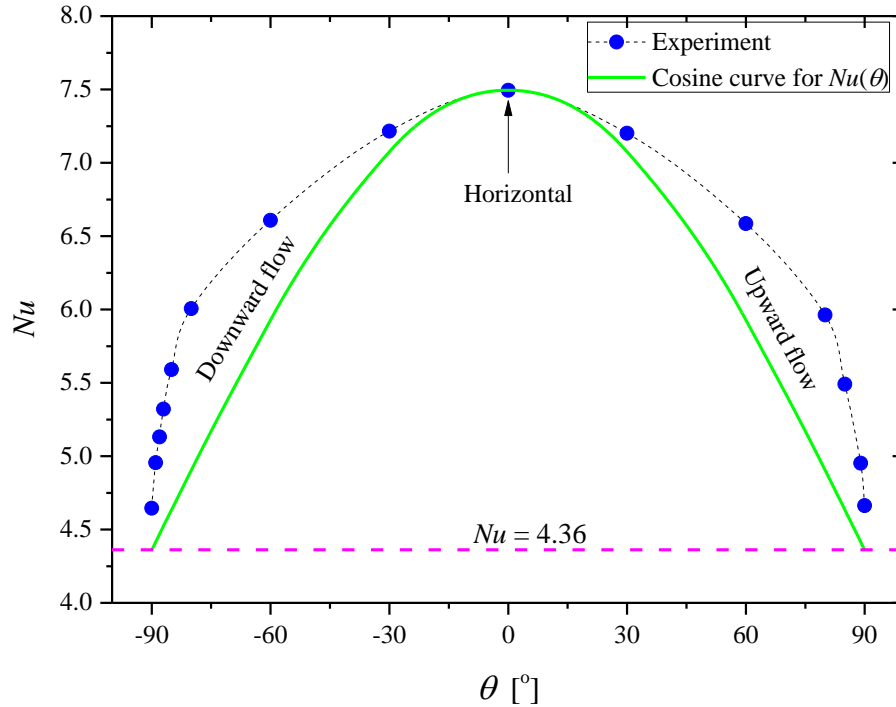


Fig. 5.8: Average fully developed laminar Nusselt numbers as a function inclination angle for a bulk Reynolds number of 1 600 and a heat flux of 6 kW/m².

For horizontal flow, the buoyancy forces, F_b , acted perpendicular to the flow direction and $g\cos\theta = g$ when $\theta = 0^\circ$, while for vertical flow it acted parallel to the flow and $g\cos\theta = 0$ when $\theta = \pm 90^\circ$. Therefore, a $g\cos\theta$ correction gave the correct answers for vertical and horizontal flow. As indicated in Fig. 5.7, the components of the buoyancy force acted in both the radial and axial directions of the fluid flow for inclined orientations. However, the axial component of the buoyancy force was negligible for vertical upward and downward results, because the Nusselt numbers were approximately equal to the forced convection Nusselt numbers as shown in Section 4.3. The horizontal results indicated that the component of the buoyancy force normal to the axis of the fluid flow was the main contributing factor for the heat transfer enhancement and should therefore be used in quantifying the buoyancy effect on heat transfer for inclined tubes.

Because the inclination angle influenced the buoyancy forces, it was decided to adjust the Grashof numbers and modified Grashof numbers in Eqs. 3.15 and 3.16 as follows:

$$Gr_\theta = Gr\cos\theta \quad 5.2$$

and

$$Gr_{\theta}^* = Gr^* \cos\theta \quad 5.3$$

The corresponding Rayleigh numbers were thus:

$$Ra_{\theta} = Gr_{\theta} Pr \quad 5.4$$

and

$$Ra_{\theta}^* = Gr_{\theta}^* Pr \quad 5.5$$

This is similar to the approach followed by Rolle [134], who defined an “inclined plane Grashof number” for free convection from a flat plate. In this study, it is referred to as the “inclined tube Grashof number” or “inclined tube Rayleigh number”.

The Nusselt number enhancement due to inclination angle was a function of Pr , Re and Gr_{θ} or Gr_{θ}^* and could therefore be accounted for by making use of the Reynolds number and inclined tube Rayleigh number:

$$Nu_{MC} = 0.053 \left(\frac{Ra_{\theta}^{0.2}}{Re^{0.1}} \right)^{2.9} \quad 5.6$$

or in terms of the modified Rayleigh number:

$$Nu_{MC} = 0.032 \left(\frac{Ra_{\theta}^{*0.15}}{Re^{0.08}} \right)^{3.48} \quad 5.7$$

When using constant heat fluxes, the use of Eq. 5.7 is more convenient [9, 18, 21, 40], because the temperature differences used to determine the Grashof numbers and thus Rayleigh numbers in Eq. 5.6 are normally not known while the heat fluxes are.

Eq. 5.1 (with Eqs. 6.1, 5.6 and 5.7) were valid for $-90^{\circ} \leq \theta \leq 90^{\circ}$, $593 \leq Gr_{\theta} \leq 18\,040$, $3\,346 \leq Gr_{\theta}^* \leq 146\,014$, $1\,000 \leq Re \leq 3\,500$ and $3 \leq Pr \leq 7$. As will be shown in Chapter 6, for $600 \leq Re \leq 1\,000$ and $\theta = \pm 90^{\circ}$, $Ra_{\theta}^* = 0$, and thus, $Nu_{MC} = 0$. With our experimental set-up we could not conduct experiments at lower Reynolds numbers than approximately 600, because the outlet temperatures became too high.

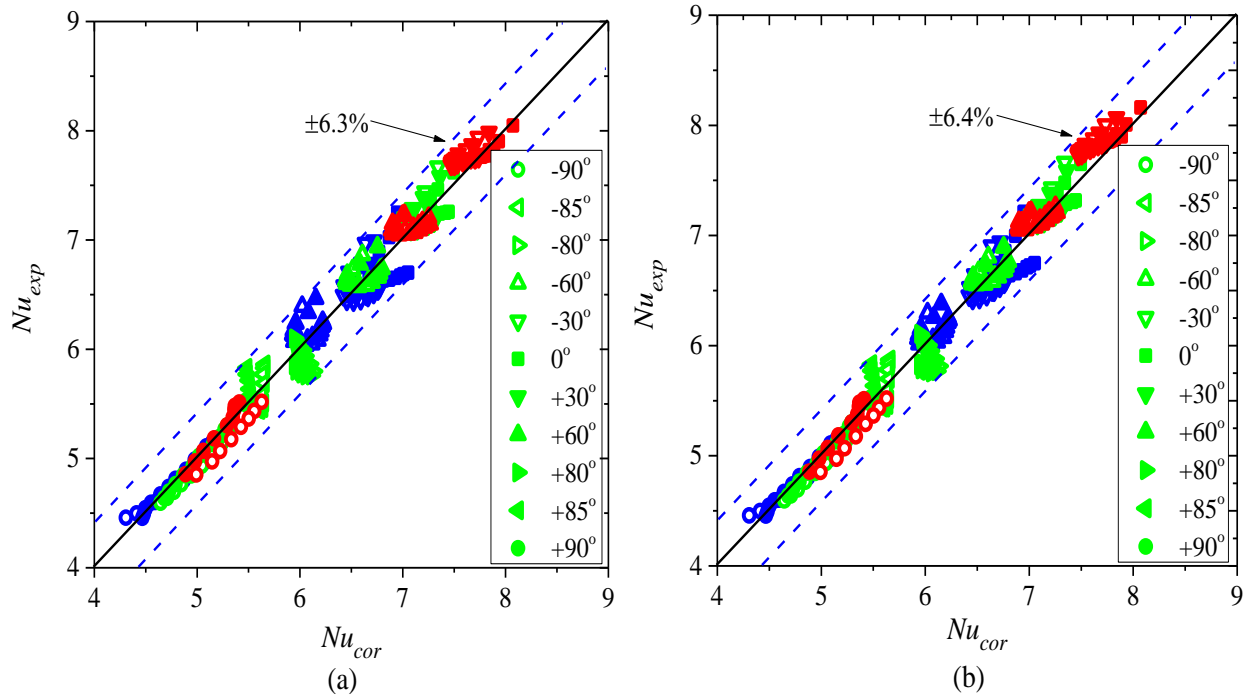


Fig. 5.9: Comparison of the average laminar Nusselt number correlation Eq. 5.1 for fully developed flow with experimental results for the different inclination angles and heat fluxes using Eq. 6.5 and (a) Eq. 5.6 and (b) Eq. 5.7. The blue, green and red markers represent heat fluxes of 4 kW/m^2 , 6 kW/m^2 , and 8 kW/m^2 , respectively.

Fig. 5.9 compares the experimental Nusselt numbers at different heat fluxes and inclination angles with the calculated values (Nu_{cor}) from Eq. 5.1 with Eq. 5.6 in Fig. 5.9(a) and with Eq. 5.7 in Fig. 5.9(b). In Fig. 5.9(a), where the Grashof numbers were determined from the measured temperature differences, the maximum deviation was 6.3% and the average deviation was 1.8%. In Fig. 5.9(b), where the Grashof numbers were determined from the measured heat fluxes, the maximum deviation was 6.4% and the average deviation was 1.7%.

Fig. 5.10 compares the average fully developed Nusselt numbers at a bulk Reynolds number of approximately 1 600 and a heat flux 6 kW/m^2 for different inclination angles with the Nusselt numbers predicted using Eq. 5.1 (with Eq. 5.6 and Eq. 5.7). The average deviation was 1.8% and the maximum difference was 3.9%. The inclined tube Grashof numbers (Eqs. 5.2 and 5.3) were also used in the mixed convection laminar flow correlation of Morcos and Bergles [130] and the average deviation between the Nusselt numbers predicted using Eq. 5.1 with Eq. 5.7 and the correlation of Morcos and Bergles [130] was 2.8%. A maximum deviation of 20% was found for vertical flows (forced convection) because their correlation did not account for variable property forced convection Nusselt numbers which changed with Reynolds number, as will be shown in Chapter 6. The inclined tube modified Grashof number, $Gr\theta^*$, was evaluated at the film temperature.

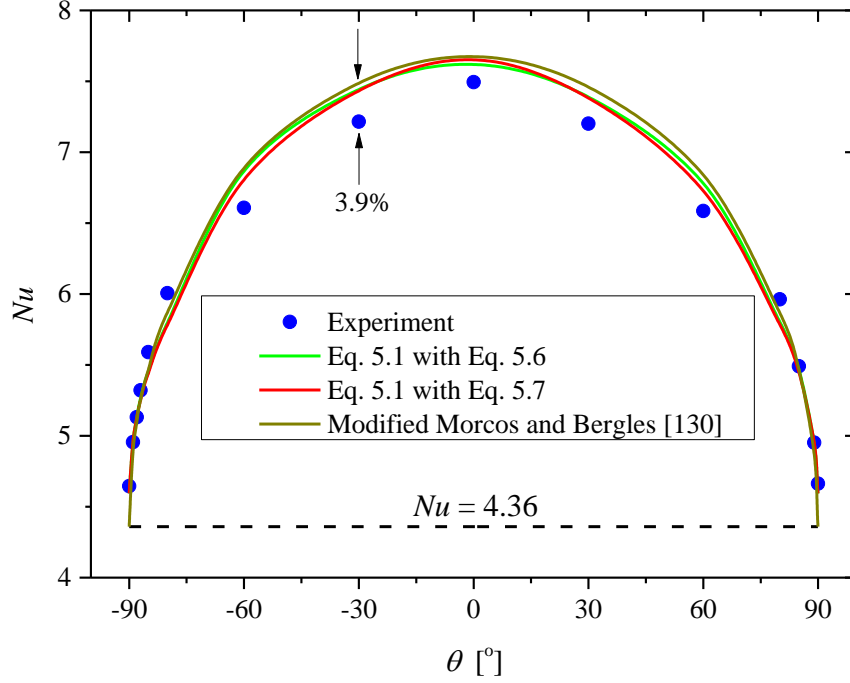


Fig. 5.10: Comparison of average fully developed Nusselt number correlations, Eq. 5.1 (with Eq. 5.6 and Eq. 5.7) with the experimental data at a bulk Reynolds number of approximately 1 600 and a heat flux of 6 kW/m² for different inclination angles.

For the fully developed isothermal friction factors, Fig. 5.1 indicated that the friction factors were approximately equal to the Poiseuille correlation ($64/Re$) for all inclination angles. Similar to the approach used by Tam and Ghajar [20] and Tam *et al.* [56] for the diabatic friction factors, the Poiseuille friction factors were multiplied with the bulk-to-wall-viscosity ratios (μ_b/μ_w), as a function of the inclined tube Grashof and Prandtl numbers:

$$f = \left(\frac{64}{Re}\right) \left(\frac{\mu_b}{\mu_w}\right)^{0.0016Gr_\theta^{0.67} Pr^{0.011}} \quad 5.8$$

and in terms of modified inclined Grashof numbers:

$$f = \left(\frac{64}{Re}\right) \left(\frac{\mu_b}{\mu_w}\right)^{0.0016Gr_\theta^*{}^{0.56} Pr^{0.011}} \quad 5.9$$

Eqs. 5.8 and 5.9 were valid for $-90^\circ \leq \theta \leq 90^\circ$, $593 \leq Gr_\theta \leq 18\,040$, $3\,346 \leq Gr_\theta^* \leq 146\,014$, $1.04 \leq \mu_b/\mu_w \leq 1.25$, $1\,000 \leq Re \leq 3\,500$ and $3 \leq Pr \leq 7$. As will be shown in Chapter 6, for

$600 \leq Re \leq 1000$ and $\theta = \pm 90^\circ$, the friction factors were not a function of Grashof number and were considered as forced convection friction factors; thus $f = 64/Re$.

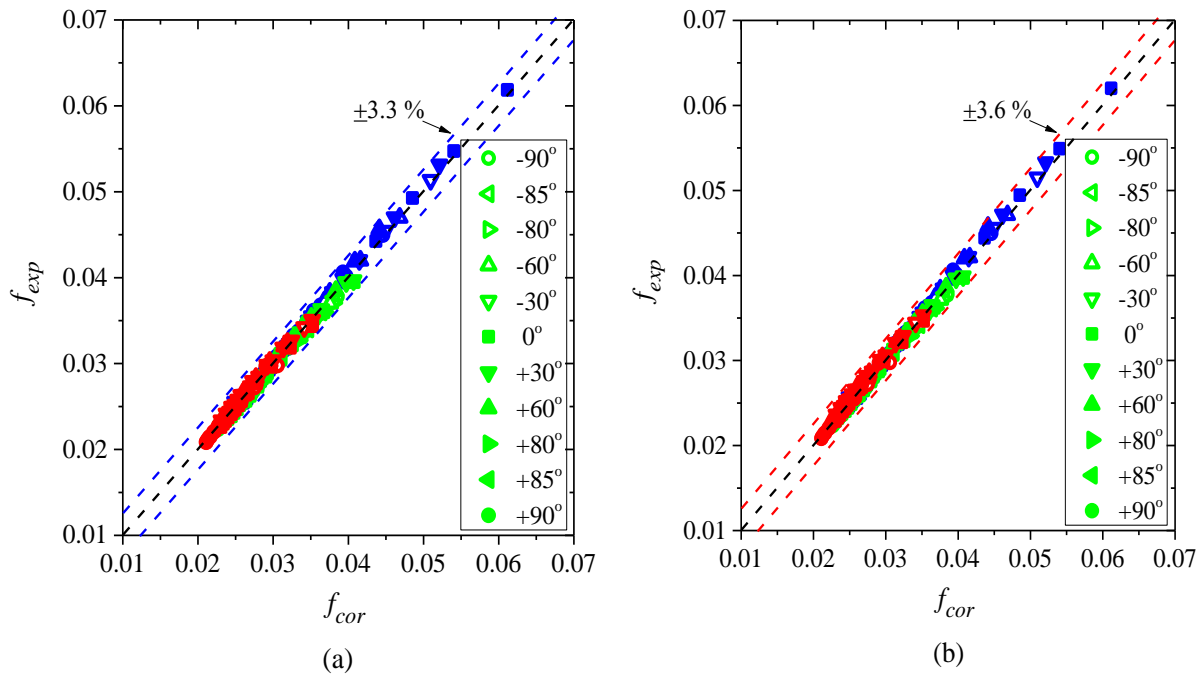


Fig. 5.11: Comparison of the laminar fully developed diabatic friction factor correlations with the experimental results for the different inclination angles at different heat fluxes using (a) Eq. 5.8 and (b) Eq. 5.9. The blue, green and red markers represent heat fluxes of 4 kW/m², 6 kW/m², and 8 kW/m², respectively.

The experimental friction factors at different heat fluxes and inclination angles were compared to the calculated values from Eq. 5.8 in Fig. 5.11(a) and with Eq. 5.9 in Fig. 5.11(b). In Fig. 5.11(a), where the Grashof numbers were determined from the measured temperature differences, the maximum deviation was 3.3% and the average deviation was 1%. In Fig. 5.11(b), where the Grashof numbers were determined from the measured heat fluxes, the maximum deviation was 3.6% and the average deviation was 1%.

5.3.3. Transitional flow

Fig. 5.12 compares the average fully developed Colburn j -factors at a heat flux of 6 kW/m² for different inclination angles as a function of the bulk fully developed Reynolds number. As there was no significant difference in the results for upward and downward flow (Fig. 5.6), only results for upward flow were given.

In the laminar flow regime, the Colburn j -factors decreased with increasing Reynolds numbers, as expected. Furthermore, at a fixed Reynolds number, the laminar Colburn j -factors decreased with increasing inclination angle from horizontal to vertical flow.

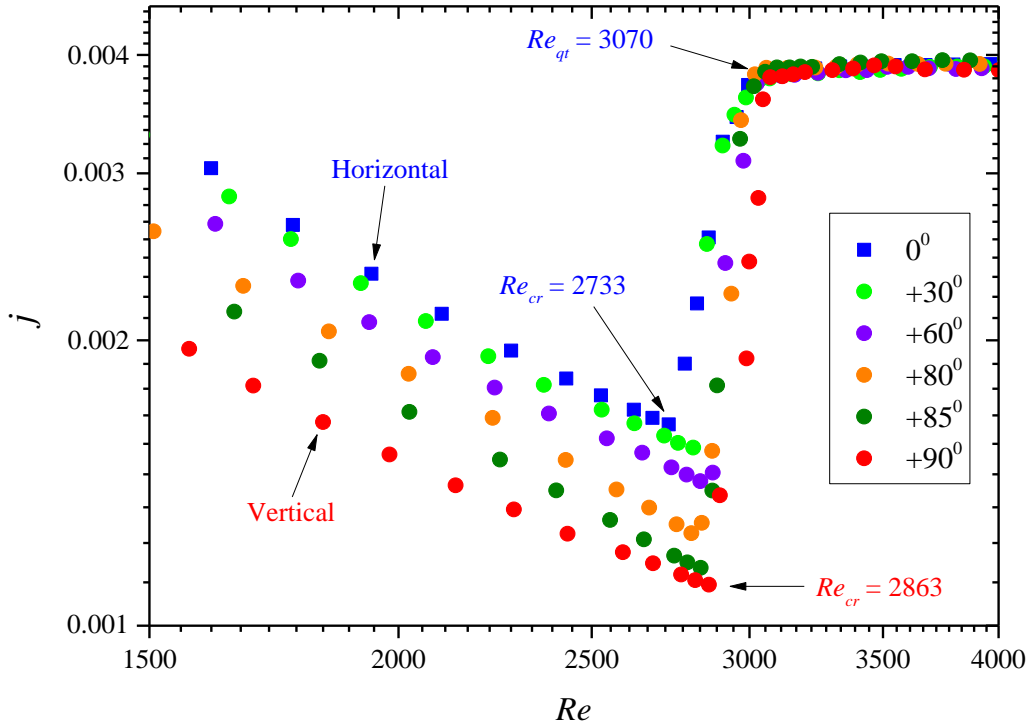


Fig. 5.12: Comparison of the average fully developed Colburn j -factors as a function of Reynolds number for upward flow at different inclination angles at constant heat flux of 6 kW/m^2 .

The critical Reynolds number (Re_{cr}) at which the transitional flow regime started, as defined by Everts and Meyer [21], corresponded to the point where the gradient of the laminar Colburn j -factor changed from a negative to a positive gradient. Fig. 5.12 indicates that for horizontal flow ($\theta = 0^\circ$), the critical Reynolds number was 2 733. The transitional flow regime ended (Re_{qt}) for horizontal flow at a Reynolds number of approximately 3 070, where the flow entered the quasi-turbulent flow regime. Fig. 5.12 also indicates that the critical Reynolds numbers increased with increasing inclination angle from 2 733 for horizontal flow to 2 863 for vertical flow. Everts and Meyer [21] found that buoyancy effects caused transition to occur earlier. Hence, as the buoyancy effects decreased due to increasing inclination angle, the start of the transitional flow regime was delayed.

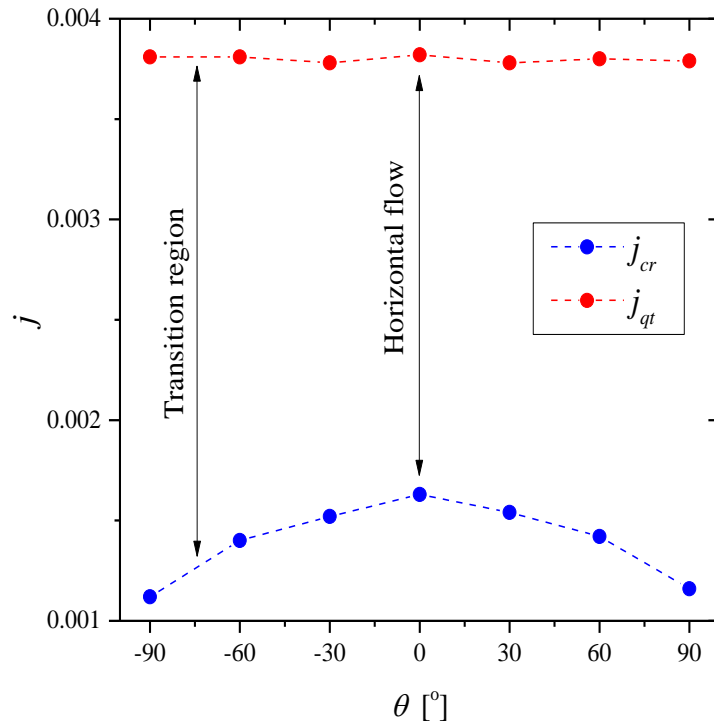


Fig. 5.13: Comparison of the Colburn j -factors at the start, j_{cr} , and end, j_{qt} , of the transitional flow regime as a function of inclination angle at a heat flux of 6 kW/m².

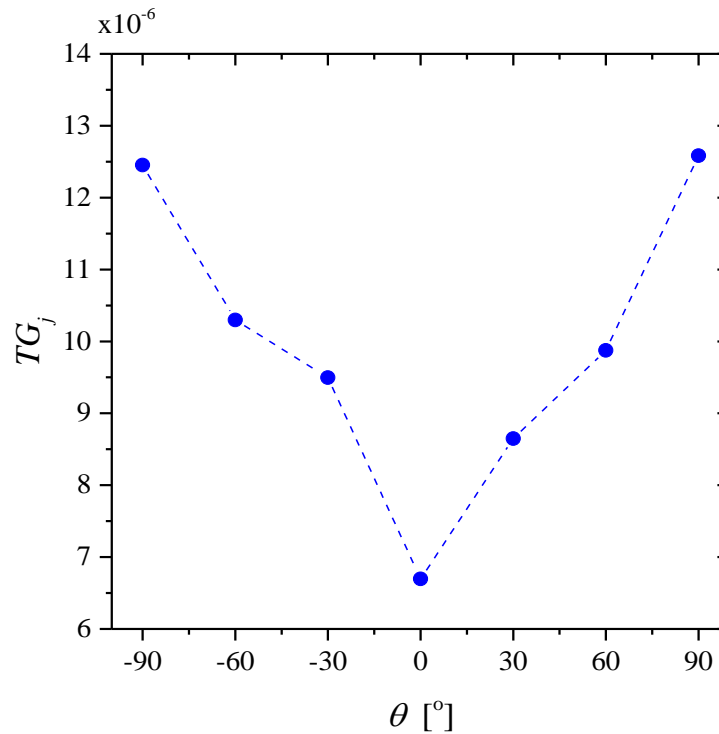


Fig. 5.14: Comparison of transition gradients of the Colburn j -factors (TG_j) as a function of inclination angle at a heat flux of 6 kW/m².

To investigate the Colburn j -factors in the transitional flow regime, Fig. 5.13 compares the Colburn j -factors at the start, j_{cr} , and end, j_{qt} , of the transitional flow regime as a function of inclination angle. As expected, the maximum Colburn j -factor at the start of the transitional flow regime occurred at the horizontal orientation (0°), where buoyancy forces were at its maximum, and decreased as the inclination angle increased in the upward and downward flow directions. However, the Colburn j -factors at the end of the transitional flow regime remained constant at 0.00389, which confirmed that the heat transfer coefficients at the end of the transitional flow regime was independent of inclination angle (or Grashof number). The effect of buoyancy decreased with increasing Reynolds number in the transitional flow regime because of the increase in mass flow rates (inertia forces) that enhanced mixing (turbulence) and therefore dominated buoyancy effects. At a quasi-turbulent Reynolds number of 3 500, all 11 Colburn j -factor values of the different inclination angles were within 0.1% of the average value of 0.00389. The turbulent flow regime, (not shown in Fig. 5.12) was similar to the quasi-turbulent flow regime in which the inertia forces were much higher than the buoyancy forces. The results were therefore Grashof number independent, as was found by Meyer and Everts [18] and Everts and Meyer [21, 40].

Fig. 5.14 compares the transition gradients (Eq. 3.21 as defined by Everts and Meyer [21]) as a function of inclination angle. This figure indicates that the transition gradient increased from horizontal to vertical flow. This was because the critical Reynolds numbers at the start of the transitional flow regime increased with inclination angle (due to decreasing buoyancy effects) while the end of the transitional flow Reynolds numbers (which is the start of the quasi-turbulent flow regime) remained relatively constant (Fig. 5.15). A similar trend was also found in the transition gradients of the friction factors, where it increased with an increase in the inclination angle from horizontal to vertical flow.

To investigate the effects of flow direction and buoyancy on the boundaries of the transitional flow regime, Fig. 5.15 compares the Reynolds numbers at which the transitional flow regime started and ended as a function of inclination angle in the upward and downward flow directions at a heat flux of 6 kW/m^2 . It should be noted (taken into consideration the uncertainties) that this graph which was generated from the Colburn j -factors results, compares very well with Fig. 5.4 which was generated from the friction factor results. The good agreement can be expected, because Everts and Meyer [40] recently showed that there is a direct relationship between heat transfer and pressure drop in the transitional flow regime.

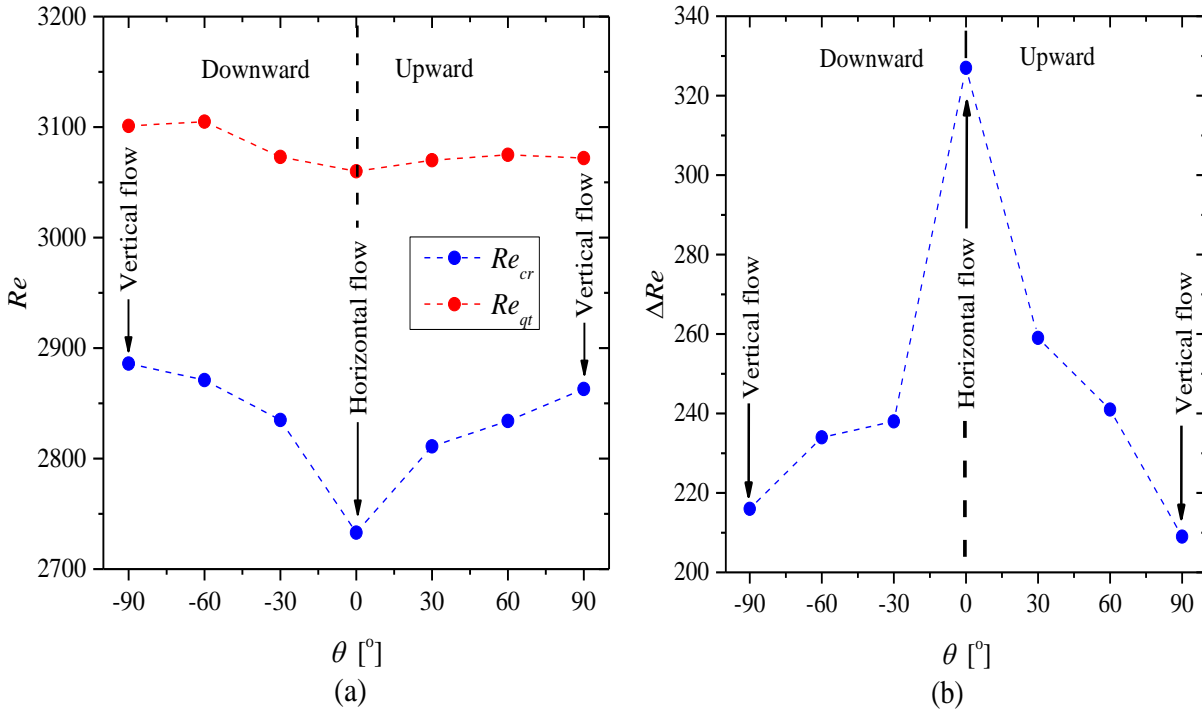


Fig. 5.15: Comparison of (a) the Reynolds numbers at which the transitional flow regime started and ended and (b) the width of the transitional flow regime as a function of inclination angle at a heat flux of 6 kW/m².

When the inclination angle was increased and decreased from the horizontal, ($\theta = 0^\circ$) to the vertical upward flow ($\theta = +90^\circ$) and vertical downward flow ($\theta = -90^\circ$), the critical Reynolds numbers, Re_{cr} , increased. However, similar to the results in Fig. 5.12, the Reynolds numbers, Re_{qt} , at which the transitional flow regime ended remained relatively constant for all inclination angles. Fig. 5.15(b) compares the width of the transitional flow regime, ΔRe (Eq. 3.21), as a function of inclination angle. This graph indicates that that the width of the transitional flow regime was a maximum for horizontal flow and decreased as the inclination angle increased in the upward and downward flow directions to vertical flow, where buoyancy was insignificant (forced convection condition). Thus, the maximum width of the transitional flow regime was found for horizontal flow where the buoyancy forces were the largest. This is similar to the findings of Everts and Meyer [21] that at the onset of mixed convection conditions, buoyancy effects first disturbed the transition process and caused the width of the transitional flow regime to increase. As the buoyancy effects increased significantly, it assisted the flow to transition from laminar to turbulent and caused the width of the transitional flow regime to decrease.

5.3.4. Schematic summary

Because it is challenging from the experiments to clearly and easily define the general characteristics of the transitional flow regime at different inclination angles, the heat transfer and pressure drop results are summarised schematically in Fig. 5.16(a) and (b) respectively, as a function of Reynolds number. The blue, orange, green and red curves represent the horizontal (0°), $\pm 30^\circ$, $\pm 60^\circ$ and vertical ($\pm 90^\circ$) inclination angles.

In the laminar flow regime (Fig. 5.16(a)), the Nusselt numbers for vertical flow converged to the forced convection Nusselt number of 4.36. At a fixed Reynolds number, the Nusselt numbers increased with decreasing inclination angle from vertical upward or downward ($\theta = \pm 90^\circ$) to horizontal ($\theta = 0^\circ$) flow, due to the increase in the inclined tube Grashof number (buoyancy). The experimental data also indicated that the Prandtl numbers during this process increased (especially near the wall) which contributed towards increased Rayleigh numbers (product of the Grashof and Prandtl numbers). A significant increase in Nusselt number occurred as buoyancy effects became significant when the inclination angle was changed with 30° from vertical ($\pm 90^\circ$) to $\theta = \pm 60^\circ$. A similar increase of 30° from horizontal flow ($\theta = 0^\circ$) caused a relatively small change in the Nusselt number. The reason is that the buoyancy effects already occurred when the tube was in a horizontal orientation and the 30° change in inclination angle just slightly decreased the inclined tube Grashof number. A similar behaviour was observed with the laminar fully developed diabatic friction factors in Fig. 5.16(b), where the friction factors for a fixed Reynolds number increased as the inclination angle decreased from vertical flow ($\theta = \pm 90^\circ$) to horizontal flow ($\theta = 0^\circ$) flow. The friction factors for vertical flow converged to the forced convection and isothermal friction factors of $64/Re$.

As indicated by points A to D in Fig. 5.16, the critical Reynolds numbers, Re_{cr} , increased as the inclination angle increased from horizontal to vertical. However, the Reynolds numbers at which the transitional flow regime ended, Re_{qt} , remained relatively constant (at point X) for the inclination angles. As the Grashof number decreased due to increased inclination angle, the width of the transitional flow regime decreased. Furthermore, dotted line A-X (horizontal flow) and dotted line D-X (vertical flow) indicate that the transition gradients of the Nusselt numbers (TG_{Nu}) in (Fig. 5.16(a)) and that of the friction factors (TG_f) in (Fig. 5.16(b)) increased with increasing inclination angle.

In the quasi-turbulent flow regime, inclination angle had a negligible effect on the heat transfer and pressure drop results, because the turbulent motion of the fluid completely suppressed the buoyancy effects. The turbulent flow regime is expected to be similar to the quasi-turbulent flow regime.

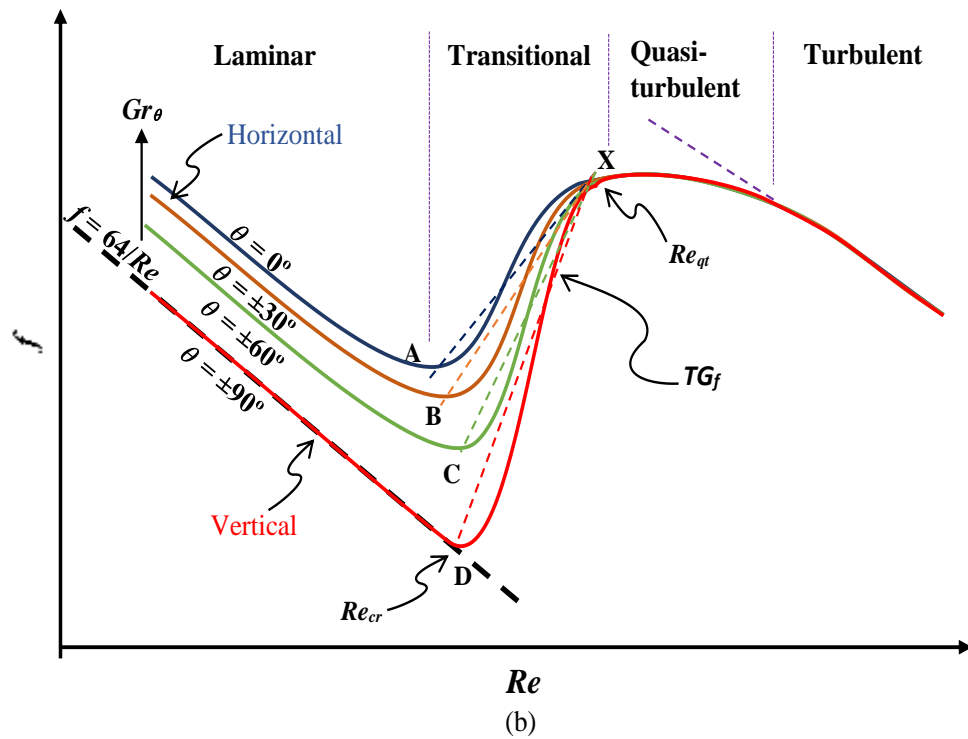
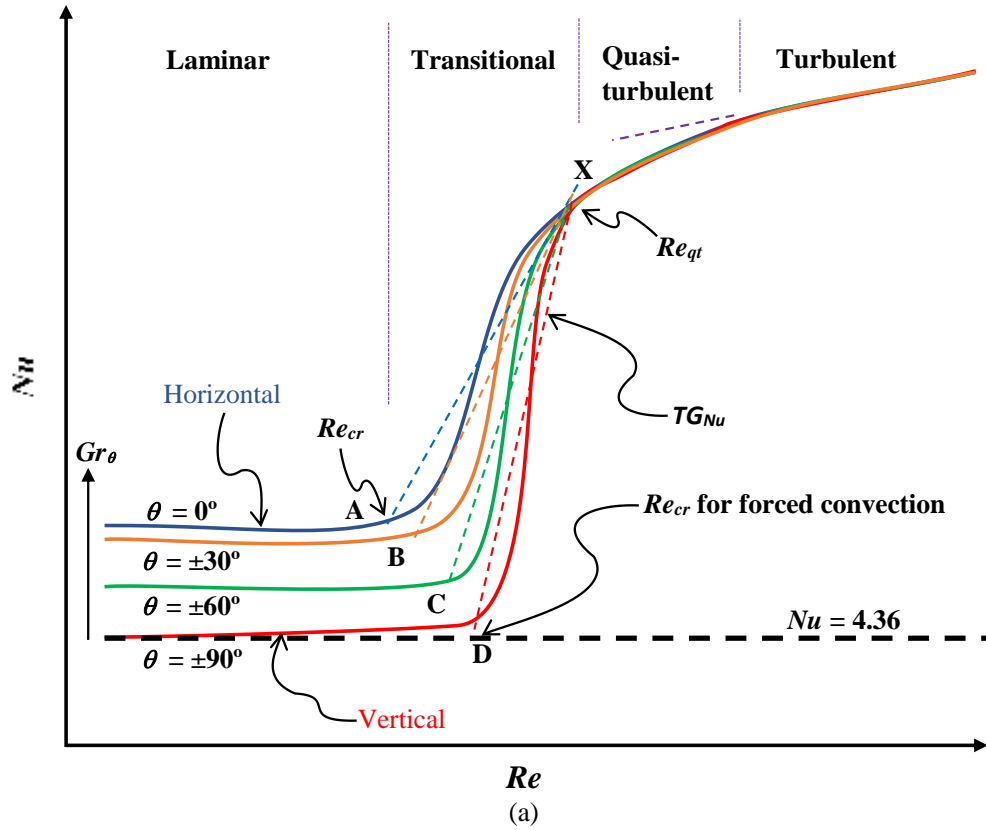


Fig. 5.16: Schematic representation of (a) the Nusselt number and (b) the friction factor, as a function of Reynolds number for upward and downward flow at different inclination angles and a constant heat flux.

5.4. Developing flow heat transfer for horizontal and vertical flow

Fig. 5.17 compares the heat transfer results for developing and fully developed flow at horizontal (0°) and vertical upward ($+90^\circ$) inclinations as function of local Reynolds number. Only the vertical upward flow results have been included, because Fig. 5.6 indicated that there was no significant difference in the results of upward and downward flows. In the laminar flow regime, the green line represents the Nusselt number of 4.36 for fully developed forced convection heat transfer, while the orange line represents the correlation of Meyer and Everts [18] for developing and fully developed mixed convection heat transfer. Furthermore, points A-H in Fig. 5.17 corresponds to points A-H in Fig. 5.18.

Fig. 5.17(a) indicates that near the inlet of the test section (at $x/D_i = 33$), the laminar Colburn j -factors were higher than the fully developed line for forced convection conditions ($Nu = 4.36$). There was no difference between the results for horizontal and vertical flows, because buoyancy effects were suppressed by the thin boundary layers and the results fell into the Forced Convection Developing (FCD) region as defined by Meyer and Everts [18]. Although a similar trend was observed in Fig. 5.17(b), the Colburn j -factors were less than in Fig. 5.17(a) because the heat transfer coefficients decreased along the tube length as the flow developed [18].

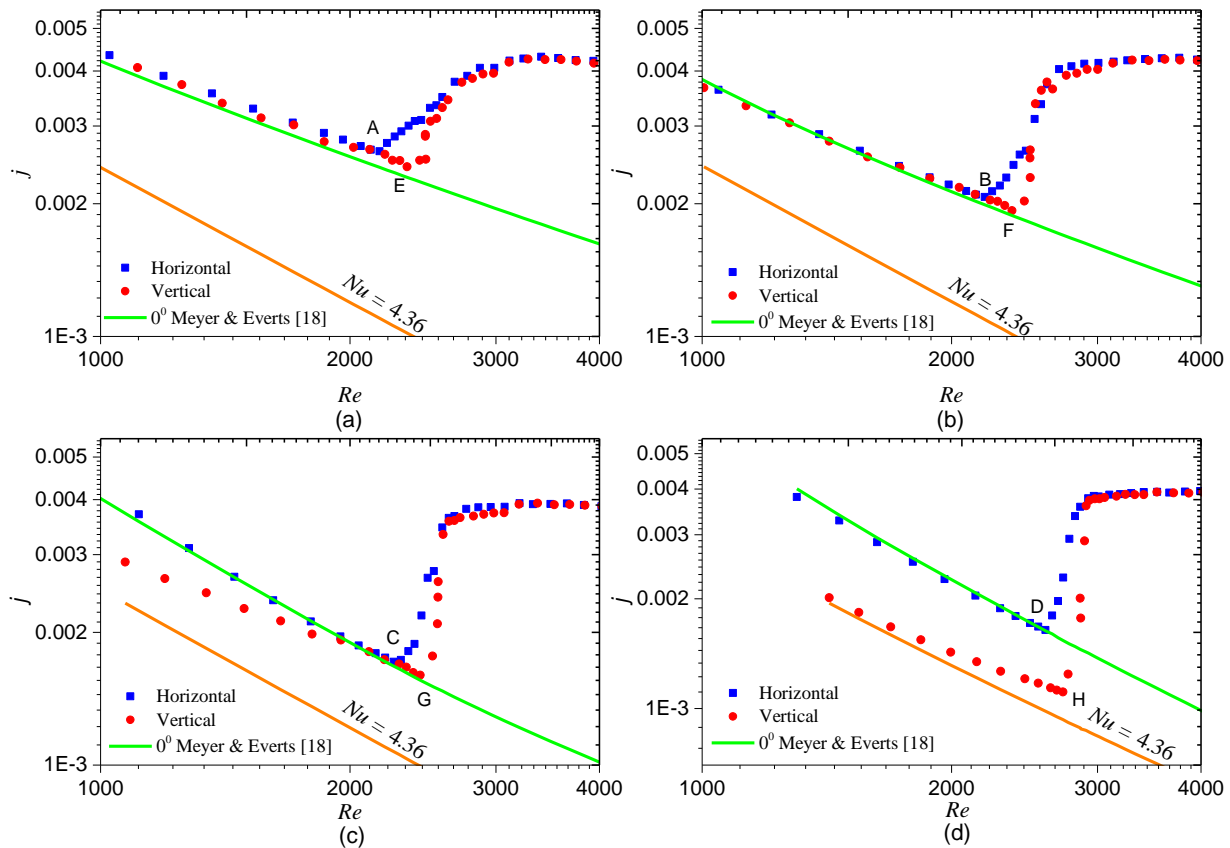


Fig. 5.17: Comparison of local developing and fully developed Colburn j -factors as function of (a) $x/D_i = 33$, (b) $x/D_i = 63$, (c) $x/D_i = 151$ and (d) $x/D_i = 592$, as a function of local Reynolds numbers for horizontal and vertical flow at a heat flux of 6 kW/m^2 .

As the flow continued downstream to $x/D_i = 151$ (Fig. 5.17(c)), the Colburn j -factors for horizontal flow corresponded very well to the correlation of Meyer and Everts [18]. However, the Colburn j -factors for vertical flow were less than for horizontal flow, because buoyancy effects were negligible, while it became significant for horizontal flow. The Colburn j -factors vertical flow remained higher than the theoretical forced convection Nusselt number of 4.36, which indicated that the flow was still developing.

Fig. 5.17(d) indicates that at $x/D_i = 592$, the Colburn j -factors for vertical flow corresponded well (average deviation of 9%) with the forced convection Nusselt number of 4.36, especially for Reynolds numbers less than 2 000. Furthermore, the Colburn j -factors for horizontal flow were significantly higher than for vertical flow, because buoyancy effects enhanced the heat transfer inside the test section.

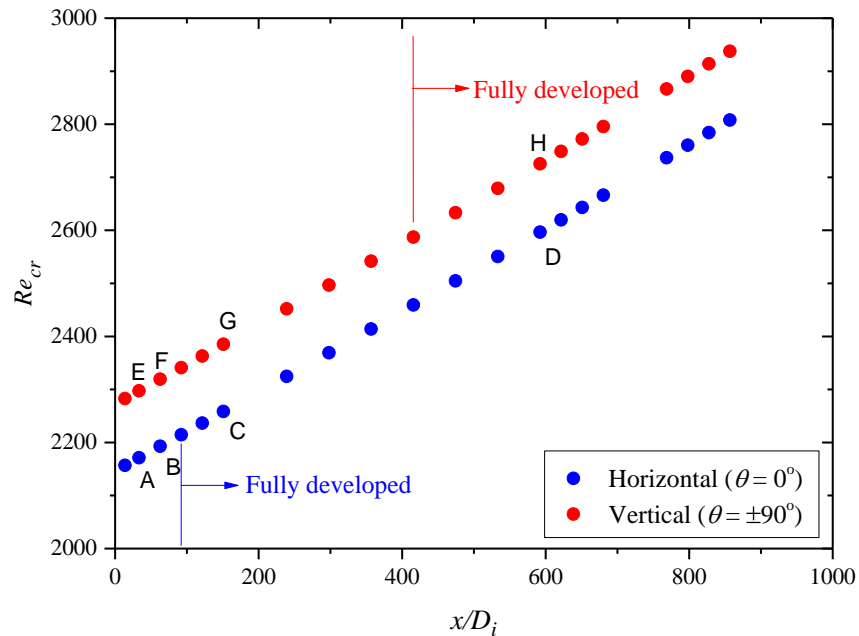


Fig. 5.18: Comparison of the local critical Reynolds numbers as a function of axial location of the tube for developing and fully developed flows of horizontal and vertical inclinations in Fig. 5.17.

Fig. 5.17 also indicates that the start of the transitional flow regime was delayed for vertical flow compared to horizontal flow along the entire tube length. The increased critical Reynolds numbers of vertical flow compared with horizontal flow was as expected because Everts and Meyer [21] found that buoyancy effects caused transition to occur earlier and buoyancy effects were significant for horizontal flow but negligible for vertical flow. The end of the transitional flow regime occurred at approximately the same Reynolds number for both horizontal and vertical flow. Fig. 5.18 compares the Reynolds numbers at which the transitional flow regime started in Fig. 5.17 for horizontal (points A - D) and vertical (points E - H) as a function of axial position. Similar to

the horizontal flow results of Everts and Meyer [21], the critical Reynolds numbers increased along the tube length for both horizontal and vertical flows. This was only due to the variation of viscosity with temperature and transition actually occurred at the same mass flow rate in the entire test section [21].

5.5. Conclusions and recommendations

The heat transfer and pressure drop characteristics of a single-phase mixed convective flow in the laminar and transitional flow regimes of smooth inclined tubes heated at a constant heat flux were experimentally investigated in this chapter. To account for the effect of inclination angle on the laminar Nusselt numbers and the friction factors, a simple *inclined tube Grashof/Rayleigh number* was defined. The laminar heat transfer coefficients were expressed as a forced convection part plus an additional enhancement part caused by mixed convection. Similarly, the laminar friction factors were expressed as the forced convection part multiplied by the enhancement part. Fully developed average laminar Nusselt number and friction factor correlations for inclined tubes were developed as a function of the inclined tube Grashof/Rayleigh numbers.

Buoyancy effects were found to be negligible for vertical upward and downward flow and both the heat transfer and pressure drop results were dominated by forced convection only. It was also found that the influences of buoyancy near vertical inclination angles was stronger than near horizontal inclination angles which caused the laminar heat transfer and pressure drop to increase rapidly near vertical inclination angles.

Both the heat transfer and pressure drop results indicated that the Reynolds number at which the transitional flow regime started in the fully developed region increased as the inclination angle increased from horizontal to vertical flow, while the end of the transitional flow regime remained relatively constant for all the inclination angles. This caused the width of the transitional flow regime to decrease as the inclination angle increased. Furthermore, inclination of the test section decreased the buoyancy effects (inclined tube Grashof number) and increased the transition gradient. Because buoyancy had a negligible effect on the quasi-turbulent flow regime, the results were independent of inclination angle. Furthermore, flow directions (upward and downward flows) had negligible influence on the heat transfer coefficients and friction factors. Overall it was concluded that inclination of heated tubes changed the way buoyancy forces acted on the fluid flow and changed the magnitude of the Grashof numbers and thus, transitional flow Reynolds numbers.

As the analysis in this chapter was for constant heat flux conditions, it is therefore recommended that the heat transfer and pressure drop in the laminar and transitional flow regime for constant wall temperature conditions be investigated for both heating and cooling conditions. Furthermore, the effect of tube diameters needs to be investigated as this can change the magnitude of the inclined tube Grashof numbers and thus affect the heat transfer and pressure drop in both the

laminar and transitional flow regimes. This is important especially for the vertical orientations, whether if the increase in diameter and thus Grashof numbers can cause the buoyancy effects to become significant, and change the flow condition from forced to mixed convection at higher laminar Reynolds numbers and the entire transitional flow regime.

6. Forced convection heat transfer and pressure drop

6.1. Introduction

This chapter investigates the heat transfer and pressure drop in the laminar and transitional flow regimes for pure forced convection conditions using vertical upward and downward flows (as confirmed from the laminar flow result validations in Sections 4.3 and 6.2). The heat transfer characteristics of the developing and fully developed regions as well as the fully developed pressure drop characteristics are analyzed. The general notation used in most graphs in this chapter was solid circle markers (●) for upward flows and empty circle markers (○) for downward flows. It should be noted that the solid circle markers used in the legends of most graphs were to differentiate the colours of the heat fluxes used for all the flow orientations. Furthermore, for clarification, only the vertical upward flow results were included in some of the graphs and not the downward results as well, because it was concluded from Fig. 4.3 and Fig. 4.4 that flow direction had no influence on the results.

6.2. Laminar flow

The comparisons of the results were made based on Nusselt numbers, heat fluxes and Reynolds numbers for vertical upward and downward flows in the laminar flow regimes. Limited results with the flow in a horizontal orientation were also included in this section. A revised fully developed laminar forced convection Nusselt number correlation is developed.

6.2.1. Heat transfer

Fig. 6.1 compares the forced and mixed (from Chapter 5) convection laminar Nusselt numbers for the same heating conditions but at different orientations. This figure indicates that for vertical flow, the average Nusselt numbers were approximately the same for all the heat fluxes (1 – 8 kW/m²), indicating negligible or no buoyancy effects (Grashof numbers). However, for horizontal flow, the Nusselt numbers increased with increasing heat flux due to buoyancy effects, indicating mixed convection heat transfer.

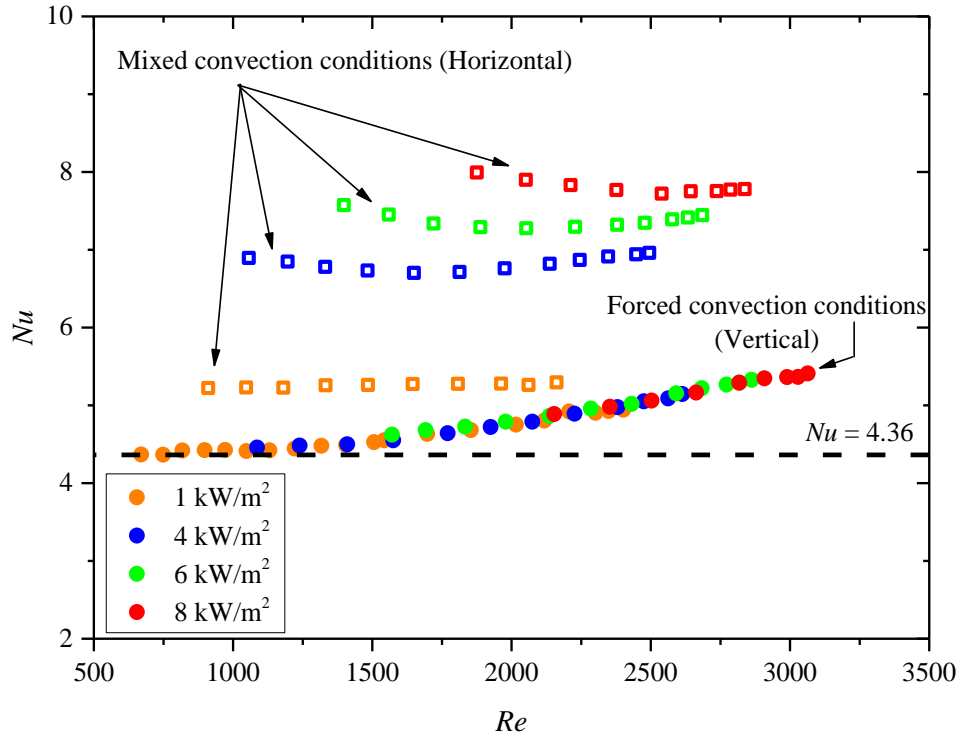


Fig. 6.1: Comparison of the average fully developed laminar Nusselt numbers as a function Reynolds number at various heat fluxes for vertical upward flow (forced convection heat transfer). Results for mixed convection horizontal flow (empty square markers) were included for comparison at the same heating conditions.

The fully developed forced convection Nusselt numbers in Fig. 6.1 were not constant at 4.36, but increased slightly with increasing Reynolds numbers for all the heat fluxes. However, Fig. 4.4 confirmed that this increase was not due to entrance effects, because the flow was fully developed from $x/D_i \geq 416$ at a Reynolds number of 2 100 and the Nusselt numbers in Fig. 6.1 were the average of $680 < x/D_i < 886$. This figure therefore indicates that the fully developed forced convection Nusselt numbers were a function of Reynolds number and were not constant at 4.36. Literature [66, 68-75, 77, 135] reported that the deviation of the forced convection Nusselt numbers from the constant property Nusselt number of 4.36, were generally due to changes in fluid properties (the specific properties were normally not stated and/or the specific reasons were vague). The fluid properties changed with temperature either due to changes in heat flux or mass flow rate.

Fig. 6.2 contains a schematic representation of the changes in temperatures, pressure drops, heat transfer coefficients, Reynolds numbers and viscosities along the tube length in both the developing and fully developed regions. In the fully developed region, points A and B represent

the bulk property/quantity as well as the pressure drop between points 1 – 2 and points 2 – 3, respectively. The maximum increase in fluid temperature (red line) between points A and B (1 m apart) occurred at a Reynolds number of 2 153 (mass flow rate of 0.00474 kg/s) and a heat flux of 8 kW/m². For this case, the changes in fluid properties between the two points A and B were as follows: an increase in thermal conductivity and specific heat capacity of 0.8% and 0.04%, and a decrease in density, viscosity and Prandtl number of 0.3%, 13% and 12%, respectively. Thus, in general, the local changes in the fluid properties along the tube length were negligible, except for the changes in viscosity (blue line in Fig. 6.2) and thus Prandtl number, which were orders of magnitude more than for the other properties.

Because of the changes in viscosities (blue line), the local Reynolds number (green line) at position A ($Re_A = 1\,955$) increased with 13% to point B ($Re_B = 2\,193$). Furthermore, the decreasing viscosity also caused the pressure drops (calculated from Eq. 3.5) to decrease with 10% from $\Delta P_A = 174$ Pa to $\Delta P_B = 156$ Pa. Therefore, dP/dx decreased in the axial direction and was not constant.

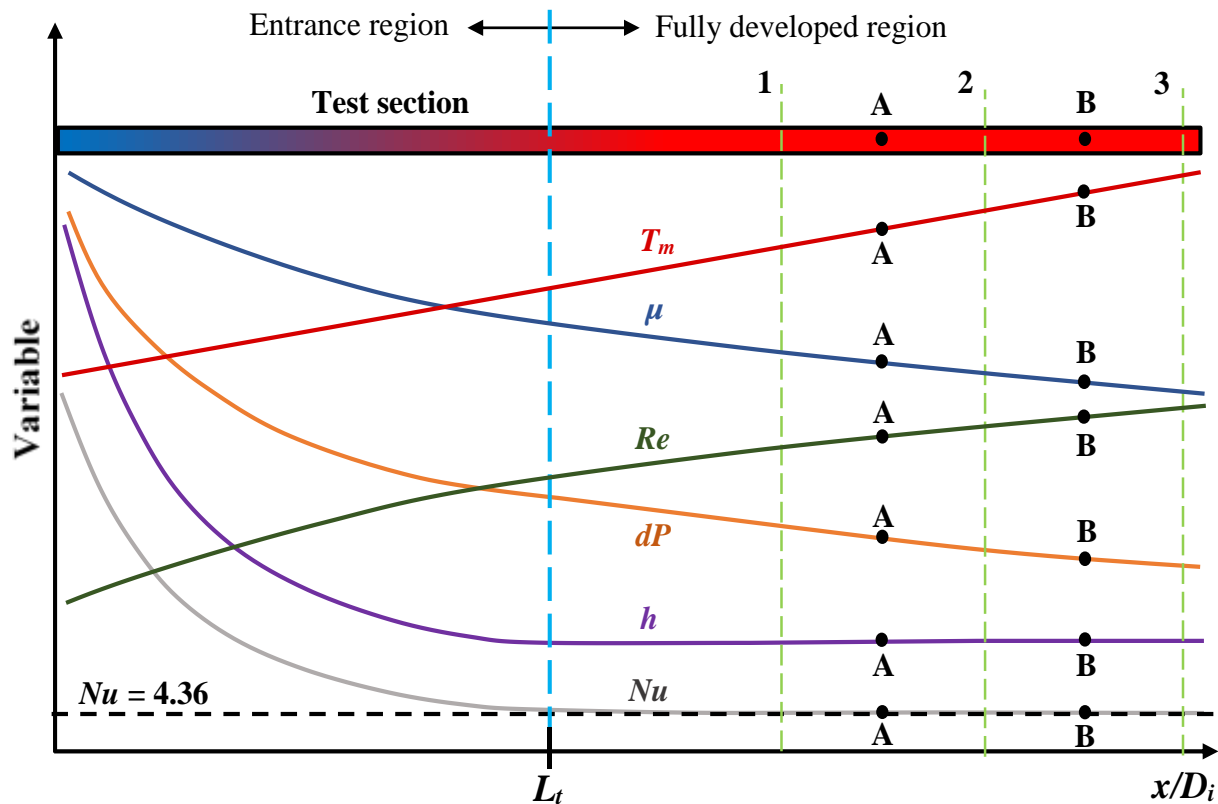


Fig. 6.2: Schematic representation of the variation of the mean fluid temperature, T_m , (red), viscosity, μ , (blue), Reynolds number, Re , (green), pressure drop, dP , (orange), heat transfer coefficient, h , (purple) and the Nusselt number, Nu , (grey) in the flow direction along the axial location of the test section tube for a constant heat flux boundary condition.

Fig. 6.3(a) compares the heat transfer coefficients as a function of mass flow rate for different heat fluxes. This figure indicates that for fixed mass flow rates of 0.002, 0.005 and 0.008 kg/s, an increase in heat flux from points 1 to 3 (brown), 4 to 8 (cyan) and 9 to 12 (black), respectively, led to increased heat transfer coefficients. Furthermore, for mass flow rates greater than 0.003 kg/s, the heat transfer coefficients increased slightly with increasing mass flow rates.

To account for the changes in fluid properties, the heat transfer coefficients in Fig. 6.3(a) were plotted in terms of the non-dimensional Nusselt number as a function of Reynolds number (which is the non-dimensional mass flow rate) in Fig. 6.3(b). Points 1 to 12 in Fig. 6.3(a) correspond to the same points in Fig. 6.3(b). For a fixed mass flow rate (for instance points 1-3 in Fig. 6.3(a)), an increase in heat flux caused an increase in thermal conductivity and a decrease in viscosity, which led to decreasing Nusselt numbers and increasing Reynolds numbers (points 1-3 in Fig. 6.3(b)). The result was that the Nusselt numbers and Reynolds numbers accounted for the changes in fluid properties and all the Nusselt numbers of the different heat fluxes (thus different Grashof numbers) collapsed onto a single line. Therefore, for forced convection $Nu \neq g(Gr)$, while $Nu = g(Gr)$ for mixed convection [18]. However, the Nusselt numbers increased with 26% from 4.36 at a Reynolds number of 600 to 5.48 at a Reynolds number of 3 064. Therefore, although most textbooks state that $Nu \neq f(Re)$ for laminar forced convection, the experimental data proved that $Nu = f(Re)$ for $Re \geq 1\ 000$. At a Reynolds number of 3 064 corresponding to the highest heat flux of 8 kW/m², $T_{b,FD}$ was 38.6°C and the Prandtl number was 4.46. The thermal entrance length was thus 3.49 m (based on $L_t = 0.05RePrD_i$), which confirmed that up to a Reynolds number of 3 064, the flow remained fully developed within $680 \leq x/D_i \leq 886$. The increasing Nusselt numbers with Reynolds number were thus not due to developing flow.

The constant forced convection laminar Nusselt number of 4.36 was derived from the velocity and temperature distributions. The velocity distribution was obtained from the momentum equation (Eq. 6.1) for fully developed laminar incompressible flow by applying a force balance to a differential volume element [11-15, 136]:

$$\frac{\mu}{r} \frac{d}{dr} \left(r \frac{du}{dr} \right) = \frac{dP}{dx} \quad 6.1$$

When assuming $\mu = \text{constant}$ and $dP/dx = \text{constant}$, Eq. 6.1 was solved by assuming that the left side of the equation was only a function of r and the right side was only a function of x . For the equality $f(r) = g(x)$ to hold for any value of r and x , they have to be equal to the same constant, therefore $dP/dx = \text{constant}$. The well-known parabolic radial velocity distribution was then obtained by integrating Eq. 6.1 twice [11-15, 136]:

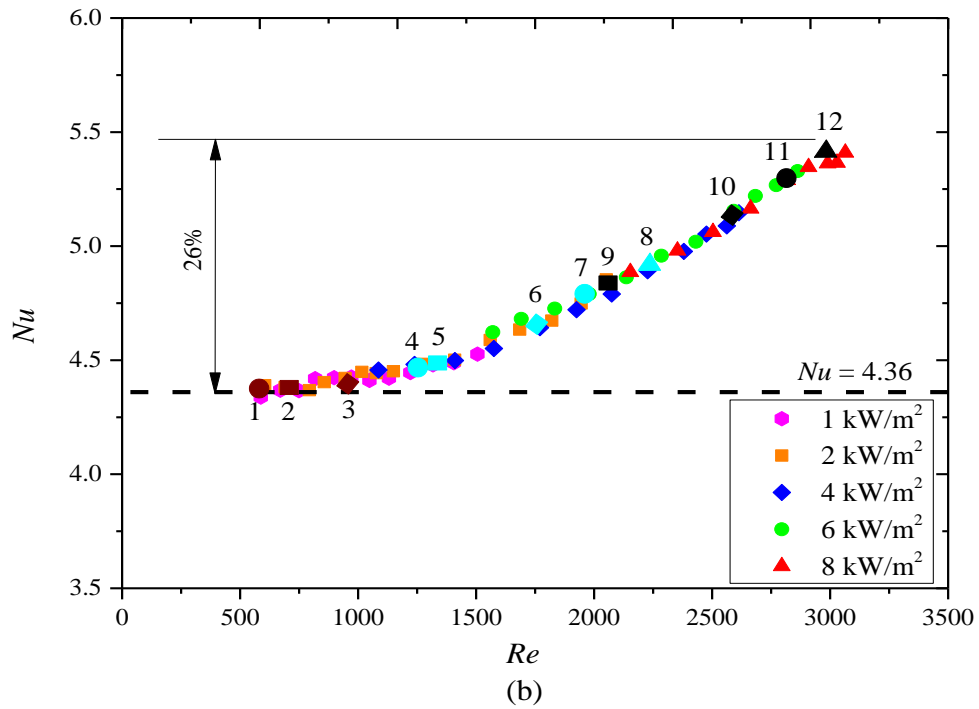
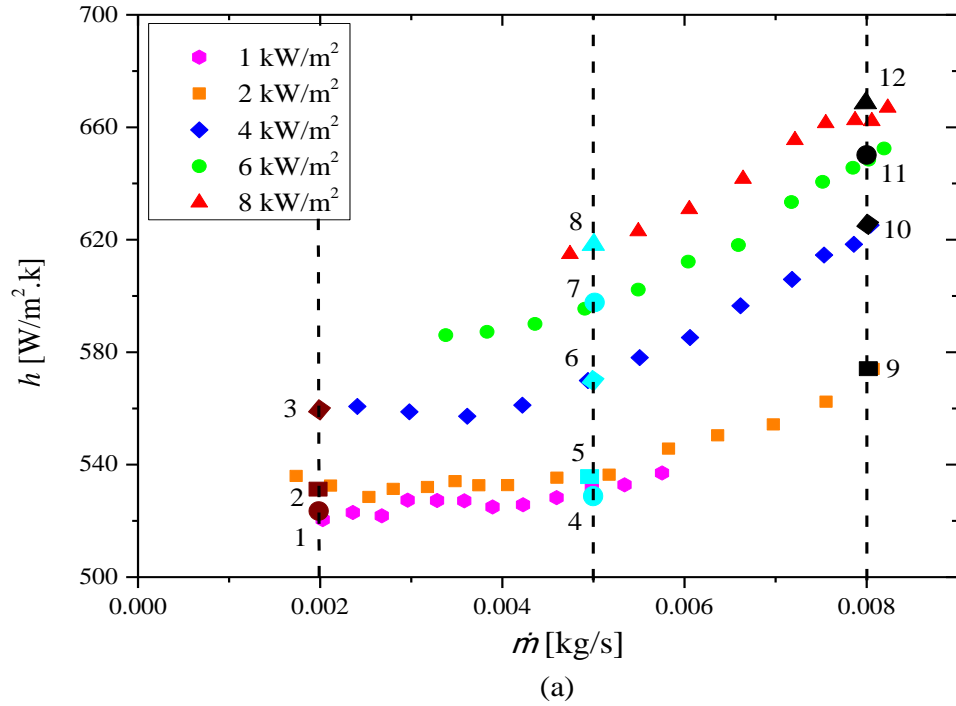


Fig. 6.3: Comparison for upward flow of (a) the heat transfer coefficients as a function mass flow rate and (b) the Nusselt numbers as a function of Reynolds number for different heat fluxes.

$$u(r) = \frac{(D_i/2)^2}{4\mu} \left(\frac{dP}{dx} \right) \left(1 - \frac{r^2}{(D_i/2)^2} \right) \quad 6.2$$

Although it was found that both the viscosity and dP/dx were not constant, but decreased along the tube length, the average fluid velocity did not change significantly along the tube length due to the negligible change in density ($\dot{m} = \rho u A$; as the cross-sectional area and mass flow rate remained constant). Furthermore, it is later shown in Fig. 6.5 (Section 6.2.2) that the friction factors corresponded very well to $64/Re$, which confirms that the velocity profile remained parabolic.

The energy equation was obtained by applying an energy balance on a differential volume element, which was then solved to obtain the radial temperature distribution of the fluid [11-15, 136]:

$$T(r) = T_w - \frac{\dot{q} \left(\frac{D_i}{2} \right)^2}{k} \left(\frac{3}{4} - \frac{r^2}{\left(\frac{D_i}{2} \right)^2} + \frac{r^4}{4 \left(\frac{D_i}{2} \right)^4} \right) \quad 6.3$$

From the conservation of energy principle, it followed that the energy transported by the fluid through a cross-section must be equal to the energy transported through the same cross section if the fluid was at a constant temperature, T_m . By assuming constant density and specific heat, the mean fluid temperature, T_m , was expressed as [11-15, 136]:

$$T_m = \frac{2}{V_{avg} (D_i/2)^2} \int_0^{D_i/2} T(r) u(r) r dr \quad 6.4$$

By substituting the velocity (Eq. 6.2) and temperature (Eq. 6.3) profiles into Eq. 6.4 and combining it with $\dot{q} = h(T_w - T_m)$, a constant Nusselt number of 4.36 (for a constant heat flux boundary condition) that is independent of Reynolds number and Prandtl number, was obtained for a circular tube. It should be noted that this was obtained for constant fluid properties and the variable fluid property results of this study indicated that the Nusselt numbers increased with increasing Reynolds number for Reynolds numbers greater than 1 000.

From the friction factor results (Fig. 6.5) it was concluded that the velocity profile was not significantly affected by the variable fluid properties and remained parabolic, because the friction factors correlated very well with $64/Re$. However, the variable fluid properties significantly affected the temperature profile and thus the thermal boundary layer thickness. Although the flow was fully developed, the mean fluid temperature increased linearly with axial location. This led to a decrease in viscosity and Prandtl number of approximately 13% and 12%, respectively. The Prandtl number represents the ratio of the diffusivity of momentum to the diffusivity of heat. A

decreasing Prandtl number therefore indicated that the diffusivity of heat increased along the tube length, which affected the temperature profile and led to a change in Nusselt number.

From Fig. 6.3 it follows that for Reynolds numbers less than 1 000, the change in Nusselt number with Reynolds number was very small and the Nusselt numbers remained approximately constant. This can also be explained with the Prandtl numbers. As the Reynolds numbers were increased, the diffusivity of momentum increased. At low Reynolds numbers, a significant temperature gradient existed along the tube length, therefore a small increase in Reynolds number led to a significant decrease in temperature and thus increase in Prandtl number. The increase in Prandtl number was mainly due to the increase in momentum diffusivity and not due to the decrease in heat diffusivity. Thus, the temperature profile was not significantly affected, which explains why the Nusselt numbers corresponded well with the constant Nusselt number of 4.36.

A revised fully developed laminar forced convection Nusselt number correlation that accounts for the increase in Nusselt number with Reynolds number, was obtained by a simple power curve fit through all the forced convection heat transfer results for vertical upward and downward flows (Fig. 6.4(a)):

$$Nu_{FC} = 4.36 + 5.36 \times 10^{-9} Re^{2.39} \quad 6.5$$

Eq. 6.5 is valid for Reynolds numbers between 600 and 3 000 (as long as transition does not occur). It should also be noted that the start of the transitional flow regime in horizontal tubes typically occurs in the Reynolds number range of 2 100-2 300. However, this Reynolds number range is significantly affected by inlet geometry, tube diameter and heat flux [21]. Everts and Meyer [21] found that, for mixed convection conditions, buoyancy effects caused transition to occur earlier (at lower mass flow rates); however, the critical Reynolds numbers increased due to the decreasing viscosity with increasing temperature. Similarly, for forced convection conditions in vertical tubes, increasing heat fluxes significantly increased the critical Reynolds numbers to a Reynolds number range of 2 500-3 100 (as will be shown in Section 6.3), due to the decreasing viscosity with increasing temperature. Fig. 6.4(b) shows the deviation of Eq. 6.5 from all the upward and downward flow results. From this figure it follows that all the experimental data were within 2.5% of the correlation, and the average deviation was 1.6%. The equation therefore accurately describes the physics of the laminar forced convection Nusselt number dependency on Reynolds number.

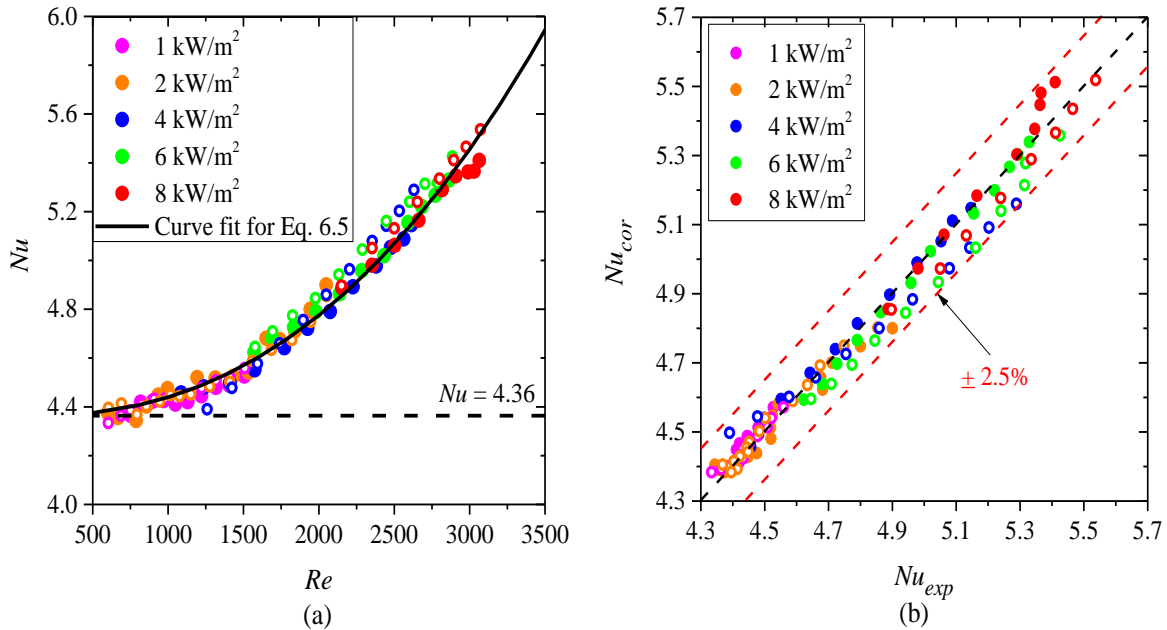


Fig. 6.4: (a) A linear curve fit through the average laminar forced convection Nusselt numbers as a function of Reynolds number and (b) Comparison of the revised fully developed laminar forced convection Nusselt number correlation (Eq. 6.5) with the vertical upward and downward flow experimental data at different heat fluxes.

6.2.2. Pressure drop and heat transfer analogy

The laminar fully developed friction factors were compared as a function of Reynolds number for different heat fluxes and flow directions in Fig. 6.5. Similar to the heat transfer results, this figure indicates that heat flux and flow direction had no influence on the friction factors. The friction factors corresponded very well to the isothermal friction factors of $64/Re$ (solid black line in Fig. 6.5) with an average and maximum deviation of only 0.9% and 2.8%, respectively. Again, this confirmed that the experimental data presented in this section is forced convection heat transfer because it was different from the mixed convection conditions where the friction factors were a function of Grashof number [18, 56]. For instance, for horizontal flow (in Chapter 5), mixed convection caused the magnitude of the friction factors to increase by approximately 20% from $64/Re$ at a heat flux of 8 kW/m².

The relationship between the heat transfer and pressure drop is investigated in Fig. 6.6 in terms of the ratio of friction factors to the Colburn j -factors, f/j , as a function of Reynolds number for both upward and downward flows. This figure indicates that the f/j -ratio of the different heat fluxes were relatively constant with Reynolds number. The slight differences between the heat fluxes were due to the difference in Prandtl numbers, because the Colburn j -factor was a function of Prandtl number. To account for this, the f/j -ratio was divided by $Pr^{1/3}$ and plotted as a function of

Reynolds number in Fig. 6.6(b). A linear curve fit was done through all the data points and Eq. 6.6 was obtained as:

$$\frac{(f/j)}{Pr^{\frac{1}{3}}} = 15.78 - 0.0013Re \quad 6.6$$

By substituting the Colburn j -factor with Eq. 3.14, the revised forced convection friction factors were obtained as:

$$f_{FC} = \frac{Nu_{FC}(15.88 - 0.0014Re)}{Re} \quad 6.7$$

Because it was known that forced convection conditions existed, the Nusselt numbers was substituted with the revised forced convection Nusselt number (Eq. 6.5):

$$f_{FC} = \frac{64}{Re} + \frac{4.8}{Re} - 0.00569 - 7 \times 10^{-12}Re^{2.39} + 8.46 \times 10^{-8}Re^{1.39} \approx \frac{64}{Re} \quad 6.8$$

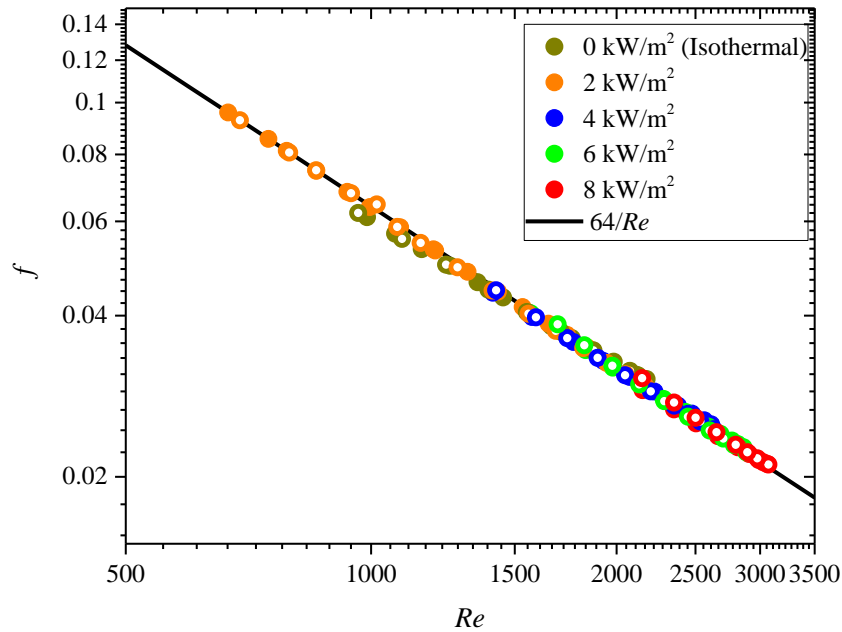


Fig. 6.5: Comparison of the forced convection diabatic friction factors as a function of Reynolds numbers for vertical upward and downward flow at different heat fluxes.

The last two terms of Eq. 6.8 were negligible because of the small coefficients of 10^{-12} and 10^{-8} . Furthermore, the sum of the second ($4.8/Re$) and third terms (0.00569) was very small and negligible. For example, at a Reynolds number of 1 000, the influence of the second and third terms were 1.4%, which was less than the pressure drop uncertainty of 8.5%. Therefore, the maximum contribution of the last four terms in Eq. 6.8 of all the Reynolds numbers was less than 2.2%.

Eq. 6.8 therefore reduced to $64/Re$ with a maximum deviation of 2.2%. The experimental data also correlated well with $64/Re$ with a maximum deviation of 2.9%. Therefore, it was concluded that the fluid properties had no significant influence on the forced convection friction factors and were approximately equal to $64/Re$.

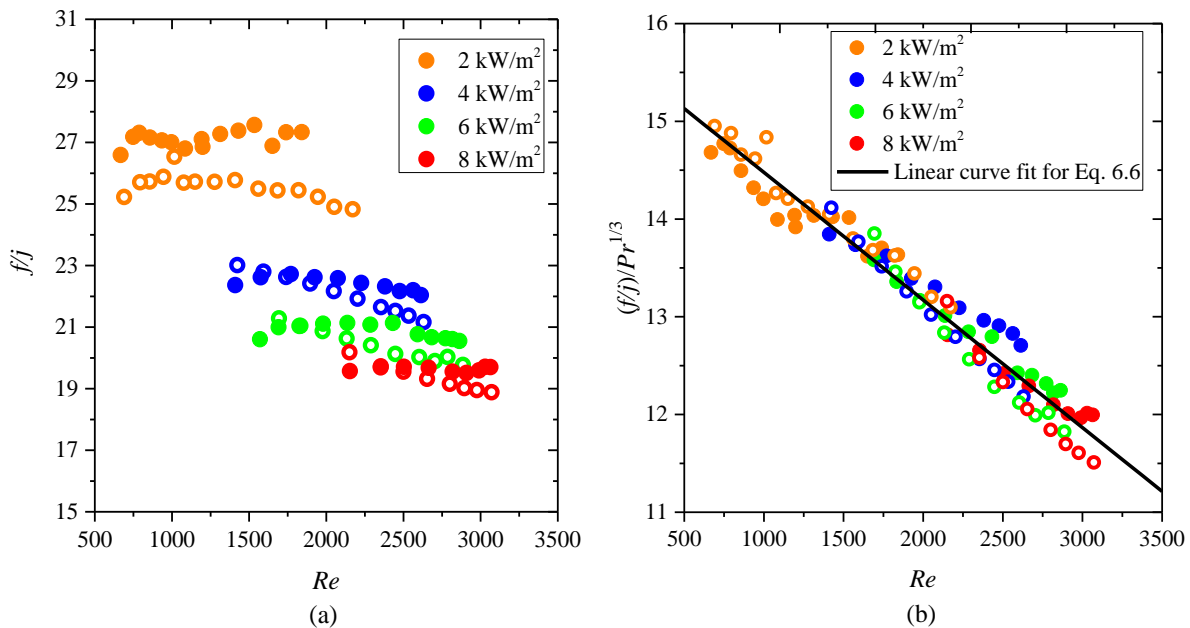


Fig. 6.6: Comparison of (a) ratio of f/j as a function Reynolds numbers and (b) a linear curve fit through the experimental results for $(f/j)/Pr^{1/3}$ as a function of Reynolds number for both upward and downward flows at different heat fluxes.

6.3. Transitional flow

The heat transfer and pressure drop results were compared at different heat fluxes for vertical upward and downward flows for pure forced convection conditions. The boundaries of the transitional flow regime in the developing and fully developed regions were also investigated.

6.3.1. Heat transfer

Fig. 6.7 compares the fully developed forced convection Nusselt numbers as a function of Reynolds number for vertical upward and downward flows. This figure indicates that transition occurred at the same critical Reynolds numbers for both upward and downward flow, but was delayed with increasing heat flux. The fact that, for a specific heat flux, transition occurred at the same critical Reynolds number for both upward and downward flow, proved again that the buoyancy effects were negligible, and that pure forced convection existed.

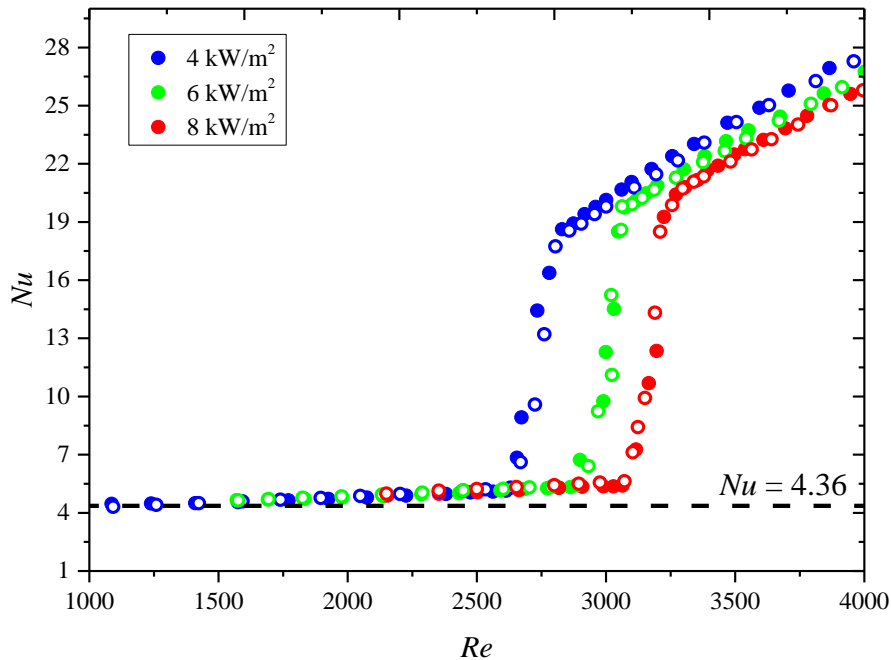


Fig. 6.7: Average fully developed Nusselt numbers as a function of Reynolds number for vertical upward (●) and downward (○) flows at different heat fluxes.

The fact that higher heat fluxes caused transition to occur at a higher Reynolds number was also found in the mixed convection studies by Ghajar and Tam [35], Meyer and Everts [18] and Everts and Meyer [21]. Although the trends were the same, the specific values of the transitional flow regime were not the same. At the same heat flux, the forced convection critical Reynolds numbers were higher. For example, at a heat flux of 8 kW/m² the critical Reynolds number was 3 070 for forced convection (vertical flow), while it was 2 889 for mixed convection (horizontal flow from Chapter 5). This is as expected because the Grashof numbers of the vertical forced convection cases were higher than for the corresponding horizontal mixed convection cases, and the results of Everts and Meyer [21] showed that the critical Reynolds number increased with increasing Grashof number.

Investigating the raw data of the results in Fig. 6.7, showed that the delay in transition between the different heat fluxes was primarily because of the changes in the viscosity – transition always occurred at the same mass flow rate for all the heating cases, which corresponded to the mass flow rate of isothermal flow. As explained by Everts and Meyer [21], heating caused the viscosity of the fluid to decrease along the tube length, therefore the Reynolds numbers increased. It can therefore be concluded that transition was purely driven by mass flow rate for forced convection heat transfer, while the combined effect of heating and buoyancy affected transition in mixed convection conditions [21, 35].

The Reynolds numbers at which the transitional flow regime started, Re_{cr} , and ended, Re_{qt} , were plotted for the lowest heat flux of 1 kW/m^2 and the highest heat flux of 8 kW/m^2 in Fig. 6.8(a). Similar to the results obtained by Everts and Meyer [21, 40], the start of the transitional flow regime occurred at the same moment in time along the entire test section, but the local Reynolds numbers increased linearly along the axial location of the tube due to the decreasing viscosity. Furthermore, the gradient of the critical Reynolds numbers increased with increasing heat flux (from 1 to 8 kW/m^2), due to the increased temperature gradient along the tube length [21]. From the solid markers in Fig. 6.8(a) it follows that the end of the transitional flow regime, Re_{qt} , decreased along the axial location in the developing region and then increased linearly in the fully developed region. Also, the gradients of the Reynolds numbers at which the transitional flow regime started and ended for each heat flux in the fully developed region were approximately the same.

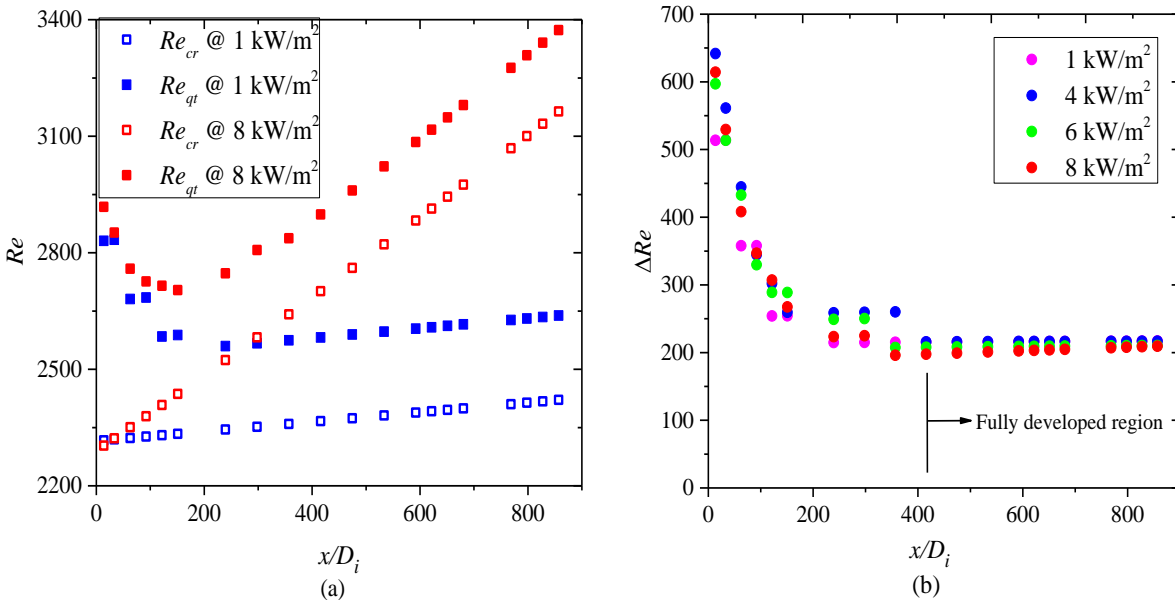


Fig. 6.8: Comparison for vertical upward flow of (a) Reynolds numbers at which the transitional flow regime started, Re_{cr} , and ended, Re_{qt} and (b) width of the transitional flow regime, ΔRe , as a function axial location for different heat fluxes.

Fig. 6.8(b) compares the differences between the Reynolds numbers at which the transitional flow regime started and ended using the width of the transitional flow regime, ΔRe . For all the different heat fluxes ($1 - 8 \text{ kW/m}^2$), the width of the transitional flow regime was a maximum near the inlet of the test section and decreased along the axial location up to the fully developed region where it converged to a constant value of approximately 210. The width of the transitional flow regime became constant at $x/D_i \geq 416$, corresponding to the laminar forced convection thermal entrance length in Fig. 4.4. From Fig. 6.8(b) it follows that, for both developing and fully developed flows, heating did not significantly affect the width of the transitional flow regime, unlike mixed convection where the width of the transitional flow regime was affected by the buoyancy effects due to increases in heat flux [21] or inclination angle (Fig. 5.15).

Up to now, only two sets of correlations were available for predicting the start and end of the transitional flow regime for mixed convection in the developing and fully developed region of smooth tubes. The first set of correlations were developed by Ghajar and Tam [38] and were a function of axial location only. However, as found by Everts and Meyer [21] for mixed convection heat transfer and also shown in Fig. 6.7 for forced convection heat transfer, heating caused the critical Reynolds numbers to increase.

Everts and Meyer [21] therefore developed the second set of correlations that accounted for both changes in axial position and buoyancy effects (Grashof number). The correlations are valid for forced and mixed convection heat transfer in the developing and fully developed region. However, for pure forced convection heat transfer, as in this study, the buoyancy forces have negligible or no influence on the boundaries of the transitional flow regime. The mixed convection correlation of Everts and Meyer [21] underpredicted the forced convection transitional flow Reynolds numbers by 11% because it considers the effect of buoyancy on the transitional flow Reynolds numbers.

For pure forced convection heat transfer, the critical Reynolds numbers were divided by the Prandtl number ratio (Pr_b/Pr_w) to account for the effects of heating and plotted as a function axial location in Fig. 6.9(a). A linear curve fit was done through all the data points at different heat fluxes for both upward and downward flows to obtain the following correlation to determine the forced convection critical Reynolds number, Re_{cr} :

$$Re_{cr} = \left(1958 + 0.5 \frac{x}{D_i}\right) \frac{Pr_b}{Pr_w} \quad 6.9$$

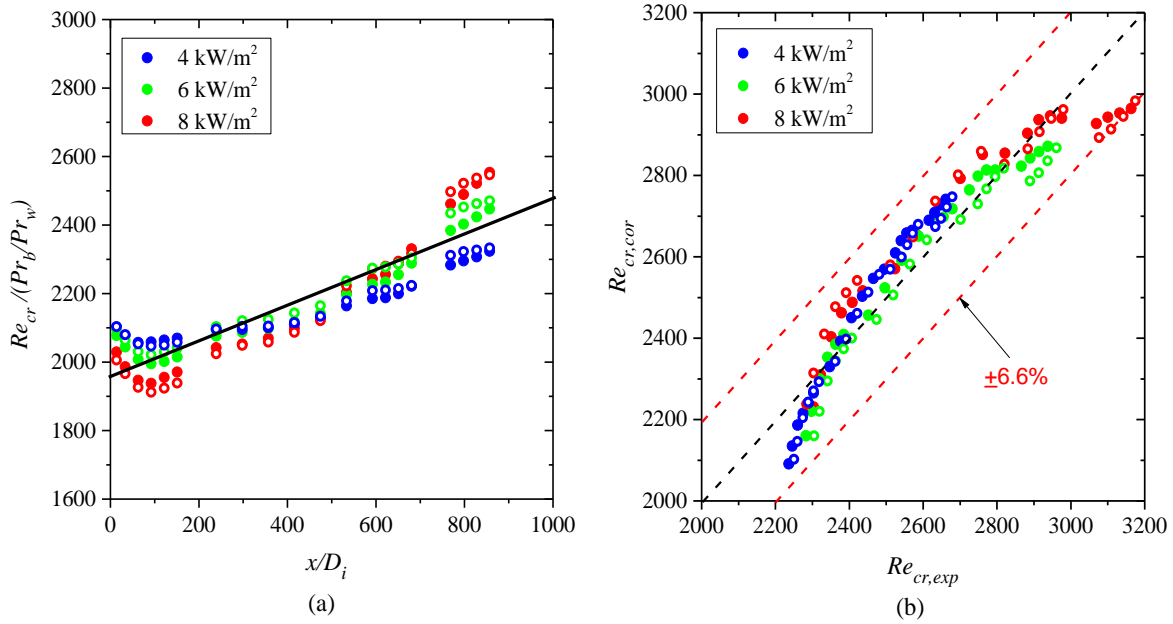


Fig. 6.9: Comparison of (a) $Re_{cr}/(Pr_b/Pr_w)$ as a function of axial location and (b) the critical Reynolds numbers calculated from Eq. 6.9 with experimental data for upward and downward flow at different heat fluxes.

Eq. 6.9 is valid for forced convection heat transfer (independent of Grashof number) and for $1.01 \leq Pr_b/Pr_w \leq 1.25$, $14 \leq x/D_i \leq 886$ and $3.5 \leq Pr \leq 8.1$. As shown by Ghajar and Tam [35], the inlet geometry has an effect on the transitional flow regime. This equation is therefore only valid for a square-edged inlet as was used during the experiments for this study. Fig. 6.9(b) indicates that the average deviation of the correlation (Eq. 6.9) from the experimental data was 2.5% and the maximum deviation was 6.6%.

For the end of the transitional flow regime, the Reynolds number, Re_{qt} , was divided by Pr^3 , and plotted in Fig. 6.10(a). A power curve fit was done through all the experimental data of upward and downward flows at different heat fluxes to obtain the following correlation:

$$Re_{qt} = 8770Pr^{-2/3} \quad 6.10$$

Eq. 6.10 is valid for forced convection heat transfer (independent of Grashof number) and for $3.5 \leq Pr \leq 8.1$ and $14 \leq x/D_i \leq 886$. This equation is also valid for a square-edged inlet only. The comparison of Eq. 6.10 with the experimental data is shown in Fig. 6.10(b) where the average deviation was 2.3% and the maximum deviation was 9.5%.

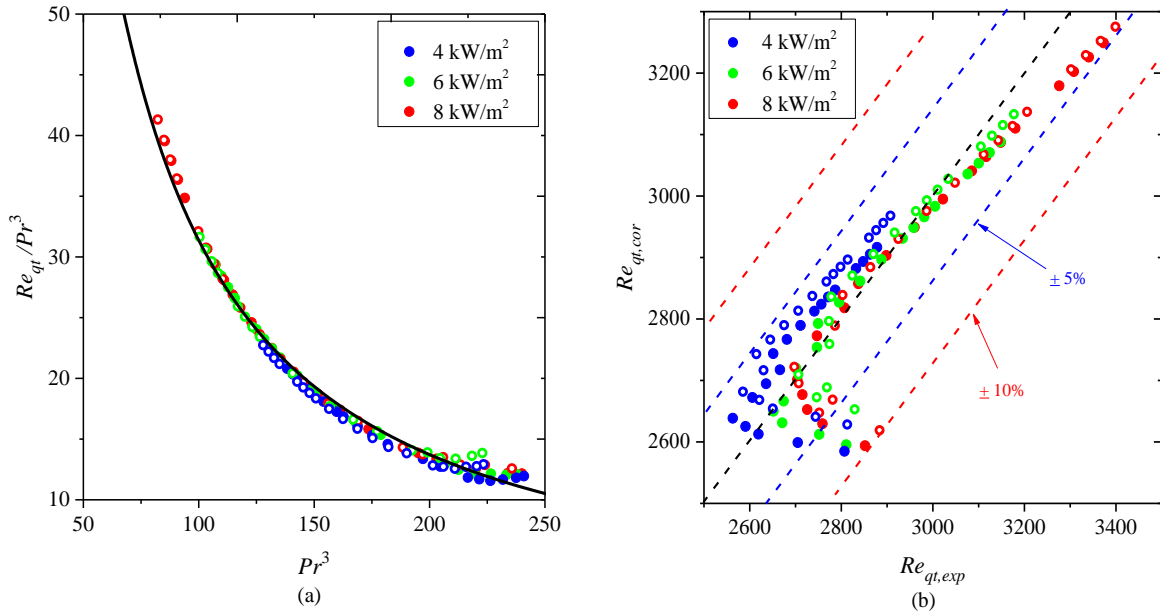


Fig. 6.10: Comparison of (a) Re_{qt}/Pr^3 as a function of axial location and (b) the Reynolds numbers at which the transitional flow regime ended calculated from Eq. 6.10 with experimental data in the upward and downward flow directions at different heat fluxes.

6.3.2. Pressure drop in the transitional flow regime

Fig. 6.11 shows the forced convection friction factors as a function of bulk Reynolds numbers (Reynolds number at the center of the two pressure taps in Fig. 3.3) for the heat fluxes of 0 (isothermal), 4, 6, and 8 kW/m² for upward and downward flows.

Similar to Fig. 6.7, transition was independent of flow direction, but was delayed as the heat fluxes increased. The critical Reynolds number at which the transitional flow regime started for isothermal flow was a minimum of 2 270 and then increased with increasing heat flux up to a maximum of 3 070 at a heat flux of 8 kW/m² (Fig. 6.11). As expected, transition occurred for all the heat fluxes (including isothermal flow) at the same mass flow rate of approximately 0.0081 kg/s and the increasing Reynolds numbers were only due to the decreasing viscosities with increasing temperatures. Similarly, the end of the transitional flow Reynolds numbers also increased with increasing heat flux and occurred at approximately the same mass flow rate for the fully developed friction factors.

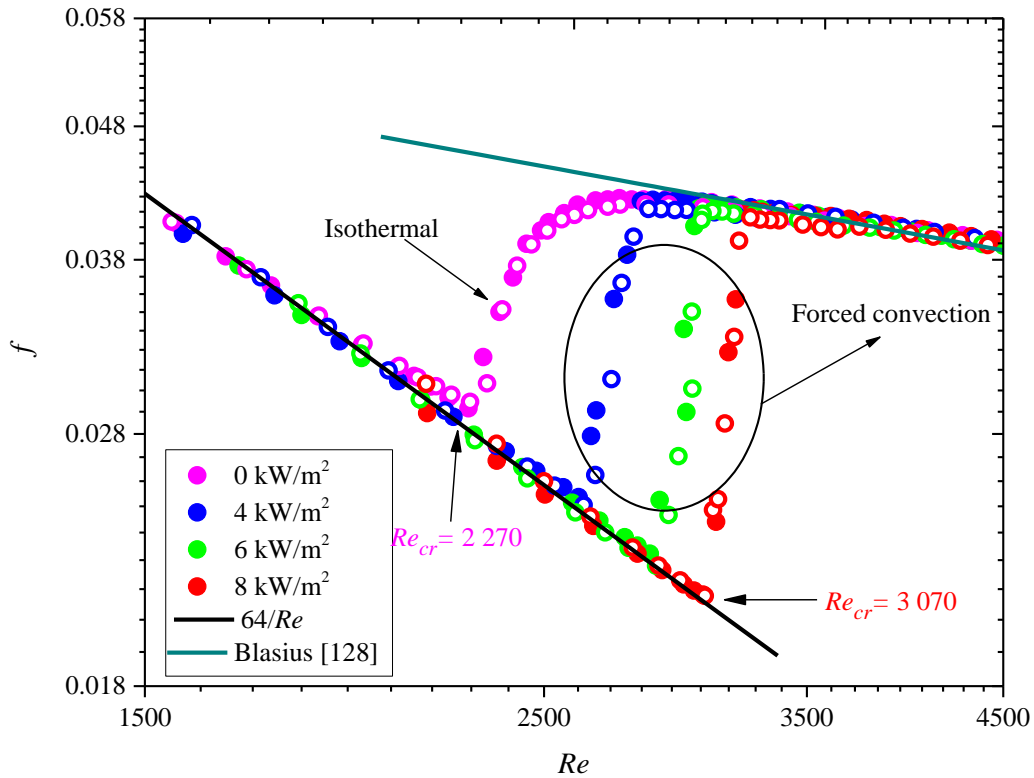


Fig. 6.11: Comparison of the fully developed friction factors as a function of Reynolds number at different heat fluxes for vertical upward and downward flow. The heat flux of 0 kW/m² was for isothermal flow.

As the Reynolds numbers at which the transitional flow regime started (Re_{cr}) and ended (Re_{qt}) increased simultaneously with increasing heat flux, the width of the transitional flow regime, ΔRe , remained relatively constant. Again, this is different from mixed convection conditions where the width of the transitional flow regime was significantly affected by the buoyancy effects due to increases in heat flux [21] or inclination angle (Fig. 5.15).

Similar to the laminar flow regime, all the friction factors in the quasi-turbulent and turbulent flow regimes were approximately the same for the various heat fluxes in the upward and downward flow configurations.

6.4. Conclusions and recommendations

Previous experimental literature showed that very limited works were conducted on internal forced convection in the transitional flow regime. Most probably because it is very challenging to perform experiments in the forced convection flow regime. Therefore, the aim of this chapter was to experimentally investigate the effect of different heat fluxes on the forced convection heat transfer and pressure drop characteristics in the laminar and transitional flow regimes of a smooth circular

tube. To ensure forced convection conditions and negligible buoyancy effects, experiments were conducted with the test section in a vertically upward and downward orientation.

It was found that flow direction had a negligible effect on the Nusselt numbers for Reynolds numbers higher than 600. Furthermore, the fully developed laminar forced convection Nusselt numbers were not constant at 4.36, for a constant heat flux boundary condition, but were a function of Reynolds number, but independent of Grashof number. Heat flux had no influence on the magnitude of the fully developed forced convection friction factors in the laminar flow regime, and the friction factors corresponded well with $f = 64/Re$. A revised laminar fully developed forced convection Nusselt number correlation, which is a function of Reynolds number, was developed for flow in smooth tubes.

The Reynolds numbers at which the transitional flow regime started and ended in the fully developed region increased simultaneously as the heat flux increased for pure forced convection conditions. Furthermore, the width of the transitional flow regime was the same for all heat fluxes and decreased along the length of the tube in the developing region up to the fully developed region where it remained constant. Correlations were developed to determine the boundaries of the transitional flow regime for pure forced convection. It was concluded from both the heat transfer and pressure drop results that transition occurred at the same mass flow rate for all heat fluxes, which corresponded to the isothermal flow case. However, the Reynolds numbers increased with increasing heat flux due to the decreasing viscosity with increasing temperature.

It is recommended that laminar forced convection Nusselt number for constant wall temperature conditions be investigated experimentally for comparison with the constant property Nusselt number of 3.66 and also with the revised Nusselt number for constant heat flux conditions. Furthermore, forced convection heat transfer should also be investigated using different channels such as rectangular channels with different aspect ratios as this can change how the velocity and temperature profiles develop and thus affect the forced convection heat transfer.

7. Effects of flow-calming section contents and inlet contraction ratios

7.1. Introduction

In this chapter, the effect of flow-calming section contents and inlet contraction ratios (as shown schematically in Table 3.3 and Fig. 3.2) on the heat transfer and pressure drop in the transitional flow regime were investigated. The content of this section is presented in two main parts: the calming section content (Section 7.2) and the contraction ratio (Section 7.3). Heat exchangers in practice have different contraction ratios, depending on the type and size of the inlet header or plenum geometry. This may lead to different levels of inlet disturbances that could influence the start and end of the transitional flow regime. The analysis involved both isothermal and diabatic flow conditions in order to compare the effect of heating on the different contraction ratios.

7.2. Calming section content

To investigate the effect of different content inside a flow-calming section, the heat transfer and pressure drop characteristics of the original flow-calming section (Fig. 3.2(a)) was compared to an empty flow-calming section (Fig. 3.2(b)) using two different contraction ratios. The flow-calming section diameters were 170 mm and 56 mm, leading to contraction ratios of 33 and 11. All the flow-calming and inlet sections were of the same length.

7.2.1. Pressure drop characteristics

Fig. 7.1(a) and (b) show the friction factor results for the original and empty flow-calming sections (as shown in Fig. 3.2) with contraction ratios of 11 and 33 respectively and a square-edged inlet geometry. Also included are $f = 64/Re$ and the Blasius [128] correlations. For both contraction ratios (Fig. 7.1(a) and (b)), the results showed no significant difference between the two flow-calming sections in all the flow regimes. For each contraction ratio, transition occurred at approximately the same critical Reynolds number. For the contraction ratio of 11 (Fig. 7.1(a)), the critical Reynolds numbers at which the transitional flow regime started were 2 300 and 2 280 for the empty and original flow-calming section respectively, while for the contraction ratio of 33 (Fig. 7.1(b)) it was 2 218 and 2 200 respectively. Similarly, Fig. 7.1 indicates that the transitional flow regime ended at approximately the same Reynolds numbers for both flow-calming sections.

Fig. 7.1(c) and (d) compares the isothermal friction factors of the original and an empty flow-calming sections with a re-entrant inlet and a contraction ratio of 11 and 33 respectively. Similar to the square-edged inlet, the flow-calming section content had a negligible influence on the

friction factors in all the flow regimes and transition occurred at approximately the same Reynolds numbers.

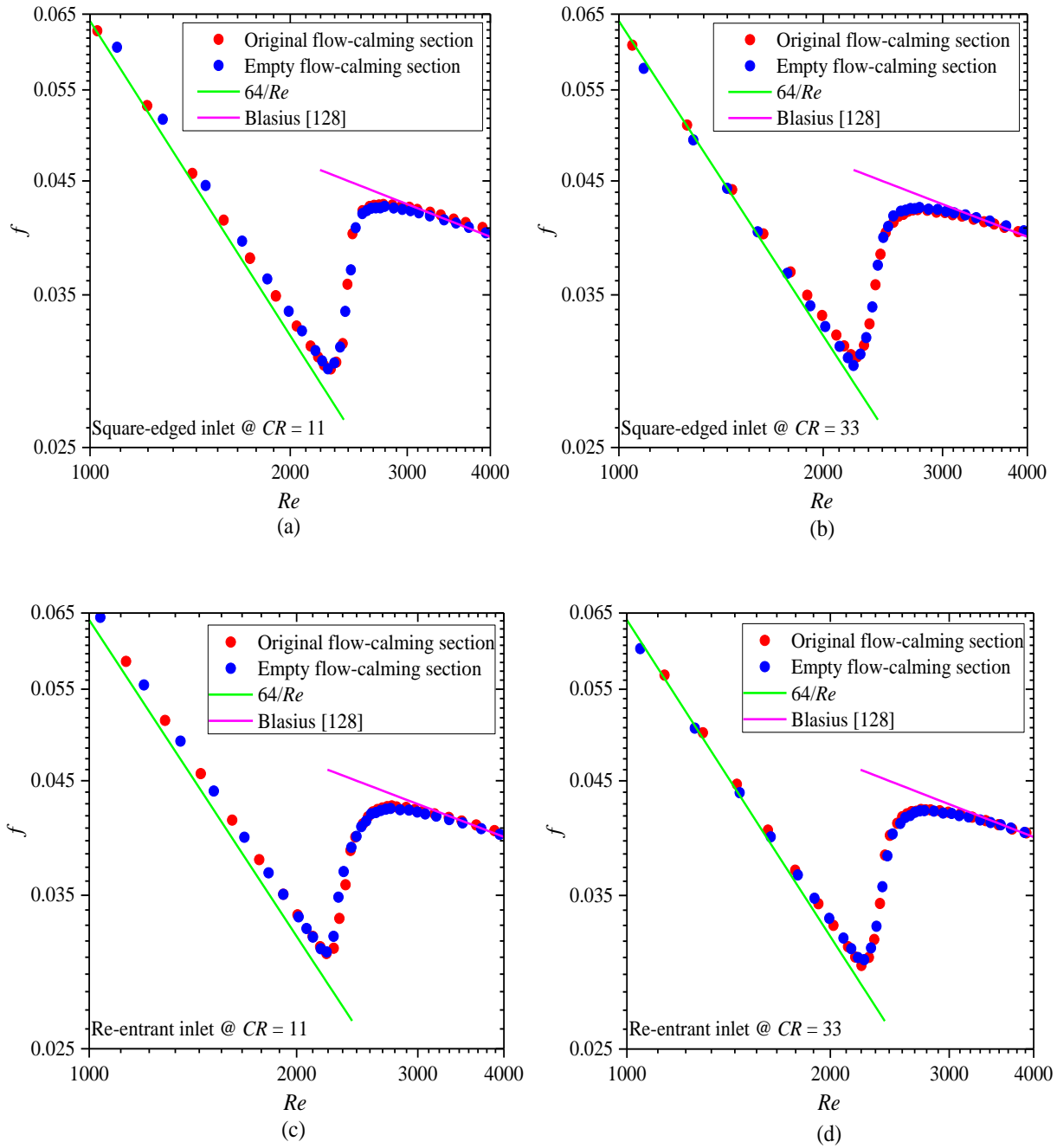


Fig. 7.1: Comparison of isothermal friction factors as a function of Reynolds number using the original and empty flow-calming sections with a square-edged inlet and contraction ratios, CR , of (a) 11 and (b) 33, and also with a re-entrant inlet for contraction ratios of (c) 11 and (d) 33.

It was therefore concluded that the flow-calming section contents had no influence on the isothermal friction factors in all flow regimes, or on the boundaries of the transitional flow regime, when square-edged and re-entrant inlets were used. Although it was not shown in this report, similar results and conclusions were found for the diabatic friction factors at different heat fluxes of 4, 6 and 8 kW/m².

7.2.2. Heat transfer characteristics

Fig. 7.2 compares the heat transfer coefficients in terms of the Colburn j -factors as a function of Reynolds numbers for the different flow-calming sections, contraction ratios and inlet geometries at a heat flux of 8 kW/m², specifically for the fully developed part (indicated in Fig. 3.3) of the test section between thermocouple stations 16 to 21 ($680 \leq x/D_i \leq 886$). This was the maximum heat flux tested with the lowest uncertainties. Similar to the friction factor results, Fig. 7.2 indicates that the flow-calming section contents had no influence on the Colburn j -factors in all the flow regimes when square-edged (Fig. 7.2(a) and (b)) and re-entrant (Fig. 7.2(c) and (d)) inlet geometries were used. Furthermore, the transitional flow regime also started and ended at approximately the same Reynolds numbers. It was expected that the same conclusions could be made from the friction factor and Colburn j -factor results, because Everts and Meyer [40] showed that a direct relationship between pressure drop and heat transfer existed in the transitional flow regime.

A possible reason for the negligible difference might be that the effects of the flow-calming section contents diminished in the empty inlet section between the flow-calming section and the test section (the length of this section might be a contributing factor). Tam and Ghajar [52] found that different screen sizes placed near the outlet of the flow-calming section had a significant influence on the local heat transfer coefficients when a bell-mouth inlet was used. The reason for this was because of the bell-mouth geometry that gradually contracts from the flow-calming section (close to the screen) to the inlet of the test section. This caused the disturbances generated by the screens to be transferred to the test section, unlike the square-edged and re-entrant inlets where these disturbances were suppressed in the inlet section.

Although it is not shown in this report, similar results and conclusions were found with the other heat fluxes of 4 and 6 kW/m² and contraction ratios of 11 and 33, where the flow-calming section contents had no influence on the heat transfer coefficients in all the flow regimes using square-edged and re-entrant inlets.

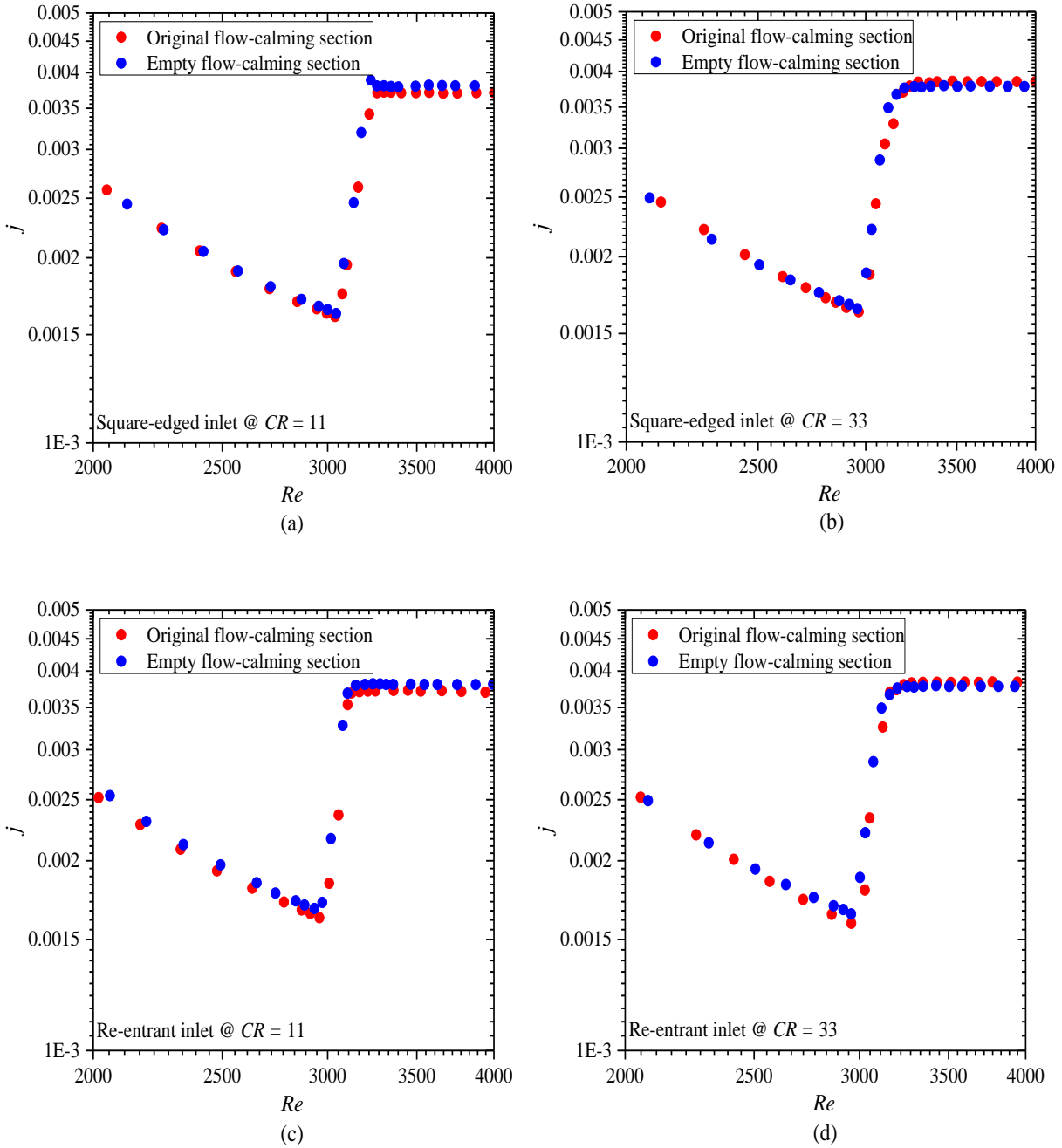


Fig. 7.2: Comparison of the fully developed Colburn j -factors as a function of Reynolds number for the original and empty flow-calming sections at a heat flux of 8 kW/m^2 for (a) square-edged with a contraction ratio of 11, (b) square-edged with a contraction ratio of 33, (c) re-entrant with a contraction ratio of 11 and a (d) re-entrant with a contraction ratio of 33.

7.3. Contraction ratio

It was concluded in Sections 7.2.1 and 7.2.2 that the content of the flow-calming section had no influence on the pressure drop and heat transfer characteristics for square-edged and re-entrant inlet geometries. An empty flow-calming section was therefore used to investigate the effect of contraction ratio, because it was challenging to construct a long flow-calming section with a small tube diameter of less than 26 mm, using the same flow-calming section contents and arrangements as in Fig. 3.2(a). Four different contraction ratios (5, 11, 15 and 33), with equal flow-calming and inlet section lengths, were compared using square-edged and re-entrant inlets. A hydrodynamically fully developed inlet (Fig. 3.2(c)) and a 90° bend inlet (Fig. 3.2(d)) were also compared.

7.3.1. Pressure drop characteristics

Fig. 7.3 shows the fully developed isothermal and diabatic friction factors for the different contraction ratios using the square-edged and re-entrant inlet geometries. Also included are the results for the hydrodynamically fully developed (empty black circles) and the 90° bend (stars) inlets. Similar to the results obtained in the previous studies [35, 41, 48, 53, 55] that investigated different inlet geometries, Fig. 7.3 indicates that the friction factors in the laminar and quasi-turbulent flow regimes were unaffected by the contraction ratio. The isothermal friction factors (Fig. 7.3(a) and (b)) correlated well with the $f = 64/Re$ and Blasius [128] correlations, but the laminar diabatic friction factors were significantly higher than $f = 64/Re$ due to buoyancy effects [21, 53]. However, the isothermal and diabatic friction factors in the transitional flow regime of both inlet geometries were affected. For the square-edged inlet in Fig. 7.3(a) and (c), transition was delayed as the contraction ratio decreased from 33 to 5.

This explains why Olivier and Meyer [48] found a delay in transition for the isothermal friction factors when the contraction ratio decreased from 9.6 to 7.3 due to different test section diameters (15 mm and 19 mm) with the same flow-calming section and a square-edged inlet. The protrusion of the tube into the inlet section by one-diameter for the re-entrant inlet (Fig. 3.2(b)) led to increased inlet disturbances when compared to the square-edged inlet. This caused transition to occur much earlier for the re-entrant inlet (Fig. 7.3(b) and (d)) than the square-edged inlet (Fig. 7.3(a) and (c)) as was also found by Ghajar and Tam [35, 52, 53, 55] and Olivier and Meyer [48].

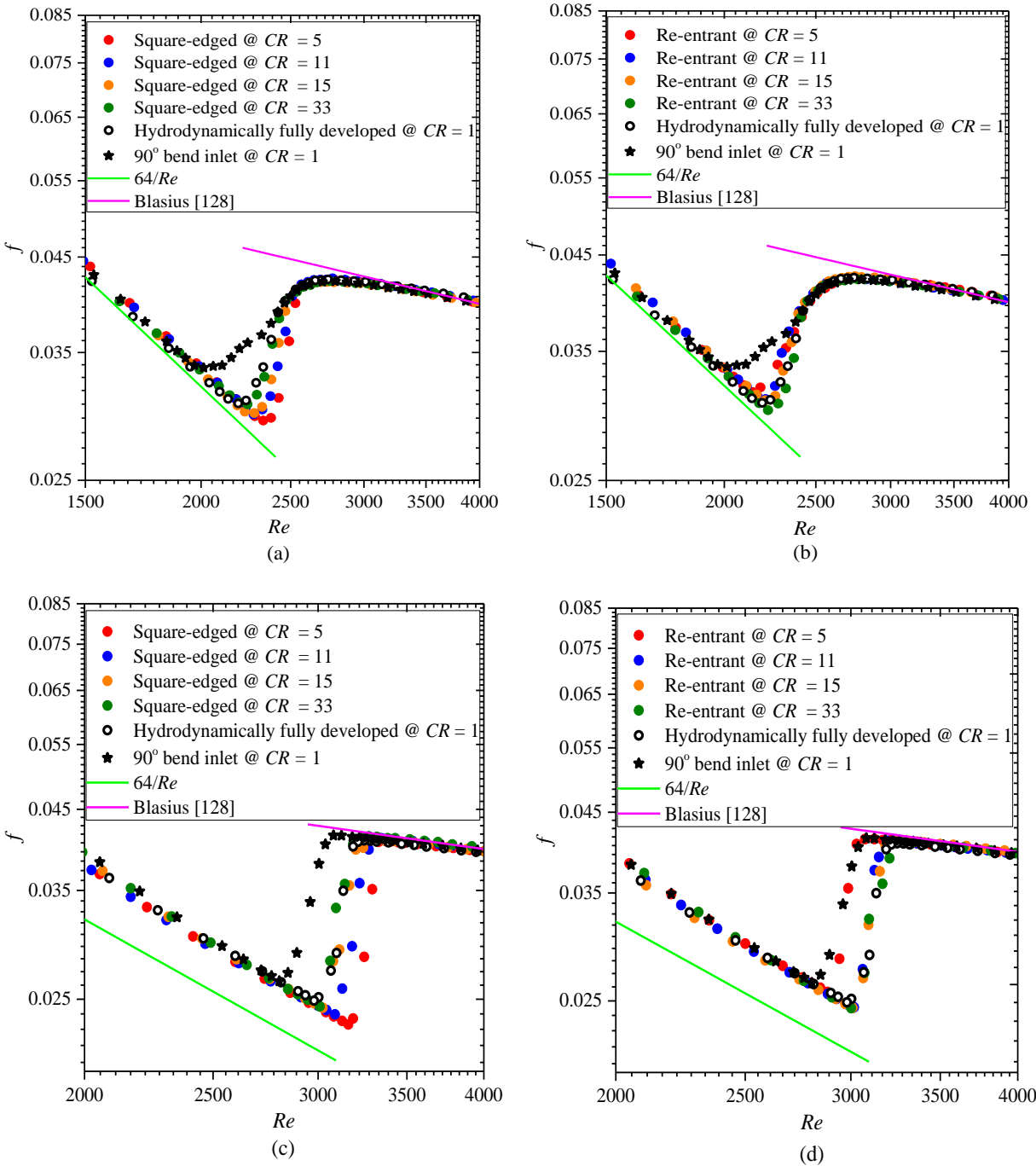


Fig. 7.3: Comparison of isothermal friction factors for (a) a square-edged and (b) a re-entrant inlet, as well as diabatic friction factors at a heat flux of 8 kW/m^2 for (c) a square-edged and (d) a re-entrant inlet, as a function of Reynolds number.

Fig. 7.3(b) and (d) also indicate that for a re-entrant inlet, transition was delayed for increasing contraction ratios, which is opposite than what was found for the square-edged inlet. Furthermore, due to the increased disturbance caused by the tube protrusion of the re-entrant inlet, the effect of the contraction ratio was less than for the square-edged inlet. The inlet disturbances caused by tube protrusion decreased with increasing contraction ratio, which explains why transition was delayed. From Fig. 7.3(c) and (d) it follows that the difference between the diabatic friction factors in the transitional flow regime for contraction ratios of 15 and 33 were small. It can therefore be assumed that there will be a negligible difference between the transitional flow friction factors of higher contraction ratios.

Fig. 7.3 indicates that the hydrodynamically fully developed inlet results were similar to the results obtained using the maximum contraction ratio of 33 for both the square-edged and re-entrant inlets. This means that as the contraction ratios increased and approached infinity, the effects of the inlet disturbances on the transitional flow regime became negligible and results approached those of the hydrodynamically fully developed inlet. However, as the contraction ratio decreased and approached 1, transition was significantly affected (especially at lower contraction ratios between 5 and 1), and was significantly delayed for the square-edged inlet and occurred much earlier for the re-entrant inlet. As expected, transition occurred earlier for the 90° bend inlet than for the other inlets and contraction ratios because of the significantly high inlet disturbances generated by the 90° bend at the inlet.

7.3.2. Heat transfer characteristics

Fig. 7.4 compares the heat transfer results in terms of the Colburn j -factors for different inlet geometries and contraction ratios at a constant heat flux of 8 kW/m². As expected, the laminar and quasi-turbulent flow regimes in Fig. 7.4 showed no significant differences between the contraction ratios. Similar to the friction factor results (Fig. 7.3), a decrease in the contraction ratio caused a delay in the entire transitional flow regime for the square-edged inlet (Fig. 7.4(a)), while transition occurred earlier for the re-entrant inlet (Fig. 7.4(b)). It can therefore also be concluded that for a fixed flow-calming section, an increase in test section diameter will not only affect the transitional flow regime due to the changes of the buoyancy effects [21], but also due to the changes in the inlet contraction ratio.

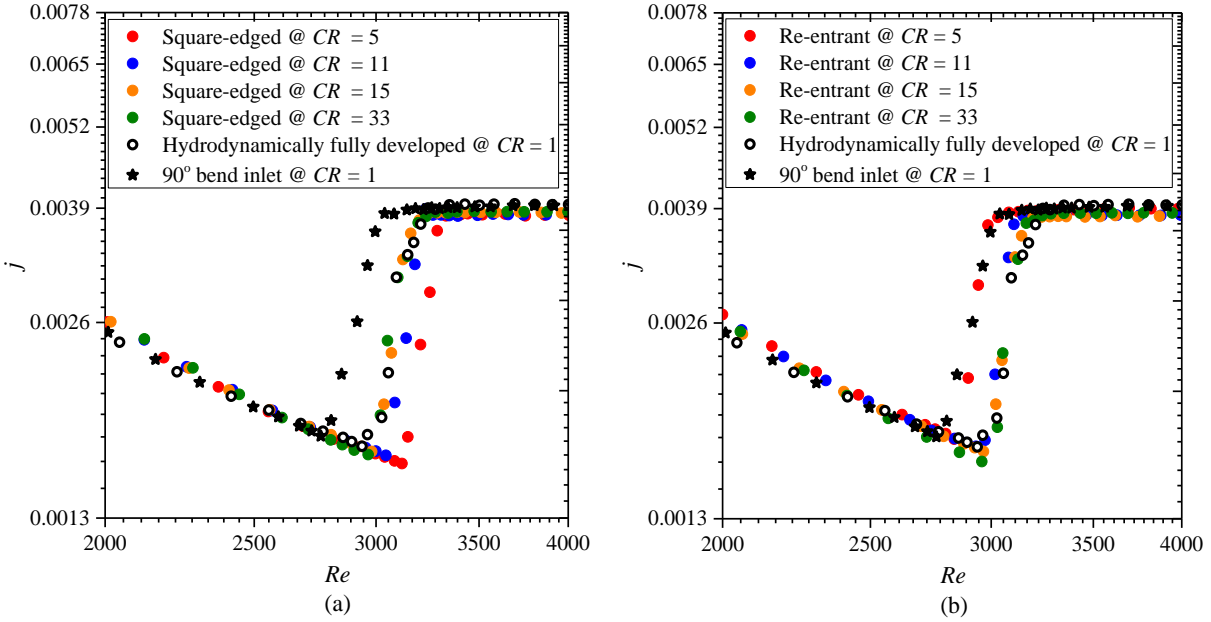


Fig. 7.4: Comparison of the fully developed Colburn j -factors as a function of Reynolds number for different contraction ratios using (a) square-edged inlet and (b) re-entrant inlet at a heat flux of 8 kW/m^2 .

To investigate the effect of inlet disturbances on the boundaries of the transitional flow regime, Fig. 7.5 compares the Reynolds numbers at which the transitional flow regime started (red) and ended (blue) for the different types of inlets as a function of contraction ratio at a heat flux of 8 kW/m^2 . For the square-edged inlet, both the Reynolds numbers at which the transitional flow regime started (Re_{cr}) and ended (Re_{qt}) decreased with increasing inlet contraction ratios. Therefore, a lower contraction ratios led to a smoother inlet that caused transition to be delayed [41]. However, for the re-entrant inlet, the Reynolds numbers at which the transitional flow regime started and ended increased with increasing contraction ratio but remained lower than for the square-edged inlet.

As the contraction ratio decreased, the disturbances increased, which caused transition to occur earlier (at lower Reynolds numbers). At the maximum contraction ratio of 33, the transitional flow Reynolds numbers for both inlets were approximately the same and also corresponded to the hydrodynamically fully developed (FD) inlet. This implies that the boundaries of the transitional flow regime were affected by the different inlet geometries when the contraction ratios were relatively low, but not when the contraction ratio was higher than 33. The 90° bend inlet had the lowest Reynolds numbers for both the start and end of the transitional flow regime. This was as expected because a greater inlet disturbance was created at the inlet of the test section due to the 90° bend. Furthermore, Fig. 7.5 also indicated that the width of the transitional flow regime ($\Delta Re = Re_{qt} - Re_{cr}$, as defined by Everts and Meyer [21]) for the square-edged and re-entrant inlet geometries, increased with increasing contraction ratio.

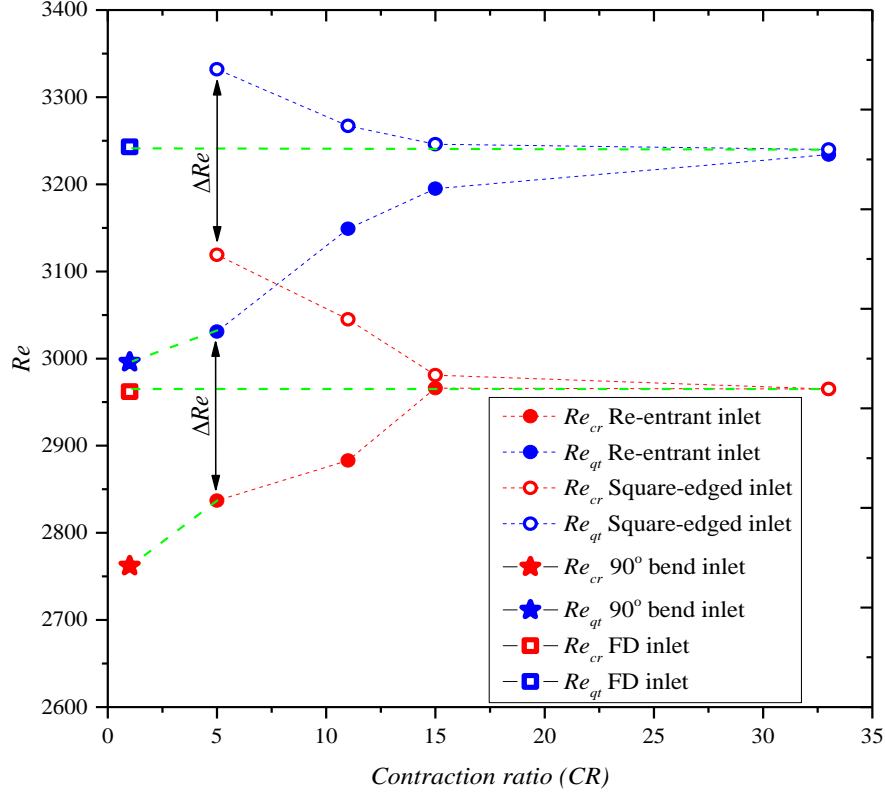


Fig. 7.5: Comparison of the Reynolds numbers at which the transitional flow regime started (Re_{cr}) and ended (Re_{qt}) as a function of contraction ratio for the different inlet geometries at a heat flux of 8 kW/m^2 . “FD” in the legend indicates hydrodynamic fully developed inlet.

The Reynolds numbers at which the transitional flow regime started (Fig. 7.6(a)) and ended (Fig. 7.6(b)) are compared for the square-edged and re-entrant inlets as a function of heat flux. As expected [35], both the Reynolds numbers at which the transitional flow regime started and ended increased with increasing heat flux. However, the rate of this increase differed for the different inlets and contraction ratios. Fig. 7.6(c) and (d) compare the difference between the transitional flow Reynolds numbers of the square-edged and re-entrant inlets, $\Delta Re_{inlets} = Re_{squ} - Re_{ree}$, at the start and end of the transitional flow regime, as a function of heat flux.

At lower contraction ratios (≤ 11), the rate of increase of Reynolds numbers with heat flux for the square-edged inlet was slightly more than for the re-entrant inlet. However, at higher contraction ratios (> 11), the difference between the transitional flow Reynolds numbers of the square-edged and re-entrant inlets became negligible. According to Nagendra [110], for all flow regimes, the influence of inlet disturbances decreased with increasing values of $ReRa(D/L)$ and become insignificant for $ReRa(D/L) > 10^6$. At the maximum heat flux of 8 kW/m^2 and a contraction ratio of 5, the value of $ReRa(D/L)$ was 1.42×10^5 . This is why for heat fluxes lower than 8 kW/m^2 , the effect of inlet disturbances on the transitional flow regime were significant for all the inlets.

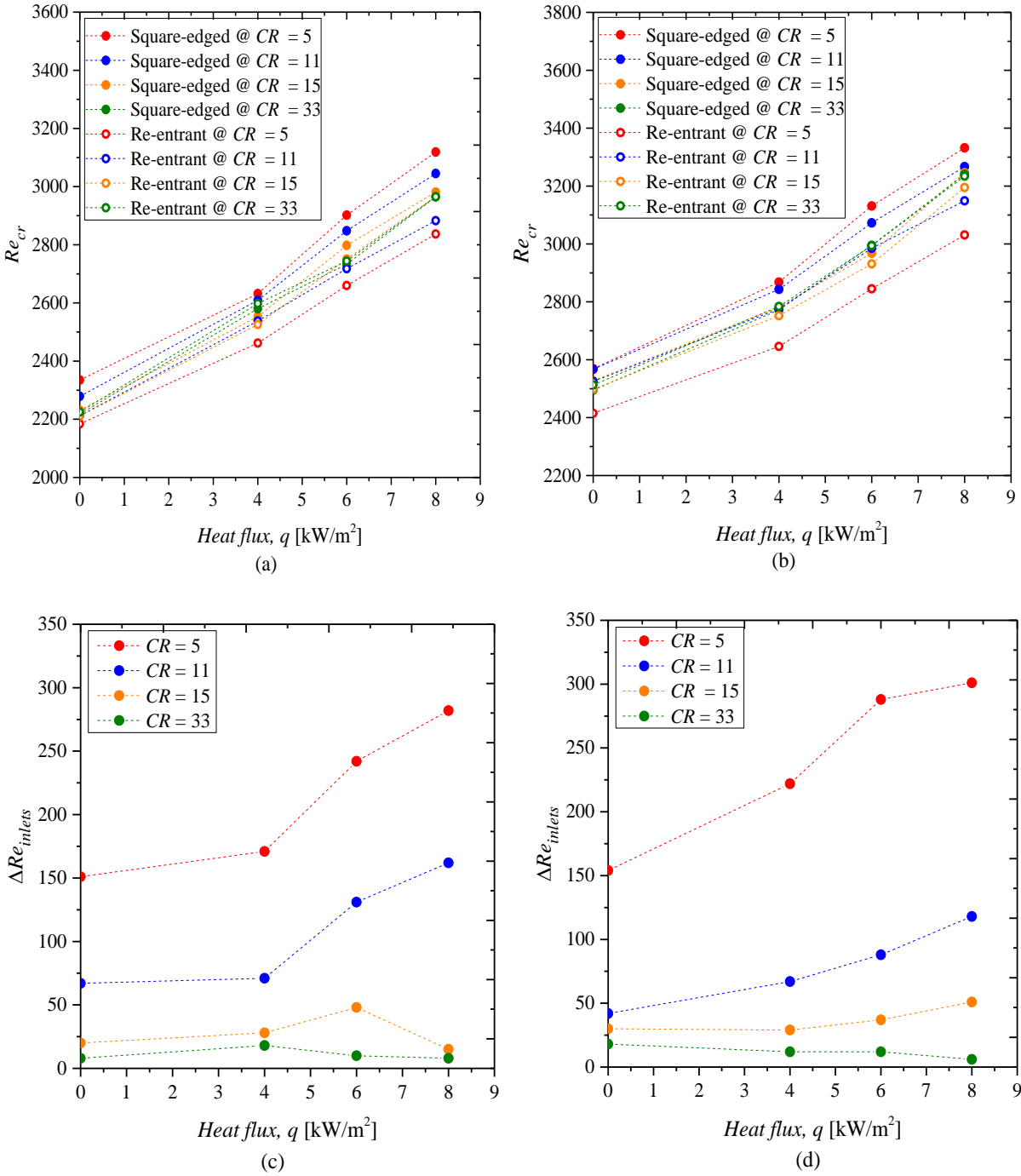


Fig. 7.6: Comparison of the Reynolds number at which the transitional flow regime (a) started and (b) ended, as well as the difference between the square-edged and re-entrant inlets at the (c) start ($\Delta Re_{inlets} = Re_{squ} - Re_{ree}$) and (d) end ($\Delta Re_{inlets} = Re_{squ} - Re_{ree}$) of the transitional flow regime, as a function of heat flux.

Mori *et al.* [111] found that for high levels of inlet disturbances, the critical Reynolds numbers increased with increase in Rayleigh numbers, because buoyancy effects suppressed the disturbances generated at the inlet. This explains why for lower contraction ratios such as 5 and 11, the difference between the Reynolds numbers of the square-edged and re-entrant inlets increased with increasing heat flux (Gr or Gr^*) in Fig. 7.6(c) and (d). The green markers in Fig. 7.6 indicate that at the maximum contraction ratio (33), the Reynolds number difference (ΔRe_{inlets}) at both the start (Fig. 7.6(c)) and end (Fig. 7.6(d)) of the transitional flow regime remained approximately zero for all the heat fluxes.

7.3.3. Schematic summary

Fig. 7.7 gives an easier schematic representation of the influence of contraction ratio on the fully developed heat transfer coefficients for a square-edged inlet (blue lines) and a re-entrant inlet (green lines). As was found by previous studies [35, 41, 48, 53, 55] different inlet conditions did not affect the heat transfer coefficients in the laminar, quasi-turbulent and turbulent flow regimes; however, the transitional flow regime was significantly affected. When a re-entrant inlet was used, the light green to dark green lines indicate that transition is delayed when the contraction ratio was increased up to the maximum contraction ratio of 33, which is represented by the red line. The opposite exists when a square-edged inlet was used. As indicated by the light blue to dark blue lines, an increase in contraction ratio led to an earlier transition. The “converged” solid red line not only represented the results of the square-edged and re-entrant inlet geometries when a higher contraction ratio was used, but also the hydrodynamically fully developed inlet.

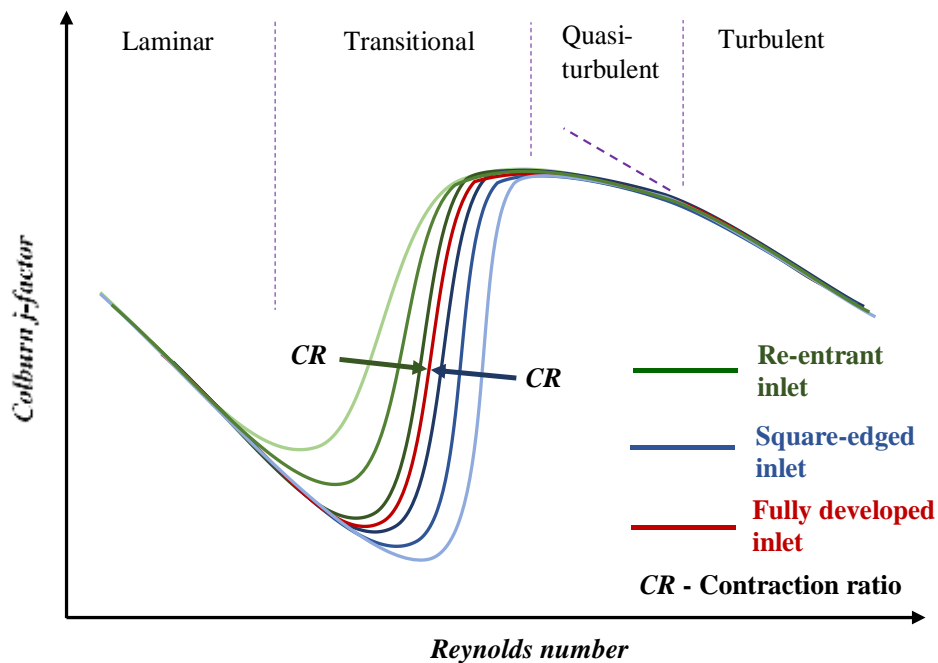


Fig. 7.7: Schematic representation of the influence of contraction ratio on the fully developed Colburn j -factor as a function of Reynolds number for a square-edged (blue) and a re-entrant (green) inlet.

Fig. 7.8 and Fig. 7.9 show qualitatively (without CFD simulations) the schematic representation of the fluid flow pattern for square-edged and re-entrant inlets respectively, with different contraction ratios. For the square-edged inlet (Fig. 7.8), as the contraction ratio decreased, the inlet cross-sectional area where the eddies formed, decreased. The fluid flow pattern to the test section therefore became smoother (with less disturbances) and transition was delayed (higher Reynolds numbers) [41]. For the re-entrant inlet (Fig. 7.9), the protrusion of the tube caused more disturbances compared with the square-edged inlet. Furthermore, as the cross-sectional area decreased (by decreasing the contraction ratio), the inlet disturbances increased as well, which caused transition to occur at lower Reynolds numbers. At higher contraction ratios (>33), the inlet geometry had a negligible influence on the transitional flow regime and the results were similar to that of a hydrodynamically fully developed inlet.

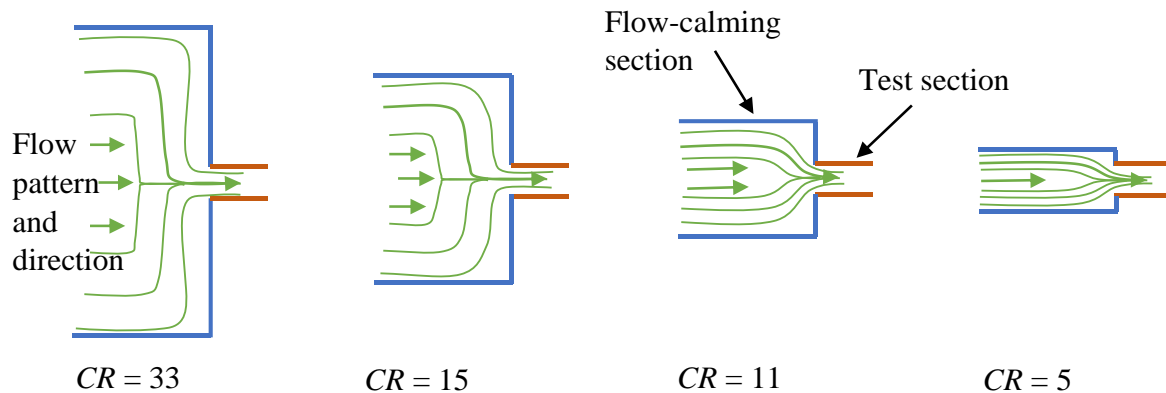


Fig. 7.8: Schematic diagram of the fluid flow pattern for a square-edged inlet with different contraction ratios.

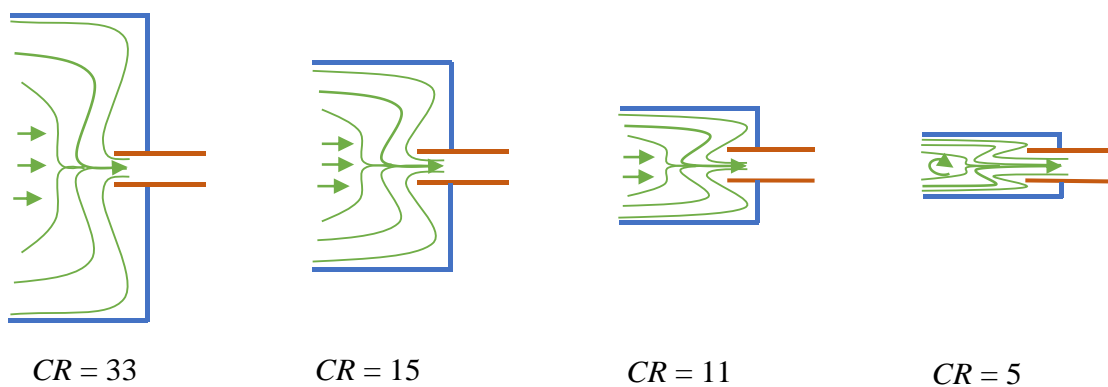


Fig. 7.9: Schematic diagram of the fluid flow pattern for a re-entrant inlet with different contraction ratios.

7.4. Conclusions and recommendations

This chapter investigated the effect of flow-calming section contents and inlet contraction ratios on the heat transfer and pressure drop characteristics of the transitional flow regime using a square-edged and re-entrant inlet. Furthermore, a hydrodynamically fully developed and 90° bend inlets were also investigated. Effects of heating on the different contraction ratios were investigated and compared between the square-edged and re-entrant inlet.

It was found that for the square-edged and re-entrant inlets, the flow-calming section contents had no influence on the heat transfer and pressure drop characteristics in the laminar, transitional and quasi-turbulent flow regimes. As the contraction ratio increased, transition occurred earlier for the square-edged inlet, while for the re-entrant inlet, transition was delayed with increasing contraction ratios. For contraction ratios larger than 33, transition occurred at approximately the same critical Reynolds numbers for both the square-edged and re-entrant inlets, which also corresponded to the critical Reynolds numbers of the hydrodynamically fully developed inlet. For the 90° bend inlet, transition occurred earlier than all the other inlet geometries and contraction ratios. The effect of heating on the transitional flow Reynolds numbers was more at lower contraction ratios than at higher contraction ratios for both the square-edged and re-entrant inlets.

It was not the purpose of this study to investigate the flow distributions and characteristics at the inlet with Computational Fluid Dynamics (CFD) analysis. It is therefore recommended that a CFD study be conducted to investigate in more detail the qualitatively descriptions of the flow for the different types of inlets.

This experimental study indicated that the boundaries of the transitional flow regime, as well as the heat transfer and pressure drop characteristics in the transitional flow regime were affected by contraction ratios. It is therefore important that future work should also quantify contraction ratios when developing correlations for specific inlets. Furthermore, the contraction ratio or size of a heat exchanger header/plenum should be considered in the design of heat exchangers operating in the transitional flow regime. What also needs to be investigated is the length (or aspect ratios) of flow-calming sections to determine what effect it will have on the transitional flow regime.

8. Summary, conclusions and recommendations

8.1. Summary

Heat exchangers are widely used in industries such as power generation, HVAC systems, manufacturing plants, transport systems (automotive, trains, aeroplanes and ships), oil, gas and chemical processing. Most heat exchangers operate in the turbulent flow regime and occasionally in the laminar or even transitional flow regimes. Although the transitional flow regime is associated with high uncertainties, it is sometimes unavoidable in heat exchangers due to design constraints, system upgrades, fouling or even changes in operating conditions that lead to lower mass flow rates. For laminar and transitional convective flow through a tube, the flow can be either forced convection or mixed convection. With mixed convection, the density differences in the radial direction lead to buoyancy effects in the fluid. To be able to distinguish between forced convection and mixed convection is very important, because the Nusselt numbers of the different conditions vary significantly.

The transitional flow regime has been receiving great attention in recent years due to its good compromise between high heat transfer and low pressure drop, making it a potential heat exchanger operating flow regime. The heat transfer and pressure drop in the transitional flow regime under various operating conditions have been extensively investigated since the 1990s. The influence of heating and inlet geometry on the transition from laminar to turbulent flow regimes were extensively investigated, mostly within horizontal tubes without inclined tubes. The Reynolds number boundaries of the transitional flow regime were quantified, and heat transfer coefficient and friction factor correlations have been developed for mixed convection conditions in horizontal tubes. However, because it was found that the heat transfer and pressure drop characteristics in the transitional flow regime were significantly affected by the inlet geometry, different correlations were developed for different inlet geometries.

The purpose of this study was to experimentally investigate the effect of tube inclination, heating and inlet contraction ratio on the single-phase heat transfer and pressure drop characteristics in the laminar and transitional flow regimes for pure forced and mixed convection conditions. To achieve this, an experimental set-up was designed, built and commissioned. The experimental set-up was validated against literature with the test section at horizontal and vertical orientations. The test section was 4.6 m long and was made from a smooth hard drawn copper tube with measured inner and outer diameters of 5.1 mm and 6.3 mm, respectively. A 6 m long test bench was designed and built to accommodate the test section together with the different flow-calming sections, as well as the different inlet geometries and contraction ratios. The test bench was pivoted at the centre and

supported at both ends so that it can be orientated at different inclination angles from -90° downward to $+90^\circ$ upward.

Depending on the type of analysis, four different types of inlet namely; square-edged and re-entrant inlet with different inlet contraction ratios (5, 11, 14 and 33), as well as hydrodynamically fully developed and 90° bend inlets were investigated. Experiments were conducted at various inclination angles from vertical upward flow ($+90^\circ$) to vertical downward flow (-90°), with horizontal flow (0°) and several other angles in between. A total of 2 679 mass flow rate measurements, 174 135 temperature measurements and 2 679 pressure drop measurements were conducted using water (Prandtl numbers between 3.5 and 8.1) as the working fluid. The Reynolds number range covered were from 400 to 6 000 at constant heat fluxes varying from 1 to 8 kW/m².

8.2. Conclusions

Performing mixed convection heat transfer and pressure drop experiments at different inclination angles generated different levels of buoyancy. To account for the effect of inclination angle on the laminar Nusselt numbers and friction factors, a simple *inclined tube Grashof/Rayleigh number* was defined. The laminar heat transfer coefficients were expressed as a forced convection part plus an additional enhancement part caused by mixed convection. Similarly, the laminar friction factors were expressed as the forced convection part multiplied by the enhancement part. Fully developed average laminar Nusselt number and friction factor correlations for inclined tubes were developed as a function of the inclined tube Grashof/Rayleigh numbers.

It was found that the influences of buoyancy near vertical inclination angles were stronger than near horizontal inclination angles which caused the laminar heat transfer and pressure drop to increase rapidly near vertical inclination angles. Both the heat transfer and pressure drop results indicated that the Reynolds number at which the transitional flow regime started in the fully developed region increased as the inclination angle increased from horizontal to vertical flow, while the end of the transitional flow regime remained relatively constant for the inclination angles. This caused the width of the transitional flow regime to decrease as the inclination angle increased. Furthermore, inclination of the test section decreased the buoyancy effects (inclined tube Grashof number) and increased the transition gradient. Because buoyancy had a negligible effect on the quasi-turbulent flow regime, the results were independent of inclination angle. Furthermore, flow directions (upward and downward flows) had negligible influence on the heat transfer coefficients and friction factors.

Buoyancy effects were found to be negligible for vertical upward and downward flow and both the heat transfer and pressure drop results were dominated by forced convection only. It was found that flow direction had a negligible effect on the forced convection Nusselt numbers for Reynolds numbers higher than 600. Furthermore, the fully developed laminar forced convection Nusselt numbers were not constant at 4.36 for a constant heat flux boundary condition, but were a function

of Reynolds number, but independent of Grashof number. Heat flux had no influence on the magnitude of the fully developed forced convection friction factors in the laminar flow regime, and the friction factors corresponded well with $f = 64/Re$. A revised laminar fully developed forced convection Nusselt number correlation, which is a function of Reynolds number, was developed for flow in smooth tubes.

The Reynolds numbers at which the transitional flow regime started and ended in the fully developed region increased simultaneously as the heat flux increased for pure forced convection conditions, although the transitional flow regime started at the same mass flow rate. Furthermore, the width of the transitional flow regime was the same for all heat fluxes and decreased along the length of the tube in the developing region up to the fully developed region where it remained constant. Correlations were developed to determine the boundaries of the transitional flow regime for pure forced convection.

When square-edged and re-entrant inlets were used, the flow-calming section contents had no influence on the heat transfer and pressure drop characteristics in the laminar, transitional and quasi-turbulent flow regimes. As the contraction ratio increased, transition occurred earlier for the square-edged inlet, while for the re-entrant inlet, transition was delayed with increasing contraction ratios. For contraction ratios larger than 33, transition occurred at approximately the same critical Reynolds numbers for both the square-edged and re-entrant inlets, which also corresponded to the critical Reynolds numbers of the hydrodynamically fully developed inlet. For the 90° bend inlet, transition occurred earlier than all the other inlet geometries and contraction ratios. The effect of heating on the transitional flow Reynolds numbers was more at lower contraction ratios than at higher contraction ratios for both the square-edged and re-entrant inlets.

Overall, it was concluded that inclination of heated tubes changed the way buoyancy forces acted on the fluid flow and changed the magnitude of the Grashof numbers and thus, transitional flow Reynolds numbers. Transition for forced convection conditions occurred at the same mass flow rate for all heat fluxes, which corresponded to the isothermal flow case. However, the Reynolds numbers increased with increasing heat flux due to the decreasing viscosity with increasing temperature. The boundaries of the transitional flow regime were significantly affected by the inlet contraction ratios for a specific inlet geometry.

8.3. Recommendations

Recommendations for future work are listed as follows:

- i. The heat transfer and pressure drop in the laminar and transitional flow regime for constant wall temperature conditions should be investigated experimentally for both heating and cooling conditions, using different inclination angles from vertical upward to vertical downward flow directions. Furthermore, laminar forced convection Nusselt numbers for constant wall temperature conditions should be investigated

- experimentally for comparison with the constant property Nusselt number of 3.66, and also with the revised laminar Nusselt number for constant heat flux conditions.
- ii. The effect of tube diameters should be investigated as this can change the magnitude of the inclined tube Grashof numbers and thus affect the heat transfer and pressure drop in both the laminar and transitional flow regimes. This is important, especially for the vertical orientations to determine whether the increase in diameter and thus Grashof numbers can cause the buoyancy effects to become significant, and change the flow condition from forced to mixed convection at higher laminar Reynolds numbers and the entire transitional flow regime.
 - iii. Forced convection heat transfer should also be investigated using different channels such as rectangular channels with different aspect ratios as this can change how the velocity and temperature profiles develop and thus affect the forced convection heat transfer.
 - iv. The effect of the length of flow-calming sections on the transitional flow regime should also be investigated.
 - v. Future work should also quantify contraction ratios when developing correlations for specific inlets.

References

- [1] D.R.E. Ewim, J.P. Meyer, S.M.A. Noori Rahim Abadi, Condensation heat transfer coefficients in an inclined smooth tube at low mass fluxes, *International Journal of Heat and Mass Transfer*, 123 (2018) 455-467.
- [2] S.P. Olivier, J.P. Meyer, M. De Paepe, K. De Kerpel, The influence of inclination angle on void fraction and heat transfer during condensation inside a smooth tube, *International Journal of Multiphase Flow*, 80 (2016) 1-14.
- [3] A.O. Adelaja, J. Dirker, J.P. Meyer, Experimental study of the pressure drop during condensation in an inclined smooth tube at different saturation temperatures, *International Journal of Heat and Mass Transfer*, 105 (2017) 237-251.
- [4] J.P. Meyer, J. Dirker, A.O. Adelaja, Condensation heat transfer in smooth inclined tubes for R134a at different saturation temperatures, *International Journal of Heat and Mass Transfer*, 70 (2014) 515-525.
- [5] S. Lips, J.P. Meyer, Experimental study of convective condensation in an inclined smooth tube. Part I: Inclination effect on flow pattern and heat transfer coefficient, *International Journal of Heat and Mass Transfer*, 55(1) (2012) 395-404.
- [6] S. Lips, J.P. Meyer, Experimental study of convective condensation in an inclined smooth tube. Part II: Inclination effect on pressure drops and void fractions, *International Journal of Heat and Mass Transfer*, 55(1) (2012) 405-412.
- [7] S. Lips, J.P. Meyer, Stratified flow model for convective condensation in an inclined tube, *International Journal of Heat and Fluid Flow*, 36 (2012) 83-91.
- [8] S. Lips, J.P. Meyer, Two-phase flow in inclined tubes with specific reference to condensation: A review, *International Journal of Multiphase Flow*, 37(8) (2011) 845-859.
- [9] M. Everts, J.P. Meyer, Flow regime maps for smooth horizontal tubes at a constant heat flux, *International Journal of Heat and Mass Transfer*, 117 (2018) 1274-1290.
- [10] B. Metais, E.R.G. Eckert, Forced, mixed and free convection regimes, *ASME J. Heat Transfer*, 86 (1964) 295-296.
- [11] Y.A. Çengel, A.J. Ghajar, *Heat and Mass Transfer: Fundamentals & Applications*, 5th ed., McGraw Hill, New York, 2015.
- [12] J.H. Lienhard, J.H. Lienhard, *A Heat Transfer Textbook*, 4th ed., Dover Publications, Newburyport, 2013.
- [13] A. Bejan, *Convection Heat Transfer*, 4th ed., J. Wiley & Sons, Hoboken, 2013.
- [14] J.P. Holman, *Heat Transfer*, 10th ed., McGraw-Hill, Boston; London, 2014.
- [15] T.L. Bergman, A.S. Lavine, F.P. Incropera, D.P. DeWitt, *Fundamentals of Heat and Mass Transfer*, 8th ed., Wiley, New York, 2017.

- [16] R.K. Shah, A.L. London, *Laminar Flow Forced Convection in Ducts*, Academic Press, New York, 1978.
- [17] T.M. Hallman, *Combined free and forced convection in a circular tube*, PhD thesis, Purdue University, Lafayette, 1958.
- [18] J.P. Meyer, M. Everts, Single-phase mixed convection of developing and fully developed flow in smooth horizontal circular tubes in the laminar and transitional flow regimes, *International Journal of Heat and Mass Transfer*, 117 (2018) 1251-1273.
- [19] Y. Sudo, K. Miyata, H. Ikawa, M. Ohkawara, M. Kaminaga, Experimental study of differences in single-phase forced-convection heat transfer characteristics between upflow and downflow for narrow rectangular channel, *Journal of Nuclear Science and Technology*, 22(3) (1985) 202-212.
- [20] L.M. Tam, A.J. Ghajar, Effect of inlet geometry and heating on the fully developed friction factor in the transition region of a horizontal tube, *Experimental Thermal and Fluid Science*, 1777(97) (1997) 52-64.
- [21] M. Everts, J.P. Meyer, Heat transfer of developing and fully developed flow in smooth horizontal tubes in the transitional flow regime, *International Journal of Heat and Mass Transfer*, 117 (2018) 1331-1351.
- [22] M. Iqbal, J.W. Stachiewicz, Influence of tube orientation on combined free and forced laminar convection heat transfer, *Journal of Heat Transfer*, 88(1) (1966) 109-116.
- [23] A. Al-Sammarraie, R. Jassem, T. K. Ibrahim, Mixed convection heat transfer in inclined tubes with constant heat flux, *European Journal of Scientific Research*, 97(1) (2013) 144-158.
- [24] H.A. Mohammed, Y.K. Salman, Combined convection heat transfer for thermally developing aiding flow in an inclined circular cylinder with constant heat flux, *Applied Thermal Engineering*, 27(8) (2007) 1236-1247.
- [25] J. Orfi, N. Galanis, C.T. Nguyen, *Laminar mixed convection in the entrance region of inclined pipes with high uniform heat fluxes*, American Society of Heating, Refrigerating and Air-Conditioning Engineers, Inc., Atlanta, GA (United States), 1998.
- [26] G.S. Barozzi, E. Zanchini, M. Mariotti, Experimental investigation of combined forced and free convection in horizontal and inclined tubes, *Meccanica*, 20(1) (1985) 18-27.
- [27] T. Maré, N. Galanis, I. Voicu, J. Miriel, Experimental analysis of mixed convection in inclined tubes, *Applied Thermal Engineering*, 26(14-15) (2006) 1677-1683.
- [28] J. Orfi, N. Galanis, C.T. Nguyen, Laminar fully developed incompressible flow with mixed convection in inclined tubes, *International Journal of Numerical Methods for Heat & Fluid Flow*, 3(4) (1993) 341-355.
- [29] J. Orfi, N. Galanis, C.T. Nguyen, Bifurcation in steady laminar mixed convection flow in uniformly heated inclined tubes, *International Journal of Numerical Methods for Heat & Fluid Flow*, 9(5) (1999) 543-567.
- [30] J. Orfi, N. Galanis, Developing laminar mixed convection with heat and mass transfer in horizontal and vertical tubes, *International Journal of Thermal Sciences*, 41(4) (2002) 319-331.

- [31] D. Choudhury, S.V. Patankar, Combined forced and free laminar convection in the entrance region of an inclined isothermal tube, *Journal of Heat Transfer*, 110(4) (1988) 901-909.
- [32] G.C. Vliet, Natural convection local heat transfer on constant-heat-flux inclined surfaces, *Journal of Heat Transfer*, 91(4) (1969) 511-516.
- [33] T. Fujii, H. Imura, Natural-convection heat transfer from a plate with arbitrary inclination, *International Journal of Heat and Mass Transfer*, 15(4) (1972) 755-767.
- [34] N. Rani, H. Setia, M. Dutt, R. Wanchoo, Natural convection heat transfer from inclined cylinders: A unified correlation, *International Journal of Mathematical, Computational, Physical and Quantum Engineering*, 8(1) (2014) 100-105.
- [35] A.J. Ghajar, L.M. Tam, Heat transfer measurements and correlations in the transition region for a circular tube with three different inlet configurations, *Experimental Thermal and Fluid Science*, 8(1) (1994) 79-90.
- [36] A.J. Ghajar, L.M. Tam, Laminar-transition-turbulent forced and mixed convective heat transfer correlations for pipe flows with different inlet configurations, *American Society of Mechanical Engineers, Heat Transfer Division, (Publication) HTD*, (1991) 15-23.
- [37] L.M. Tam, A.J. Ghajar, Transitional heat transfer in plain horizontal tubes, *Heat Transfer Engineering*, 27(5) (2006) 23-38.
- [38] A.J. Ghajar, L.M. Tam, Flow regime map for a horizontal pipe with uniform wall heat flux and three inlet configurations, *Experimental Thermal and Fluid Science*, 10(3) (1995) 287-297.
- [39] A.J. Ghajar, L.M. Tam, S.C. Tam, Improved heat transfer correlation in the transition region for a circular tube with three inlet configurations using artificial neural networks, *Heat Transfer Engineering*, 25(2) (2004) 30-40.
- [40] M. Everts, J.P. Meyer, Relationship between pressure drop and heat transfer of developing and fully developed flow in smooth horizontal circular tubes in the laminar, transitional, quasi-turbulent and turbulent flow regimes, *International Journal of Heat and Mass Transfer*, 117 (2018) 1231-1250.
- [41] J.P. Meyer, S.M. Abolarin, Heat transfer and pressure drop in the transitional flow regime for a smooth circular tube with twisted tape inserts and a square-edged inlet, *International Journal of Heat and Mass Transfer*, 117 (2018) 11-29.
- [42] J. Dirker, J.P. Meyer, D.V. Garach, Inlet flow effects in micro-channels in the laminar and transitional regimes on single-phase heat transfer coefficients and friction factors, *International Journal of Heat and Mass Transfer*, 77 (2014) 612-626.
- [43] A.I. Bashir, M. Everts, J.P. Meyer, Influence of inlet contraction ratios on the heat transfer and pressure drop characteristics of single-phase flow in smooth circular tubes in the transitional flow regime, *Experimental Thermal and Fluids Science*, 109 (2019) 109892.
- [44] J.P. Meyer, T.J. McKrell, K. Grote, The influence of multi-walled carbon nanotubes on single-phase heat transfer and pressure drop characteristics in the transitional flow regime of smooth tubes, *International Journal of Heat and Mass Transfer*, 58(1-2) (2013) 597-609.
- [45] J.P. Meyer, J.A. Olivier, Heat transfer and pressure drop characteristics of smooth horizontal tubes in the transitional flow regime, *Heat Transfer Engineering*, 35(14-15) (2014) 1246-1253.

- [46] J.P. Meyer, J.A. Olivier, Heat transfer and pressure drop characteristics of circular smooth tubes in the transitional flow regime, in: 19th International Congress of Chemical and Process Engineering, CHISA 2010 and 7th European Congress of Chemical Engineering, ECCE-7, 2010.
- [47] D.D. Ndenguma, J. Dirker, J.P. Meyer, Transitional flow regime heat transfer and pressure drop in an annulus with non-uniform wall temperatures, *International Journal of Heat and Mass Transfer*, 108 (2017) 2239-2252.
- [48] J.A. Olivier, J.P. Meyer, Single-phase heat transfer and pressure drop of the cooling of water inside smooth tubes for transitional flow with different inlet geometries (RP-1280), *HVAC&R Research*, 16(4) (2010) 471-496.
- [49] D.D. Ndenguma, J. Dirker, J.P. Meyer, Heat transfer and pressure drop in annuli with approximately uniform internal wall temperatures in the transitional flow regime, *International Journal of Heat and Mass Transfer*, 111 (2017) 429-441.
- [50] J.P. Meyer, J.A. Olivier, Transitional flow inside enhanced tubes for fully developed and developing flow with different types of inlet disturbances: Part II – Heat transfer, *International Journal of Heat and Mass Transfer*, 54(7-8) (2011) 1598-1607.
- [51] J.P. Meyer, J.A. Olivier, Transitional flow inside enhanced tubes for fully developed and developing flow with different types of inlet disturbances: Part I – Adiabatic pressure drops, *International Journal of Heat and Mass Transfer*, 54(7) (2011) 1587-1597.
- [52] L.M. Tam, A.J. Ghajar, The unusual behavior of local heat transfer coefficient in a circular tube with a bell-mouth inlet, *Experimental Thermal and Fluid Science*, 16(3) (1998) 187-194.
- [53] A.J. Ghajar, K.F. Madon, Pressure drop measurements in the transition region for a circular tube with three different inlet configurations, *Experimental Thermal and Fluid Science*, 5(1) (1992) 129-135.
- [54] A.J. Ghajar, C.C. Tang, W.L. Cook, Experimental investigation of friction factor in the transition region for water flow in minitubes and microtubes, *Heat Transfer Engineering*, 31(8) (2010) 646-657.
- [55] L.M. Tam, A.J. Ghajar, Effect of inlet geometry and heating on the fully developed friction factor in the transition region of a horizontal tube, *Experimental Thermal and Fluids Science*, 1777(97) (1997) 52-64.
- [56] K.H. Tam, L.M. Tam, A.J. Ghajar, Effect of inlet geometries and heating on the entrance and fully-developed friction factors in the laminar and transition regions of a horizontal tube, *Experimental Thermal and Fluid Science*, 44 (2013) 680-696.
- [57] J.P. Meyer, A.I. Bashir, M. Everts, Single-phase mixed convective heat transfer and pressure drop in the laminar and transitional flow regimes in smooth inclined tubes heated at a constant heat flux, *Experimental Thermal and Fluids Science*, 109 (2019) 109890.
- [58] S.M. Abolarin, M. Everts, J.P. Meyer, Heat transfer and pressure drop characteristics of alternating clockwise and counter clockwise twisted tape inserts in the transitional flow regime, *International Journal of Heat and Mass Transfer*, 133 (2019) 203-217.
- [59] S.M. Abolarin, M. Everts, J.P. Meyer, The influence of peripheral u-cut twisted tapes and ring inserts on the heat transfer and pressure drop characteristics in the transitional flow regime, *International Journal of Heat and Mass Transfer*, 132 (2019) 970-984.

- [60] A.I. Bashir, M. Everts, J.P. Meyer, R. Bennacer, Single-phase forced convection heat transfer and pressure drop in circular tubes in the laminar and transitional flow regimes, *Experimental Thermal and Fluids Science*, 109 (2019) 109891.
- [61] O. Reynolds, An experimental investigation of the circumstances which determine whether the motion of water in parallel channels shall be direct or sinuous and of the law of resistance in parallel channels, *Philos. Trans. R. Soc.*, (1883) 935-982.
- [62] F.M. White, *Fluid Mechanics*, 6th ed., McGraw-Hill, Singapore, 2009.
- [63] S. Kakaç, R.K. Shah, A. Win, *Handbook of single-phase convective heat transfer*, in, Wiley, New York :, 1987.
- [64] F. Kreith, R.M. Manglik, *Principles of Heat Transfer*, 8 ed., Cengage Learning, Boston, MA 2018.
- [65] M. Everts, Single-phase mixed convection of developing and fully developed flow in smooth horizontal circular tubes in the laminar, transitional, quasi-turbulent and turbulent flow regimes, PhD thesis, University of Pretoria, Pretoria, 2018.
- [66] S. Kakaç, The effect of temperature-dependent fluid properties on convective heat transfer, in: S. Kakaç, R.K. Shah, W. Aung (Eds.) *Handbook of Single-Phase Convective Heat Transfer*, Wiley, New York, 1987.
- [67] C. Nonino, S. Del Giudice, S. Savino, Temperature dependent viscosity effects on laminar forced convection in the entrance region of straight ducts, *International Journal of Heat and Mass Transfer*, 49(23) (2006) 4469-4481.
- [68] C. Nouar, Numerical solution for laminar mixed convection in a horizontal annular duct: Temperature-dependent viscosity effect, *International Journal for Numerical Methods in Fluids*, 29(7) (1999) 849-864.
- [69] L. Zhai, G. Xu, Y. Quan, G. Song, B. Dong, H. Wu, Numerical analysis of the axial heat conduction with variable fluid properties in a forced laminar flow tube, *International Journal of Heat and Mass Transfer*, 114 (2017) 238-251.
- [70] R.G. Deissler, Analytical investigation of fully developed laminar flow in tubes with heat transfer with fluid properties variable along the radius, *NACA TN 2410*, 1951.
- [71] R.L. Shannon, C.A. Depew, Forced laminar flow convection in a horizontal tube with variable viscosity and free-convection effects, *Journal of Heat Transfer*, 91(2) (1969) 251-258.
- [72] H. Herwig, The effect of variable properties on momentum and heat transfer in a tube with constant heat flux across the wall, *International Journal of Heat and Mass Transfer*, 28(2) (1985) 423-431.
- [73] L.B. Koppel, J.M. Smith, Laminar flow heat transfer for variable physical properties, *Journal of Heat Transfer*, 84(2) (1962) 157-162.
- [74] H. Zhao, X. Li, X. Wu, New friction factor and Nusselt number equations for laminar forced convection of liquid with variable properties, *Science China Technological Sciences*, 61(1) (2018) 98-109.
- [75] H. Herwig, S.P. Mahulikar, Variable property effects in single-phase incompressible flows through microchannels, *International Journal of Thermal Sciences*, 45(10) (2006) 977-981.

- [76] N. P. Gulhane, S.P. Mahulikar, Numerical study of compressible convective heat transfer with variations in all fluid properties, *International Journal of Thermal Sciences*, 49(5) (2010) 786-796.
- [77] R. Kumar, S.P. Mahulikar, Effect of temperature-dependent viscosity variation on fully developed laminar microconvective flow, *International Journal of Thermal Sciences*, 98 (2015) 179-191.
- [78] D. Huber, H. Walter, Forced convection heat transfer in the transition region between laminar and turbulent flow for a vertical circular tube, in: *Proceedings of the 2010 International Conference on Theoretical and Applied Mechanics, and 2010 International Conference on Fluid Mechanics and Heat & Mass Transfer*, World Scientific and Engineering Academy and Society (WSEAS), Corfu Island, Greece, 2010, pp. 132-136.
- [79] T. Wei, Heat transfer regimes in fully developed plane-channel flows, *International Journal of Heat and Mass Transfer*, 131 (2019) 140-149.
- [80] W. Aung, Mixed Convection in Internal Flow, in: S. Kakaç, R.K. Shah, W. Aung (Eds.) *Handbook of Single-Phase Forced Convection*, John Wiley, New York, 1987, pp. 15.11-15.51.
- [81] G.D. Raithby, K.G.T. Hollands, Natural Convection, in: W.M. Rohsenow, J.P. Hartnett, Y.I. Cho (Eds.) *Handbook of Heat Transfer*, McGraw-Hill, Boston, 1998, pp. 4.1-4.99.
- [82] S.T. McComas, E.R.G. Eckert, Combined free and forced convection in a horizontal circular tube, *Journal of Heat Transfer*, 88(2) (1966) 147-152.
- [83] R.L. Shannon, C.A. Depew, Combined free and forced laminar convection in a horizontal tube with uniform heat flux, *Journal of Heat Transfer*, 90(3) (1968) 353-357.
- [84] S.W. Hong, S.M. Morcos, A.E. Bergles, Analytical and experimental results for combined forced and free laminar convection in horizontal tubes, in: *Proceedings of the 5th International Heat Transfer Conference (IHTC-5)*, Tokyo, Japan, 1974, pp. 154-158.
- [85] K.C. Cheng, J.W. Ou, Free convection effects on graetz problem for large prandtl number fluids in horizontal tubes with uniform wall heat flux, in: *Proceedings of the 5th International Heat Transfer Conference (IHTC-5)*, Tokyo, Japan, 1974, pp. 159-163.
- [86] E.R.G. Eckert, A.J. Diaguila, Convective heat transfer for mixed, free, and forced flow through tubes, *ASME Trans*, (76) (1954) 497-504.
- [87] J.D. Jackson, M.A. Cotton, B.P. Axcell, Studies of mixed convection in vertical tubes, 10(1) (1989).
- [88] H.A. Mohammed, Laminar mixed convection heat transfer in a vertical circular tube under buoyancy-assisted and opposed flows, *Energy Conversion and Management journal*, 49 (2008) 2006-2015.
- [89] H.A. Mohammed, Y.K. Salman, Experimental investigation of mixed convection heat transfer for thermally developing flow in a horizontal circular cylinder, *Applied Thermal Engineering*, 27(8-9) (2007) 1522-1533.
- [90] H.A. Mohammed, Y.K. Salman, Combined natural and forced convection heat transfer for assisting thermally developing flow in a uniformly heated vertical circular cylinder, 34 (2007) 474-491.

- [91] C. Tian, J. Wang, X. Cao, C. Yan, A.A. Ala, Experimental study on mixed convection in an asymmetrically heated, inclined, narrow, rectangular channel, *International Journal of Heat and Mass Transfer*, 116 (2018) 1074-1084.
- [92] C. Tian, M. Yan, J. Wang, X. Cao, C. Yan, S. Yu, Experimental investigation of flow and heat transfer for natural circulation flow in an inclined narrow rectangular channel, *Progress in Nuclear Energy*, 98 (2017) 266-276.
- [93] A. Bejan, S. Lorente, L. Martins, J.P. Meyer, The constructal size of a heat exchanger, *Journal of Applied Physics*, 122(6) (2017) 064902.
- [94] S.M.A. Noori Rahim Abadi, J.P. Meyer, J. Dirker, Effect of inclination angle on the condensation of R134a inside an inclined smooth tube, *Chemical Engineering Research and Design*, 132 (2018) 346-357.
- [95] M. Mahdavi, M. Sharifpur, J.P. Meyer, Exploration of nanofluid pool boiling and deposition on a horizontal cylinder in Eulerian and Lagrangian frames, *International Journal of Heat and Mass Transfer*, 125 (2018) 959-971.
- [96] M. Nishi, B. Ünsal, F. Durst, G. Biswas, Laminar-to-turbulent transition of pipe flows through puffs and slugs, *Journal of Fluid Mechanics*, 614 (2008) 425-446.
- [97] E.K. Kalinin, S.A. Yarkho, Flow pulsations and heat transfer in the transition region between the laminar and turbulent flow regimes in a tube, *International Chemical Engineering*, 6(4) (1966) 571-574.
- [98] H.K. Tam, L.M. Tam, A.J. Ghajar, S.C. Tam, T. Zhang, Experimental investigation of heat transfer, friction factor, and optimal fin geometries for the internally microfin tubes in the transition and turbulent regions, *Journal of Enhanced Heat Transfer*, 19(5) (2012) 457-476.
- [99] S.G. Kandlikar, W.J. Grande, Evolution of Microchannel Flow Passages--Thermohydraulic Performance and Fabrication Technology, *Heat Transfer Engineering*, 24(1) (2003) 3-17.
- [100] L.M. Tam, H.K. Tam, A.J. Ghajar, W.S. Ng, I.W. Wong, K.F. Leong, C.K. Wu, The effect of inner surface roughness and heating on friction factor in horizontal micro-tubes, in: *ASME-JSME-KSME 2011 Joint Fluids Engineering Conference*, 2011, pp. 2971-2978.
- [101] A. Barba, S. Rainieri, M. Spiga, Heat transfer enhancement in a corrugated tube, *International Communications in Heat and Mass Transfer*, 29(3) (2002) 313-322.
- [102] A. García, J.P. Solano, P.G. Vicente, A. Viedma, Enhancement of laminar and transitional flow heat transfer in tubes by means of wire coil inserts, *International Journal of Heat and Mass Transfer*, 50(15) (2007) 3176-3189.
- [103] A. García, P.G. Vicente, A. Viedma, Experimental study of heat transfer enhancement with wire coil inserts in laminar-transition-turbulent regimes at different Prandtl numbers, *International Journal of Heat and Mass Transfer*, 48(21) (2005) 4640-4651.
- [104] A. García, J.P. Solano, P.G. Vicente, A. Viedma, The influence of artificial roughness shape on heat transfer enhancement: Corrugated tubes, dimpled tubes and wire coils, *Applied Thermal Engineering*, 35 (2012) 196-201.

- [105] S. Osman, M. Sharifpur, J.P. Meyer, Experimental investigation of convection heat transfer in the transition flow regime of aluminium oxide-water nanofluids in a rectangular channel, *International Journal of Heat and Mass Transfer*, 133 (2019) 895-902.
- [106] N. Galanis, A. Behzadmehr, Mixed convection in vertical ducts, in: *International Conference on Fluid Mechanics and Aerodynamics (FMA'08)*, Rhodes, Greece, 2008, pp. 6-12.
- [107] G.F. Scheele, E.M. Rosen, T.J. Hanratty, Effect of natural convection on transition to turbulence in vertical pipes, *The Canadian Journal of Chemical Engineering*, 38(3) (1960) 67-73.
- [108] A. Behzadmehr, A. Laneville, N. Galanis, Experimental study of onset of laminar – turbulent transition in mixed convection in a vertical heated tube, *International Journal of Heat and Mass Transfer*, 51(25-26) (2008) 5895-5905.
- [109] H.A. Mohammed, The effect of different inlet geometries on laminar flow combined convection heat transfer inside a horizontal circular pipe, *Applied Thermal Engineering*, 29(2) (2009) 581-590.
- [110] H.R. Nagendra, Interaction of free and forced convection in horizontal tubes in the transition regime, *Journal of Fluid Mechanics*, 57(2) (1973) 269-288.
- [111] M. Yasuo, F. Kozo, T. Shinobu, N. Masakuni, Forced convective heat transfer in uniformly heated horizontal tubes 1st report—Experimental study on the effect of buoyancy, *International Journal of Heat and Mass Transfer*, 9(5) (1966) 453-463.
- [112] M. Al-Arabi, Turbulent heat transfer in the entrance region of a tube, *Heat Transfer Engineering*, 3(3-4) (1982) 76-83.
- [113] M. Everts, Heat transfer and pressure drop of developing flow in smooth tubes in the transitional flow regime, Masters dissertation, University of Pretoria, Pretoria, 2014.
- [114] A. Bakker, R.D. LaRoche, E.M. Marshall, Laminar flow in static mixers with helical elements, in: *The Online CFM Book* (2000).
- [115] R.E. Rayle, Influence of orifice geometry on static pressure measurements, ASME paper No 59-A-234, (1959).
- [116] C.O. Popiel, J. Wojtkowiak, Simple formulas for thermophysical properties of liquid water for heat transfer calculations (from 0°C to 150°C), *Heat Transfer Engineering*, 19(3) (1998) 87-101.
- [117] C. Wang, P. Gao, S. Tan, Z. Wang, C. Xu, Experimental study of friction and heat transfer characteristics in narrow rectangular channel, *Nuclear Engineering and Design*, 250(0) (2012) 646-655.
- [118] C. Wang, P. Gao, S. Tan, Z. Wang, Forced convection heat transfer and flow characteristics in laminar to turbulent transition region in rectangular channel, *Experimental Thermal and Fluid Science*, 44 (2013) 490-497.
- [119] J. Ma, L. Li, Y. Huang, X. Liu, Experimental studies on single-phase flow and heat transfer in a narrow rectangular channel, *Nuclear Engineering and Design*, 241(8) (2011) 2865-2873.
- [120] T.S. Zhao, Q.C. Bi, Pressure drop characteristics of gas–liquid two-phase flow in vertical miniature triangular channels, *International Journal of Heat and Mass Transfer*, 44(13) (2001) 2523-2534.

- [121] F. Madrid, N. Caney, P. Marty, Study of a vertical boiling flow in rectangular mini-channels, *Heat Transfer Engineering*, 28(8-9) (2007) 753-760.
- [122] M.V. Sardeshpande, P. Shastri, V.V. Ranade, Two-phase flow boiling pressure drop in small channels, *International Journal of Heat and Fluid Flow*, 61 (2016) 636-649.
- [123] H.A. Mohammed, Laminar mixed convection heat transfer in a vertical circular tube under buoyancy-assisted and opposed flows, *Energy Conversion and Management*, 49 (2008) 2006-2015.
- [124] D.D. Joye, Comparison of correlations and experiment in opposing flow , mixed convection heat transfer in a vertical tube with Grashof number variation, *International Journal of Heat and Mass Transfer*, 39(5) (1996) 1033-1038.
- [125] P.E. Saylor, D.D. Joye, Hydrostatic correction and pressure drop measurement in mixed convection heat transfer in a vertical tube, *Industrial & Engineering Chemistry Research*, 30(4) (1991) 784-788.
- [126] P.F. Dunn, *Measurement and Data Analysis for Engineering and Science*, 2nd ed., CRC press, United States of America, 2010.
- [127] J.L. Poiseuille, *Recherches expérimentales sur le mouvement des liquides dans les tubes de très- petits diamètres*, Imprimerie Royale, (1844).
- [128] H. Blasius, *Das ähnlichkeitsgesetz bei reibungsvorgängen in flüssigkeiten*, *Forschg. Arb. Ing.-Wes.*, (1913) 131-137.
- [129] B. Metais, E.R.G. Eckert, Forced, Mixed, and Free Convection Regimes, *Journal of Heat Transfer*, 86(2) (1964) 295-296.
- [130] S.M. Morcos, A.E. Bergles, Experimental investigation of combined forced and free laminar convection in horizontal tubes, *Journal of Heat Transfer*, 97(2) (1975) 212-219.
- [131] V. Gnielinski, New equations for heat and mass-transfer in turbulent pipe and channel flow, *International Chemical Engineering*, 16(2) (1976) 359-368.
- [132] J.P. Meyer, M. Everts, N. Coetzee, K. Grote, M. Steyn, Heat transfer coefficients of laminar, transitional, quasi-turbulent and turbulent flow in circular tubes, *International Communications in Heat and Mass Transfer*, 105 (2019) 84-106.
- [133] S.V. Patankar, *Numerical Heat Transfer and Fluid Flow*, Hemisphere Publ. Corp., Washington, DC, 1985.
- [134] K.C. Rolle, *Heat and Mass Transfer*, Cengage Learning, Boston, 2016.
- [135] C.J. Ho, C.Y. Chang, C.Y. Cheng, S.J. Cheng, Y.W. Guo, S.T. Hsu, W.M. Yan, Laminar forced convection effectiveness of Al₂O₃-water nanofluid flow in a circular tube at various operation temperatures: Effects of temperature-dependent properties, *International Journal of Heat and Mass Transfer*, 100 (2016) 464-481.
- [136] D. Taler, *Numerical Modelling and Experimental Testing of Heat Exchangers*, 1st ed., Springer International Publishing, Berling-Heidelberg, 2019.